

# POLITECNICO DI TORINO

**Aerospace Engineering Master's Degree**

Master's Degree Thesis

## **Implementation of classical and advanced failure criteria for composite layered structures in FEMAP and assessment of results**



**Supervisor**

prof. Erasmo Carrera

**Candidate**

Amedeo Grasso

March 2018

## Table of contents

Table of contents.....	2
Introduction.....	5
Chapter 2 - Overview of most popular failure criteria.....	8
2.1 - Maximum stress and maximum strain criteria .....	9
2.2 - Tsai–Hill criterion .....	10
2.3 – Tsai-Wu criterion.....	10
2.4 – Hoffman criteria.....	11
2.5 – Hashin criterion.....	13
2.6 – LaRC criteria.....	14
2.6.1 - The basic knowledge of LaRC: Puck’s failure criteria .....	14
2.6.1.1 – Failure conditions for fibre failure (FF) .....	15
Tensile fibre failure criterion .....	16
Compressive “fibre kinking” failure criterion .....	16
2.6.1.2 – Failure conditions for inter-fibre failure (IFF).....	17
Mode A .....	18
Mode B .....	18
Mode C .....	19
Description of coefficients and terms used in the inter-fibre failure criteria .....	19
2.6.2 - LaRC03.....	20
2.6.2.1 - Matrix failure.....	21
2.6.2.1.1 - Matrix failure under transverse compression ( $\sigma_{22} < 0$ ) .....	21
2.6.2.1.2 - Matrix failure under Transverse Tension ( $\sigma_{22} > 0$ ) .....	24
2.6.2.2 - Fibre failure .....	26
2.6.2.2.1 - Fibre Tension Failure .....	26
2.6.2.2.2 - Fibre Compression Failure .....	27
2.6.2.3 - Matrix Damage under Biaxial Compression .....	28
2.6.3 - LaRC04.....	29
2.6.3.1 - Matrix failure.....	29
2.6.3.1.1 - Tensile Matrix failure .....	29
2.6.3.1.2 - Compressive Matrix failure.....	31
2.6.3.2 - Fibre failure .....	33
2.6.3.2.1 – Tensile fibre failure.....	33

2.6.3.2.2 – Compressive fibre failure.....	33
2.6.4 - LaRC05.....	40
2.6.4.1 - Failure model at the ply level .....	41
2.6.4.1.1 - Matrix Failure .....	41
2.6.4.1.2 - Fibre Kinking Failure .....	43
2.6.4.1.3 - Fibre Tensile Failure.....	46
Chapter 3 – The API .....	47
3.1 - Computational framework.....	47
3.1.1 - Femap .....	48
3.1.2 - Visual Basic Language .....	49
3.2 - API: Flowchart .....	50
3.3 API: Functions and GUIs.....	51
3.3.1 - Failure Index Operative Mod .....	51
3.3.2 - Sandwich Panel – Margin of Safety .....	52
Chapter 4 - API: Validation .....	54
4.1 - Validation of functions to evaluate Hoffman failure index and MOS.....	54
4.1.1 - Description of the model .....	55
Material properties .....	55
4.1.2 - Numerical Results of the analysis and comparison .....	56
4.2 – Failure indexes with LaRC05 theory validation of results. ....	59
4.2.1 – Fiber tension .....	60
4.2.2 – Matrix failure .....	62
4.2.3 – Kinking failure.....	66
4.2.4 - Failure mode.....	67
4.3 – Validation of calculation of margin of safety for sandwich panel.....	68
4.3.1 Panel with metallic skins .....	68
4.3.1.1 - Description of the model .....	68
Layup and materials data .....	69
4.3.1.2 - Numerical Results of the analysis and comparison .....	69
Upper skin – Results .....	70
Bottom skin - Results.....	70
Honeycomb – Results .....	70
4.3.2 Panel with composite laminate skins .....	71
4.3.2.1 - Description of the model .....	71
Layup and material data.....	71

4.3.2.2 - Numerical Results of the analysis and comparison .....	73
Failure index .....	74
Margin of Safety .....	74
4.3.3 - Honeycomb meshed with solid elements .....	77
4.3.3.1 - Description of the model .....	77
Layup and material data.....	77
4.3.3.2 - Numerical Results of the analysis and comparison .....	78
Chapter 5 - Common issues when using failure criteria and critical discussion....	79
5.1 - Comparison of failure indexes between classical and LaRCs criteria .....	79
5.1.1 - Unidirectional 0° E-glass/MY750 epoxy .....	79
5.1.2 - Unidirectional composite E-Glass/LY556 .....	81
5.1.3 - Cross-ply laminates .....	82
5.2 - LaRC05 vs. Hoffman results .....	83
5.2.1 - Example 1 .....	83
5.2.2 - Example 2 .....	87
Chapter 6 - Numerical results on a real case study .....	89
6.1 - Sandwich Panels .....	91
6.1.1 - Skin Analysis .....	92
6.1.2 - Honeycomb Analysis.....	93
Chapter 7 - Concluding remarks .....	95
References .....	96

## Introduction

In the aerospace and aeronautic Industry, the use of composite material is growing each year, and, the methodology for designing high-performance structures of composite materials is still evolving. As a matter of fact, further advances in the use of laminated composites are subordinate to a better understanding of their failure mechanisms. In this context having a physical model for each failure mode becomes an important point of concern, because these physical models should establish when the failure takes place, and they also describe the post-failure behavior.

However, the analysis and simulation of the failure of composite laminated structures are quite cumbersome tasks. As anticipated by Puck, who paid particularly attention to the differences in tensile and compressive strength, the failure mechanisms are very different from those of traditional metallic structures. The combination of various interfaces (fibre, matrix, layers) on a macro scale level requires a local dedicated analysis to establish the initiation of failure mechanisms of a fibre, a crack in the matrix or a delamination between two different layers.

The main failure modes of laminated fibre-reinforced composites are the following [Ref.15]:

- **Delamination:** the process through which composite materials made of different plies stacked together tend to delaminate. The bending stiffness of delaminated panels can be significantly reduced, even when no visual defect is visible on the surface or the free edges. The physics of delamination is quite understood, and one of the best numerical tools to predict the propagation of delamination consists in the use of Decohesion Elements. These elements have been developed, and implemented in commercial Finite Element (FE) codes, like ABAQUS.
- **Matrix compression failure:** what is commonly considered as matrix compression failure is actually shear matrix failure. Indeed, the failure occurs at an angle with the loading direction, which is the evidence of the shear nature of the failure process.
- **Matrix tensile failure:** the fracture on the surface resulting from this failure mode is typically normal to the loading direction. Some fiber splitting at the fracture surface usually can be observed.
- **Fibre compression failure:** this failure mode is largely affected by the resin shear behaviour and imperfections such as the initial fibre misalignment of the angle and voids. Typically, kinking bands can be observed on a smaller scale, and they are the result of the fibre micro-buckling, matrix shear failure or fiber failure.
- **Fibre tensile failure:** this failure mode is explosive. It releases large amounts of energy. In structures that cannot redistribute the load, it typically causes catastrophic failure.

Moreover, in composite structures that can accumulate damage before structural collapse, the use of failure criteria is not sufficient to predict ultimate failure. Simplified models, such as the ply discount method, can be used to predict ultimate

failure, but they cannot represent with satisfactory accuracy the quasibrittle failure of laminates that results from the accumulation of several failure mechanisms.

The study of the non-linear response of quasibrittle materials due to the accumulation of damage is important because the rate and direction of damage propagation defines the damage tolerance of a structure and its eventual collapse. Several theories have been proposed for predicting both the initial and the progressive failure of composites. Although significant progress has been made in this area, there is currently no single theory that accurately predicts failure at all levels of analysis, for all loading conditions, and for all types of fiber reinforced polymer (FRP) laminates. In fact, the mechanisms that lead to failure in composite materials have not been fully understood yet. This is especially true for compression failure, both for the matrix and fibre dominated failure modes. For instance, a physical model for matrix compression failure should predict that failure occurs when some stress state is achieved, as well as what kind of orientation should have the fracture plane and how much energy the crack formation should dissipate.

In general, the greatest difficulty in the development of an accurate and computationally efficient numerical procedure to predict damage growth concerns with the way in which should be analyzed the material micro-structural changes and how those changes to the material response should be related to. While some failure theories have a physical basis, most theories represent attempts to provide mathematical expressions that give a best fit of the available experimental data in a form that is practical from a designer's point of view.

The World Wide Failure Exercises (WWFEs), that were conceived and conducted by Soden and co-workers and Puck and Schuermann, provided an exhaustive assessment of the theoretical methods for predicting material initial failure in Fiber Reinforced Polymer composites (FRP). It underlined that, even when analyzing simple laminates that have been extensively studied and tested, the predictions of most theories different significantly from the experimental observations. During the first edition of WWFE (1996) the Puck failure criterion was indicated as one of the most effective, the predicted failure envelopes being in good correlation with the test results. After WWFE, NASA Langley Research Center revisited existing failure theories in order to identify the most accurate models and, when it was possible, to introduce some enhancements. The results of this activities is a series of criteria named LaRC, today the LaRC05 criterion was defined by extending the approach to three-dimensional stress states.

In the second chapter of this work the reader can find a critical review of the state of the art in composite failure theories, together with a consistent number of references on this subject. Beside the growth of knowledge, the development of new and less approximate failure theories allow to project structural component with minor margins. Industries can reduce costs of production. This is why:

- Less amount of material would be used,
- Minors needed weights in flight
- More detailed expectation of failure and its prevention

However, in modern software CAE classical failure theory have just been often implemented. Furthermore, the companies are skeptical about improving and using new theories. For these reasons during my activity of six months in Thales Alenia Space an API for FEMAP software was implemented in the framework of the

activity, where both classical (Hoffman) and more recent (LaRC05) failure theories to evaluate failure index were implemented.

The description of the API and its validation are the subjects of chapter 3 and 4. Then a briefly comparison of results is reported in chapter 5. Finally, the chapter 6 presents the results obtained using the API on a previous real case.

## Chapter 2 - Overview of most popular failure criteria

In the next section, is given an overview and the analytic definition of most popular two-dimensional failure criteria for anisotropic materials, including the LaRC03, 04 and 05 criteria. Many different failure criteria have been formulated in order to predict failure loads for general stress states. In this text is proposed the following classification, in which they could be grouped in two main groups firstly:

1. *Failure criteria neglecting interactions between different stress components.*
2. *Failure criteria considering interactions between different stress components.*

Criteria belonging to the first group are the simplest ones and they usually propose one inequality for each one of the three in-plane stresses (or strain) components.

In the remaining criteria, the failure in one direction may be sensitive to loads along other directions (including shear).

This last group can be divided into the following two subgroups.

- a. *Criteria proposing one single inequality to define the failure envelope.*
- b. *Criteria proposing a combination of interactive and non-interactive conditions.*

The Hoffman, Tsai–Wu, Liu–Tsai and Tsai–Hill are quadratic criteria and they belong to the first group, while the Hashin and Rotem, Hashin, Puck and Schuermann and LaRC criteria pertain to the second one.

In general, one more Failure Indexes (FI) corresponds to each failure criteria. A FI exceeding the unitary value means that failure occurs, according to the applied criterion.

Some useful definitions are reported to a better understanding of the following concepts:

- **Failure indices:** represent a phenomenological failure criterion in that only an occurrence of a failure is indicated and not the mode of failure.
- **Strength ratio:** is a more direct indicator of failure than the failure index since it demonstrates the percentage of applied load to the failure criteria. Strength ratio is defined as:  $\text{Strength Ratio (SR)} = \text{Allowable Stress} / \text{Calculated Stress}$

For example, a  $\text{SR} = 0.75$  not only indicates that a failure has occurred, but also indicates that the applied load is 25% beyond the allowable. A  $\text{FI} = 1.25$  on the other hand does not represent a percentage of failure; just that a failure condition exists [20].

## 2.1- Maximum stress and maximum strain criteria

The maximum stress and maximum strain criteria<sup>1</sup> belong to the first group, so it does not considers any interaction between different stress components. Considering one Cartesian material reference frame, in which direction 1 is the same of the fibres, the failure occurs if at least one of the following conditions are satisfied:

- $\sigma_{11} \geq X^T$  or  $\sigma_{11} \leq -X^C$ ,
  - $\sigma_{22} \geq Y^T$  or  $\sigma_{22} \leq -Y^C$ ,
  - $\tau_{12} \geq S^L$ .
- (2.1 – 1)

Where  $\sigma_{11}$  and  $\sigma_{22}$  are the in-plane normal stress components,  $\tau_{12}$  is the in-plane shear stress component. While  $X^T$  and  $X^C$  are respectively the material strength in the fibre direction under tension and compression (longitudinal tensile and compressive strengths),  $Y^T$  and  $Y^C$  are respectively the material strength normal to the fibre direction under tension and compression (transverse tensile and compressive

strengths) and  $S^L$  is the longitudinal shear strength.

The failure index is evaluated as:

$$FI = \text{MAX} \left[ \frac{\sigma_{11}}{X}, \frac{\sigma_{22}}{Y}, \frac{\tau_{12}}{S} \right] \quad (2.1 - 2)$$

with  $X = X^T$  or  $X = X^C$  if  $\sigma_{11} \geq 0$  or  $\sigma_{11} < 0$ , the same for transverse tensile.

The maximum strain criterion is obtained following the same approach of the maximum stress criterion, but taking into account corresponding strains in the conditions for failure.

After that FI is obtained, it is possible to define the corresponding failure load,  $L_F$ , as:

$$L_F = k * L, \quad (2.1 - 3)$$

where L is the acting load and  $k = 1/FI$ .

---

<sup>1</sup> Ref.1

## 2.2 - Tsai-Hill criterion

The Tsai-Hill criterion was formulated by referring to distortional energy and is thus an interactive criterion that takes into account the effect of the in-plane shear stress<sup>[6,7]</sup>.

The condition for failure is given by the following inequality

$$\left(\frac{\sigma_{11}}{X}\right)^2 - \frac{\sigma_{11}\sigma_{22}}{X^2} + \left(\frac{\sigma_{22}}{Y}\right)^2 + \left(\frac{\tau_{12}}{S^L}\right)^2 \geq 1 \quad (2.2 - 1)$$

where the failure parameters X and Y depends on the considered quadrant of the coordinate plane, being  $X = X^T$  or  $X = X^C$  if  $\sigma_{11} \geq 0$  or  $\sigma_{11} < 0$ , the same for Y.

Corresponding failure load is given by formula 2.1-1, but in this case  $k = 1/\sqrt{FI}$ .

## 2.3 - Tsai-Wu criterion

The Tsai-Wu criterion was not derived from a physical basis, but it was formulated in order to fit experimental results<sup>[8,9]</sup>. It is an interactive approach considering in-plane shear stress effects.

The failure condition is expressed by the following inequality:

$$A_{11}\sigma_{11}^2 + 2A_{12}\sigma_{11}\sigma_{22} + A_{22}\sigma_{22}^2 + A_{66}\tau_{12}^2 + B_1\sigma_{11} + B_2\sigma_{22} \geq 1 \quad (2.3 - 1)$$

where the first term of inequality is the Tsai-Wu's failure index and other terms are Tsai-WU parameters, whose expressions are given in *Tab. 1*.

Tsai-Wu parameters	
$A_{11}$	$\frac{1}{X^T X^C}$
$A_{22}$	$-\frac{1}{2\sqrt{X^T X^C Y^T Y^C}}$
$A_{12}$	$\frac{1}{Y^T Y^C}$
$A_{66}$	$\frac{1}{S^T S^C}$
$B_1$	$\frac{1}{X^T} - \frac{1}{X^C}$
$B_2$	$\frac{1}{Y^T} - \frac{1}{Y^C}$

Table 1 - Tsai-WU parameters

The  $A_{12}$  coefficient is often obtained/corrected by biaxial tests of laminae.

The failure load corresponding to the Tsai–Wu criterion is:

$$L_F = k * L,$$

where L is the acting load and k is obtained by:

$$k = \text{MIN} \left( \frac{2}{\pm B_1 \sigma_{11} \pm B_2 \sigma_{22} \sqrt{(4A_{11} + B_1^2) \sigma_{11}^2 + 2(4A_{12} + B_1 B_2) \sigma_{11} \sigma_{22} + (4A_{22} + B_2^2) \sigma_{22}^2 + 4A_{66} \tau_{12}^2}} \right) \quad (2.3 - 2)$$

## 2.4– Hoffman criteria

The following formulas were extracted by NX Nastran User’s Guide<sup>2</sup> and they were implemented in the API.

The resulting failure index in Hoffman’s theory for an orthotropic lamina in a general state of plane stress (2D) with unequal tensile and compressive strengths is given by

$$FI_{Hoffaman2D} = \left( \frac{1}{X_t} - \frac{1}{X_c} \right) \sigma_1 + \left( \frac{1}{Y_t} - \frac{1}{Y_c} \right) \sigma_2 + \frac{\sigma_1^2}{X_t X_c} + \frac{\sigma_2^2}{Y_t Y_c} + \frac{\sigma_{12}^2}{S^2} - \frac{\sigma_1 \sigma_2}{X_t X_c}, \quad (2.5 - 1)$$

Note that this theory takes into account the difference in tensile and compressive allowable stresses by using linear terms in the equation.

To calculate the strength ratio and then the margin of safety, the following terms are defined:

Hoffman’s failure index (2D) coefficients	
$F_1 = \frac{1}{X_t} - \frac{1}{X_c}$	$F_{22} = \frac{1}{Y_t Y_c}$
$F_2 = \frac{1}{Y_t} - \frac{1}{Y_c}$	$F_{66} = \frac{1}{S^2}$
$F_{11} = \frac{1}{X_t X_c}$	

Table 2 - Hoffman’s failure index (2D) coefficients

Substituting above terms into Hoffman FI equation and setting FI = 1, the following expression for SR has been obtained:

<sup>2</sup> Ref. 20

$$SR = \frac{-b + \sqrt{b^2 - 4ac}}{2a}, \quad (2.5 - 2)$$

where:

$$\begin{aligned} a &= F_{11}\sigma_1^2 + F_{22}\sigma_2^2 + F_{66}\sigma_{12}^2 - F_{11}\sigma_1\sigma_2 \\ b &= F_1\sigma_1 + F_2\sigma_2, \\ c &= -1. \end{aligned}$$

(2.5 - 3)

In case of composites modelled using solid elements, so for a 3D mesh and stress state, the relation of failure index becomes:

$$\begin{aligned} FI_{Hoff3D} &= C_1(\sigma_2 - \sigma_3)^2 + C_2(\sigma_3 - \sigma_1)^2 + C_3(\sigma_1 - \sigma_2)^2 + C_4\sigma_1 + C_5\sigma_2 + C_6\sigma_3 \\ &\quad + C_7\tau_{23}^2 + C_8\tau_{13}^2 + C_9\tau_{12}^2, \end{aligned} \quad (2.5 - 4)$$

and the new coefficients are resumed in *Tab.3*

Hoffman's failure index (3D) coefficients	
$C_1 = \frac{1}{2} \left( \frac{1}{Z_t Z_c} + \frac{1}{Y_t Y_c} - \frac{1}{X_t X_c} \right)$	$C_6 = \left( \frac{1}{Z_t} - \frac{1}{Z_c} \right)$
$C_2 = \frac{1}{2} \left( \frac{1}{X_t X_c} + \frac{1}{Z_t Z_c} - \frac{1}{Y_t Y_c} \right)$	$C_7 = \frac{1}{S_{23}^2}$
$C_3 = \frac{1}{2} \left( \frac{1}{X_t X_c} + \frac{1}{Y_t Y_c} - \frac{1}{Z_t Z_c} \right)$	$C_8 = \frac{1}{S_{13}^2}$
$C_4 = \left( \frac{1}{X_t} - \frac{1}{X_c} \right)$	$C_9 = \frac{1}{S_{12}^2}$
$C_5 = \left( \frac{1}{Y_t} - \frac{1}{Y_c} \right)$	

Table 3 - Hoffman's failure index (3D) coefficients

In each case, the following material data are required:

- $X_t, X_c$  are the maximum allowable stresses in the 1-direction in tension and compression;
- $Y_t, Y_c$  are the maximum allowable stresses in the 2-direction in tension and compression;
- $Z_t, Z_c$  are the maximum allowable stresses in the 3-direction in tension and compression;
- $S_{12}$  is the maximum allowable in-plane shear stress;
- $S_{23}$  is the maximum allowable 23 shear stress;
- $S_{13}$  is the maximum allowable 13 shear stress.

## 2.5 – Hashin criterion

In Hashin and Rotem's works<sup>3</sup>, for the first time the failure of laminated composites has been attributed to different physical phenomena: fiber-dominated and matrix-dominated failure modes. The Hashin criterion proposes a combination of four interactive and non-interactive conditions in order to distinguish between matrix or fibre failure caused by tension or compression. Firstly they were defined in *Ref.10* and subsequently they were revised in *Ref.11*. A further version of this criterion was proposed by Sun et al, according to some empirical modifications. The Hashin criterion is an interactive one, the conditions for failure being given by the following inequalities.

- a) Matrix Failure for compression ( $\sigma_{22} \geq 0$ )

$$\left(\frac{\sigma_{22}}{Y^T}\right)^2 + \left(\frac{\tau_{12}}{S^L}\right)^2 \geq 1 \quad (2.4 - 1)$$

- b) Matrix failure for tension ( $\sigma_{22} < 0$ )

$$\left(\frac{\sigma_{22}}{2S^T}\right)^2 + \frac{\left[\left(\frac{Y^C}{2S^T}\right)^2 - 1\right]\sigma_{22}}{Y^C} + \left(\frac{\tau_{12}}{S^L}\right)^2 \geq 1 \quad (2.4 - 2)$$

- c) Fibre failure for tension ( $\sigma_{11} \geq 0$ )

$$\left(\frac{\sigma_{11}}{X^T}\right)^2 + \left(\frac{\tau_{12}}{S^L}\right)^2 \geq 1 \quad (2.4 - 3)$$

- d) Fibre failure for compression ( $\sigma_{11} < 0$ )

$$-\frac{\sigma_{11}}{X^C} \geq 1 \quad (2.4 - 4)$$

In formula *b*) the term  $S^T$  is the transverse shear strengths which is very difficult to measure experimentally. An analytic relation is suggested:

$$S^T = Y^C \cos(\alpha) \left( \sin(\alpha) + \frac{\cos(\alpha)}{\tan(2\alpha)} \right), \quad (2.4 - 5)$$

where  $\alpha$  is the angle of fracture plane, which was also adopted in LaRC criteria.

---

<sup>3</sup> Ref. 10 and Ref.11

Hashin's failure index is given by the highest value among the expressions before. The failure load corresponding to the Hashin's criterion is given by:

$$L_F = kL \quad (2.4 - 6)$$

where, in the case of linear analysis, k can be found by scaling the results computed with load L by a varying factor  $k_{try}$ . After a number of iterations, if  $FI \approx 1$  then  $k = k_{try}$ .

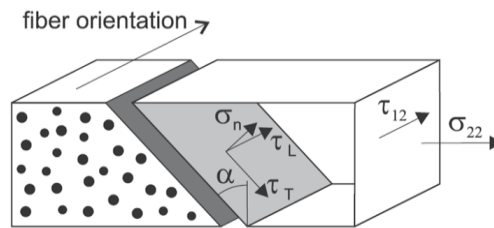


Figure 1 - Angle of fracture plane of an unidirectional lamina subjected to transverse compression and in-plane shear

## 2.6- LaRC criteria

In the first paragraph of this section origins of LaRC criteria will be briefly described, then a more detailed treatment of them will follow in the others paragraphs. Since LaRC criteria have been reviewed many times until today, only LaRC03, LaRC04 and LaRC05 have been reported to streamline the reading.

### 2.6.1 - The basic knowledge of LaRC: Puck's failure criteria

Puck provided an exhaustive assessment of the theoretical methods for predicting material initial failure in Fiber Reinforced Polymer composites. In fact, he was the first author who supported the idea of distinguishing and treating separately failure criteria the fibre failure (FF) and interfibre failure (IFF).

For a physically based theoretical treatment of the successive failure process in laminates, the Puck theory supplies at least four essential topics:

1. Non-linear stress and strain analysis before IFF,
2. Physically-based action plane related fracture criteria for IFF and FF,
3. A continuous degradation after the onset of IFF,
4. Considerations on total failure of a laminate.

Puck made a new attempt based on Hashin's concept using fundamental elements of the failure criterion by Mohr and Coulomb. Applying this model, the three-dimensional state of stress is evaluated in a realistic manner. It is assumed that besides the occurrence of fibre failure only tensile stresses and shear stresses in loading planes tangential to the fibre direction induce the inter-fibre failure of the unidirectionally reinforced composite, whereas compressive stresses in these planes obstruct failure. Moreover, by experimental observations he argued that for FRP materials, which are intrinsically brittle, have not sense to evaluate failure

using criteria similar to the well-known “Von Mises yield criterion” for ductile metals. Therefore, Puck tackles the task of modifying the ideas of Coulomb and Mohr for the application on UD-composites.

The fracture hypothesis adapted to a UD-composite element are the follows:

- "The stresses on the fracture plane are decisive for fracture". Though this is not a problem idea, it is not as easy to handle, because the location of the fracture plane is difficult to evaluate a priori.
- “The normal stress  $\sigma_n$  and the shear stress  $\tau_{nt}$  and  $\tau_{n1}$  on the fracture plane are decisive for IFF. A tensile stress  $\sigma_n$  supports the fracture, while in contrast a compressive stress ‘makes the material stronger’”.

In order to characterize certain types of stress Puck introduces the concept of ‘stressing’. Consider for instance a  $\sigma_{\perp}$ -stressing, it is quite unimportant whether we are dealing with a stress  $\sigma_2$  or  $\sigma_3$  stress or with a stress  $\sigma_n$  as shown in *Fig.2*; the decisive feature is that it is acting transverse ( $\perp$ ) to the fibre direction <sup>[12]</sup>.

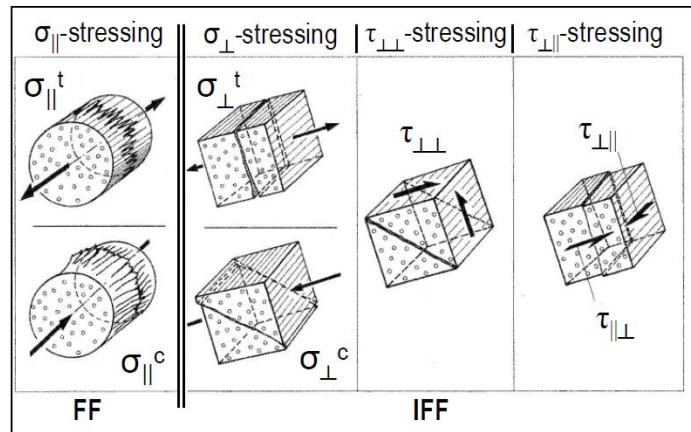


Figure 2 - The basic stressings (stressing means type of stress) of a UD-composite  $\sigma_{||}$  stressing is responsible for fibre failure (FF), while  $\sigma_{\perp}$ ,  $\tau_{\perp\perp}$ ,  $\tau_{\perp||}$  stressings cause interfibre failure (IFF). Also shown are the planes in which brittle fracture occurs ( $\tau_{\perp||}$  can not produce a fracture of its action plane, because fibres would have to be sheared off. Fracture occurs much easier on the parallel to fibre action plane in which  $\tau_{\perp||}$  with the same magnitude as  $\tau_{\perp\perp}$  is acting).

### 2.6.1.1 – Failure conditions for fibre failure (FF)

In this paragraph, will be reported results obtained by Puck studying fibre failure. For a more detailed treatment see *Ref.13*.

Puck assumed that fibre failure in a UD composite under a combined state of stress ( $\sigma_1, \sigma_2, \sigma_3, \tau_{23}, \tau_{31}, \tau_{21}$ ) will occur at the same fibre stress as that which is acting in the fibres at failure under uniaxial stress  $\sigma_1$ . Starting from this failure hypothesis he began with a failure condition for fibre instead of for the unidirectional composite:

$$\begin{aligned} \sigma_{f1} &= X_{fT} \quad \text{for } \sigma_{f1} \geq 0 \\ \sigma_{f1} &= -X_{fC} \quad \text{for } \sigma_{f1} < 0 \end{aligned} \quad (2.6.1 - 1)$$

where

- $X_{fT}, X_{fC}$  are tensile fibre strength and compressive fibre strength in fibre direction (in a UD composite),
- $\sigma_{f1}$  is the fibre stress in  $x_1$  direction.

In case of linear-elastic material behaviour it is possible to evaluate the strengths like:

$$X_{fT} = \frac{X_T}{E_1} E_{f1} = \epsilon_{1T} E_{f1} \quad \text{and} \quad X_{fC} = \frac{X_C}{E_1} E_{f1} = \epsilon_{1C} E_{f1} \quad (2.6.1 - 2)$$

where

- $\epsilon_{1T}$  and  $\epsilon_{1C}$  are tensile failure strain and compression failure strain of a unidirectional layer in  $x_1$  direction,
- $E_1$  is the elastic modulus of a unidirectional layer in the  $x_1$  direction,
- $E_{f1}$  is the fibre modulus in  $x_1$  direction,
- $X_T$  and  $X_C$  are tensile strength and compressive strength of the unidirectional layer parallel to the fibre direction.

Already at a state of stress where  $\sigma_1 = 0$ , but  $\sigma_2 \neq 0$ , stresses of opposite sign occur in fibres and matrix in a direction parallel to the fibres because of their different elastic moduli and Poisson's ratios (for  $\sigma_2 > 0$  it is  $\sigma_{f1} < 0$  and for  $\sigma_2 < 0$  it is  $\sigma_{f1} > 0$ ) [13]

Puck was able to write the following failure conditions for fibre failure under combined ( $\sigma_{f1}, \sigma_{f2}$ <sup>4</sup>) loading taking into account the above hypothesis.

Tensile fibre failure criterion

$$\frac{1}{\epsilon_{1T}} \left( \epsilon_1 + \frac{\nu_{f12}}{E_{f1}} m_{\sigma f} \sigma_2 \right) = 1 \quad \text{for } (...) \geq 1 \quad (\text{PUCK} - 1)$$

Compressive "fibre kinking" failure criterion

$$\frac{1}{\epsilon_{1C}} \left( \epsilon_1 + \frac{\nu_{f12}}{E_{f1}} m_{\sigma f} \sigma_2 \right) = -1 \quad \text{for } (...) < 1 \quad (2.6.1 - 3)$$

with  $\epsilon_{1C}$  expresses as appositive value.

Indeed, Eq. 2.6.1 -3 was modified using an empirical shear correction. In this way, Puck correlated it with experimental experience. Its last expression is:

---

<sup>4</sup>  $\sigma_{f2}$  is the fibre stress in  $x_2$  direction.



$$\begin{cases} \sigma_1 = \sigma_1 \\ \sigma_n = \sigma_2 * \cos^2 \theta \\ \tau_{nt} = -\sigma_2 \sin \theta \cos \theta \\ \tau_{n1} = \tau_{21} \cos \theta \end{cases} \quad (2.6.1 - 4)$$

where  $\theta$  is the angle between the  $x_2$  axis and the  $x_n$  axis, as it is shown in Fig.5.

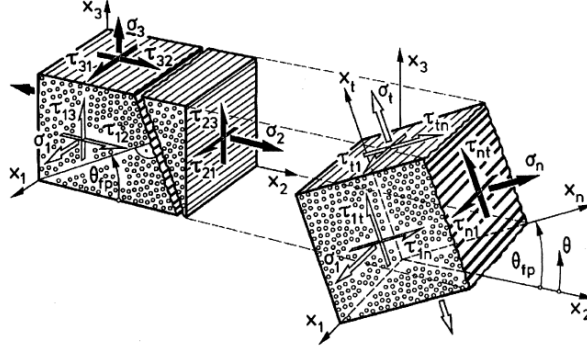


Figure 5 - Three-dimensional stresses on a UD composite element.  $(x_1, x_2, x_3)$  coordinate system is fixed to fibre direction  $(x_1)$ , laminate mid-surface  $(x_2)$  and thickness direction  $(x_3)$ . The  $(x_1, x_n, x_t)$  coordinate system is rotated by an angle  $\theta_{fp}$  from the  $x_2$  direction to the  $x_n$  direction which is normal to the fracture plane. The inter-fibre fracture is influenced by the three stresses  $\sigma_1, \tau_{nt}, \tau_{n1}$  only (according to Mohr's strength theory).

To achieve a better agreement with experimental results Puck modified introducing different assumptions the basic fracture conditions, which he found. To see all the passages the reader can examine Ref.13, in facet in this document will be only described the final form of the criteria and the basic terms to obtain them.

#### Mode A

Mode A corresponds to a fracture angle  $\theta_{fp} = 0^\circ$ . This criterion is invoked if transverse stress in the composite is greater than 0 (thus indicating a transverse crack perpendicular to the transverse loading).

So criterion worked out by Puck is expression PUCK-3:

$$\sqrt{\left(\frac{\tau_{21}}{S_{21}}\right)^2 + \left(1 - p_{\perp\parallel}^{(+)} \frac{Y_T}{S_{21}}\right)^2 \left(\frac{\sigma_2}{Y_T}\right)^2} + p_{\perp\parallel}^{(+)} \frac{\sigma_2}{S_{21}} = 1 - \left|\frac{\sigma_1}{\sigma_{1D}}\right| \quad (PUCK - 3)$$

This is available if  $\sigma_2 \geq 0$ .

#### Mode B

Mode B corresponds to a transverse compressive stress (inhibiting crack formation) with a longitudinal shear stress, which is below a fracture resistance (coupled with empirical constants). Also in this case the angle  $\theta_{fp} = 0^\circ$ .

$$\frac{1}{S_{21}} \left( \sqrt{\tau_{21}^2 + (p_{\perp\parallel}^{(-)} \sigma_2)^2} + p_{\perp\parallel}^{(-)} \sigma_2 \right) = 1 - \left| \frac{\sigma_1}{\sigma_{1D}} \right| \quad (PUCK - 4)$$

The above criterion is valid if  $\sigma_2 < 0$  and  $0 \leq \left| \frac{\sigma_2}{\tau_{21}} \right| \leq \frac{R_{\perp\perp}^A}{|\tau_{21c}|}$ .

Mode C

Mode C, which is a general case, corresponds to a transverse compressive stress (inhibiting crack formation) with a longitudinal shear stress, which is significantly large enough to cause a fracture on an inclined plane to fibre axis.

$$\left[ \left( \frac{\tau_{21}}{2(1 + p_{\perp\perp}^{(-)} S_{21})} \right)^2 + \left( \frac{\sigma_2}{Y_C} \right)^2 \right] \frac{Y_C}{(-\sigma_2)} = 1 - \left| \frac{\sigma_1}{\sigma_{1D}} \right| \quad (PUCK - 5)$$

The angle of fracture plane is obtained from the following relationship:

$$\cos \theta_{fp} = \sqrt{\frac{f_w R_{\perp\perp}^A}{(-\sigma_2)}} \quad (2.6.1 - 5)$$

The criterion for mode C is valid if  $\sigma_2 < 0$  and  $0 \leq \left| \frac{\tau_{21}}{\sigma_2} \right| \leq \frac{|\tau_{21c}|}{R_{\perp\perp}^A}$ .

A final observation to do is that in all criteria above was taken into account the phenomena of degradation of fracture resistances due to single fibre failure. In fact, single fibre breaks cause local damage in the vicinity of the breaks in the form of debonding of fibre and matrix and microcracks in the matrix. By this damage the fracture resistances  $R^A$  the composites offers to inter-fibre fracture are decreased. This is taken into account by equally decreasing all fracture resistances with a weakening factor  $f_w$ . In mathematical equations, the term  $\left| \frac{\sigma_1}{\sigma_{1D}} \right|$  was added.

Description of coefficients and terms used in the inter-fibre failure criteria

In accordance with the six stressings shown in *Fig.2*, also six corresponding strengths exist and they are designated as follows:

$$R_{\parallel}^t, R_{\parallel}^c, R_{\perp}^t, R_{\perp}^c, R_{\perp\perp}, R_{\perp\parallel}$$

It is important to note that the widely used term ‘strength’ means the experimentally determined ultimate load divided by the cross section of the plane, which is oriented perpendicularly to the applied stress. This is valid for a tensile or compressive load. If a shear strength has to be determined the shear load at failure is divided by the area of the plane in which the shear load was acting. However, in case of brittle fracture behaviour of the material this plane is in most cases not

identical with the fracture plane <sup>[12]</sup>. The fracture planes which appear when a UD-composite is loaded by a given stressing until fracture is reached, are also shown in Fig.2.

Puck's observations lead to the following conclusion: uniaxial transverse compressive stressing  $\sigma_{\perp}^c$  causes fracture in a plane which does not coincide with its action plane (so the fracture is produced mainly by shear). Also, pure  $\tau_{\perp\perp}$  causes fracture in a plane which does not have the same direction as own action plane (usually it has an angle of 45°). Only the tensile  $\sigma_{\perp}^t$ -stressing and the  $\tau_{\perp\parallel}$ -stressing produce a fracture in their action planes, i.e. their action plane is also a fracture plane.

For this reason, were defined new resistances, which has been evaluated respect the action plane:

- $R_{\perp}^{(+A)}$  – Fracture resistance of the action plane against its fracture due to transverse tensile stressing,
- $R_{\perp\perp}^A$  – Fracture resistance of the action plane against its fracture due to transverse/transverse shear stressing,
- $R_{\perp\parallel}^A$  - Fracture resistance of the stress action plane against its fracture due to transverse/parallel shear stressing.

In general, these were defined as: “The fracture resistance of an action plane is the maximum resistance, with which the action plane can resist its own fracture caused by a uniaxial  $\sigma_{\perp}^t$ -stressing or a pure  $\tau_{\perp\perp}$  or  $\tau_{\perp\parallel}$ -stressign respectively” <sup>[12]</sup>.

Other terms in above equations are:

- $p_{\perp\parallel}^{(-)}$  - it is the slope of the  $(\sigma_n, \tau_{n1})$  fracture envelope for  $\sigma_n \leq 0$  at  $\sigma_n = 0$
- $p_{\perp\perp}^{(-)}$  - it is the slope of the  $(\sigma_n, \tau_{nt})$  fracture envelope for  $\sigma_n \leq 0$  at  $\sigma_n = 0$ ,
- $Y_T$  – it is the composite transverse tensile strength,
- $Y_C$  – it's the transverse compressive strength.

To work out the final form of each criterion Puck assumed that the following coupling exist:

$$\frac{p_{\perp\perp}^{(-)}}{R_{\perp\perp}^A} = \frac{p_{\perp\parallel}^{(-)}}{R_{\perp\parallel}^A} = \left(\frac{p}{r}\right) = const \quad (2.6.1 - 6)$$

### 2.6.2 - LaRC03

In this paragraph the physically-based criteria denoted LaRC03 is described, basing on Ref. [14]. LaRC03 criterion can be employed in order to predict accurately the failure of FRP laminated panels with in-plane stress states without requiring curve-fitting parameters. It is composed by set of a set of six failure criteria

This criterion is inspired by Puck's fundamental assumption of a fragile fracture for the matrix failure in compression and consequently implements the action plane

concept, according to the Mohr–Coulomb theory. Concerning tensile matrix cracking, LaRC03 is associated with Dvorak’s fracture mechanics approach, making use of the energy release rates associated with intralaminar crack propagation. A criterion for fibre kinking is obtained by calculating the fibre misalignment under load, and applying the matrix failure criterion in the coordinate frame of the misalignment. Fracture mechanics models of matrix cracks are used to develop a criterion for matrix in tension and to calculate the associated in-situ strengths.

### 2.6.2.1 - Matrix failure

In this section, a new set of criteria is proposed for matrix fracture that is based on the concepts proposed by Hashin and the fracture plane concept proposed by Puck.

The matrix can crack under tensile or compressive loads. In the first case the failure belongs to a fracture plane normal to the plane of the plies and parallel to the fibre direction.

#### 2.6.2.1.1 - Matrix failure under transverse compression ( $\sigma_{22} < 0$ )

In case of matrix compression, the plane of fracture should not be normal to the ply, but it may have an angle, named ‘angle of fracture plane’. Mohr-Coulomb effective stresses were used to evaluate this angle. The M-C criterion is represented geometrically by the diagram illustrated in *Fig.6*. The Mohr’s circle represents a state of uniaxial compression. The angle of the plane of fracture  $\alpha_0$  is set in this example at  $53^\circ$ , which is a typical fracture angle for composites under transverse compression loading. The line AB is the tangent to Mohr’s circle at A and it is called the *Coulomb fracture line*. The M-C criterion postulates that in a state of biaxial normal stress, fracture occurs for any Mohr’s circle that is tangent to the Coulomb fracture line. The effective stress  $\tau_{eff}$  is related to the stresses  $\tau^T$  and  $\sigma_n$  acting on the fracture plane by the expression  $\tau_{eff} = \tau^T + \eta\sigma_n$ .

In the literature,  $\tan^{-1}(\eta)$  is called the angle of internal friction and it is assumed to be a material constant. When  $\eta=0$ , the M-C criterion is equivalent to the Tresca condition<sup>5</sup>.

---

<sup>5</sup> DiLandro explains the role of internal friction on the strength of carbon-fibre composites by noting the absence of chemical bonds between fibre and matrix, and that adhesion is attributed to Van der Waal’s interactions. Larson examined the relative effects of interfacial friction and roughness on the length of interfacial sliding which proceeds from the tip of an impinging fracture oriented perpendicular to the interface<sup>[16]</sup>.

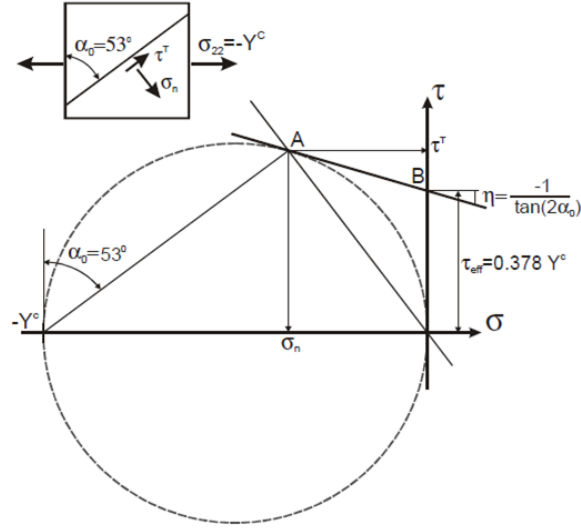


Figure 6 - Mohr's circle for uniaxial compression and the effective transverse shear

In general, the fracture plane can be subjected to transverse as well as in-plane stresses, in which case the effective stresses must be defined in both orthogonal directions as shown in equation below:

$$\begin{aligned}\tau_{eff}^T &= \langle |\tau^T| + \eta^T \sigma_n \rangle \\ \tau_{eff}^L &= \langle |\tau^L| + \eta^L \sigma_n \rangle\end{aligned}\tag{2.6.2 - 1}$$

where the terms  $\eta^T$  and  $\eta^L$  are referred to as coefficients of transverse and longitudinal influence, respectively, and the operand  $\langle x \rangle = x$  if  $x \geq 0$ ; otherwise  $x = 0$ .

Finally, the failure in matrix or this case load is expressed as a quadratic interaction between the effective shear stresses acting on the fracture plane. When stress states violate the below inequality of failure index, they are not physically admissible:

$$FI_{M_{comp}} = \left( \frac{\tau_{eff}^T}{S^T} \right)^2 + \left( \frac{\tau_{eff}^L}{S_{is}^L} \right)^2 \leq 1 \quad (LaRC03 - 1)$$

where  $S^T$  and  $S_{is}^L$  are the transverse and longitudinal shear strengths, respectively.

The subscript  $M$  indicates matrix failure. The subscript  $is$  indicating that for general laminates, the *in-situ* longitudinal shear strength rather than the strength of a unidirectional laminate should be used. Since the constraining effect of adjacent plies substantially increases the effective strength of a ply. It is assumed here that the transverse shear strength  $S^T$  is not subjected to in-situ effects.

The stress component acting on the fracture plane can be evaluate with below formulas in term of the in-plane stresses and the angle of fracture plane,  $\alpha$  (Fig 7):

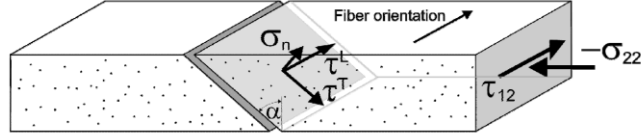


Figure 7 - Fracture of a unidirectional lamina subjected to transverse compression and in-plane shear

$$\begin{cases} \sigma_n = \cos^2(\alpha) \sigma_{22} \\ \tau^T = -\sin(\alpha) \cos(\alpha) \sigma_{22} \\ \tau^L = \tau_{12} \cos(\alpha) \end{cases} \quad (2.6.2 - 2)$$

Consequently, it is possible write effective stresses for an angle of fracture plane between  $0^\circ$  and  $90^\circ$  with the following formulas:

$$\begin{aligned} \tau_{eff}^T &= \langle -\sigma_{22} \cos(\alpha) (\sin(\alpha) - \eta^T \cos(\alpha)) \rangle \\ \tau_{eff}^L &= \langle \cos(\alpha) (|\tau_{12}| + \eta^L \cos(\alpha) \sigma_{22}) \rangle \end{aligned} \quad (2.6.2 - 3)$$

Calculation of coefficients  $\eta^T, \eta^L$  and strength  $S^T$

In this paragraph were reported just the expression of the different parameters of these formulas, for more details see *Ref. [14]*.

The coefficients  $\eta^T$  and  $\eta^L$  are obtained from the case of uniaxial transverse compression, so  $\sigma_{22} < 0$  and  $\tau_{12} = 0$ . In addition, at failure the in-plane compressive stress is equal to the matrix compressive strength,  $\sigma_{22} = -Y^C$ .

In these conditions:

1.

$$\eta^T = -\frac{1}{\tan(2\alpha_0)} \quad (2.6.2 - 4)$$

with usually  $\alpha_0 = 53^\circ \pm 2^\circ$  from Puck's study and so  $0.21 \leq \eta^T \leq 0.36$ .

For  $\alpha_0 = 45^\circ$  the coefficients would be equal to zero.

2. It is difficult to measure experimentally. Hence an expression relating the transverse shear strength to the transverse compressive strength was obtained:

$$S^T = Y^C \cos \alpha_0 \left( \sin \alpha_0 + \frac{\cos \alpha_0}{\tan(2\alpha_0)} \right) \quad (2.6.2 - 5)$$

then an angle  $\alpha_0 = 53^\circ$  gives  $S^T = 0.378 Y^C$ , however it is often approximated as  $S^T = 0.5 Y^C$  which implies  $\alpha_0 = 45^\circ$ .

3. The coefficient of longitudinal influence,  $\eta^L$ , can be determined from shear tests with varying degrees of transverse compression. In the absence of biaxial test data,  $\eta^L$  can be estimated from the longitudinal and transverse shear strengths, as proposed by Puck, so:

$$\eta^L = -\frac{S^L \cos 2\alpha_0}{Y^C \cos^2 \alpha_0} \quad (2.6.2 - 6)$$

this expression was proposed by Puck and it is useful in absence of biaxial test data.

#### Determination of the Angle of the Fracture Plane

The angle of the fracture plane for an unidirectional laminate loaded in transverse compression is a material property that is easily obtained from experimental data. However, under combined loads, the angle of the fracture plane is unknown. The correct angle of the fracture plane is the one that maximizes the failure index in *Eq. LaRC03-1*.

As it is shown in the *Fig. 8*, the fracture angle that maximizes the *FI* for small transverse stresses is  $\alpha = 0^\circ$ . When the applied transverse stress  $\sigma_{22}$  has a magnitude equal to approximately  $2/3$  of the transverse compressive strength,  $Y^C$ , the angle of the critical fracture plane switches from  $\alpha = 0^\circ$  to is  $\alpha = 40^\circ$ , and then rapidly increases to is  $\alpha = \alpha_0$ , the angle of fracture for uniaxial transverse compression [16].

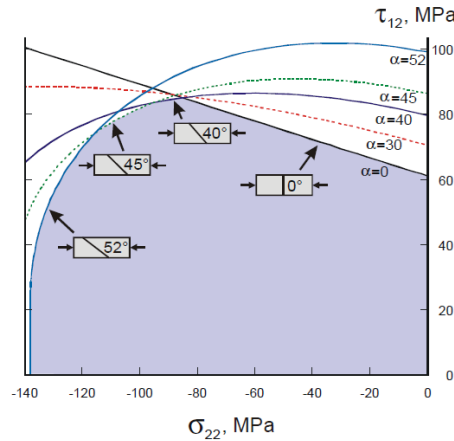


**Figure 8 - Matrix failure envelopes for a typical unidirectional E-glass/epoxy lamina subjected to in plane**

#### 2.6.2.1.2 - Matrix failure under Transverse Tension ( $\sigma_{22} > 0$ )

A failure criterion to predict matrix cracking under the presence of both in-plane shear and transverse tensile stresses should represent the “in-situ” effect occurring in laminated composites. The in-situ effect is characterized by higher transverse tensile and shear strengths of a ply when it is constrained by plies with different fibre orientations in a laminate, when compared with the strength of the same ply in

a unidirectional laminate. It also depends on the number of plies clustered together, and on the fibre orientation of the constraining plies.

The orientation of the constraining plies and the number of plies clustered together also affect the crack density and the stiffness reduction of the cracked ply. So, accurate in-situ strengths are necessary for any stress based failure criterion for matrix cracking in constrained plies, LaRC03 criterion adopted in-situ strengths calculated using fracture mechanics solutions for the propagation of cracks in a constrained ply. The reader can find a complete argumentation in *Ref. [14]*, only the main formulas and terms are only reported now.

The criterion expects the failure when the failure index, that can be expressed in terms of the ply stresses and in-situ strengths  $Y_{is}^T$  and  $S_{is}^L$ , is minor of the unit:

$$FI_{M_{tens}} = (1 - g) \frac{\sigma_{22}}{Y_{is}^T} + g \left( \frac{\sigma_{22}}{Y_{is}^T} \right)^2 + \left( \frac{\tau_{12}}{S_{is}^L} \right)^2 \leq 1 \quad (\text{LaRC03} - 2)$$

where

- $g = \text{material constant} = \frac{G_{Ic}}{G_{IIc}} = \frac{\Lambda_{22}^0}{\Lambda_{44}^0} \left( \frac{Y_{is}^T}{S_{is}^L} \right)^2$ <sup>6</sup>
- $G_{Ic}(T) = \frac{\pi a_0}{2} \Lambda_{22}^0 (Y_{is}^T)^2$ , fracture toughness for the T-direction of the mode I
- $G_{IIc}(T) = \frac{\pi a_0}{2} \Lambda_{44}^0 (S_{is}^L)^2$ , fracture toughness for the T-direction of the mode II
- $G_{Ic}(L) = \frac{\pi a_0}{4} \Lambda_{22}^0 (Y_{is}^T)^2$ , fracture toughness for the L-direction of the mode I
- $G_{IIc}(L) = \frac{\pi a_0}{4} \Lambda_{44}^0 (S_{is}^L)^2$ , fracture toughness for the L-direction of the mode II<sup>7</sup>
- $a_0 = \text{transverse slit size}$
- $\Lambda_{22}^0 = 2 \left( \frac{1}{E_2} - \frac{\nu_{21}^2}{E_1} \right)$
- $\Lambda_{44}^0 = \frac{1}{G_{12}}$

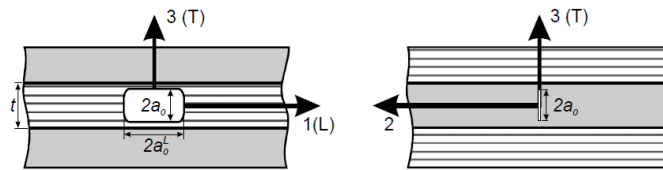


Figure 9 - Slit crack geometry

<sup>6</sup>If  $g=1$  it is possible reverts to the linear version of the criterion proposed by Wu and Reuter for the propagation of delamination in laminated composites. Furthermore eq. Larc03-2 reverts to Hashin criterion. The term  $g$  is defined identically from T-direction values or L-direction values.

<sup>7</sup>  $G_{Ic}$  and  $G_{IIc}$  are the components of the fracture toughness  $G$  pertaining to the two modes of energy release during the crack propagation. They can be measured from standard fracture tests, however Dvorak and Laws formulation for calculating is proposed.

Finally, the in-situ strengths can be calculated with different formulas basing on the geometry of the plies<sup>8</sup>, which are reported in *Tab. 4*:

Geometry	$Y_{is}^T$	$S_{is}^L$
Thin embedded plies	$\sqrt{\frac{8G_{Ic}(L)}{\pi t \Lambda_{22}^0}}$	$\sqrt{\frac{8G_{IIc}(L)}{\pi t \Lambda_{44}^0}}$
Thick embedded plies	$\sqrt{\frac{2G_{Ic}(T)}{\pi a_0 \Lambda_{22}^0}}$	$\sqrt{\frac{2G_{IIc}(T)}{\pi a_0 \Lambda_{44}^0}}$
Unidirectional Laminates	$1.12\sqrt{2}Y^T$	$\sqrt{2}S^L$

Table 4 - In-situ strengths LaRC03

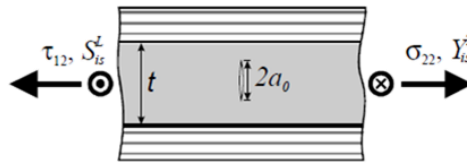


Figure 10 - Geometry of slit crack in a thick embedded ply subjected to tension and shear loads.

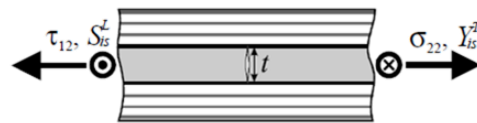


Figure 11 - Geometry of slit crack in a thin embedded ply.

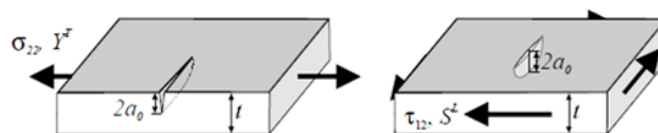


Figure 12 - Unidirectional specimens under transverse tension and shear.

## 2.6.2.2 - Fibre failure

### 2.6.2.2.1 - Fibre Tension Failure

The LaRC03 criterion for fibre tension failure is a non-interacting maximum allowable strain criterion that is simple to measure and is independent from fibre volume fraction and Young's moduli.

<sup>8</sup> Thick embedded ply: the length of the slit crack is much smaller than the ply thickness,  $2a_0 \ll t$

Thin embedded ply: having thickness smaller than the typical defect,  $t < 2a_0$

It is expressed by the follow inequality:

$$FI_{Ftens} = \frac{\varepsilon_{11}}{\varepsilon_1^T} \leq 1 \quad (\text{LaRC03} - 3)$$

#### 2.6.2.2.2 - Fibre Compression Failure

Compressive failure of aligned fibre composites occurs from the collapse of the fibres as a result of shear kinking and damage of the supporting matrix. Fibre kinking occurs as shear deformation leading to the formation of a kink band.

The first person who analysed kinking phenomenon was Argon, who assumed a local initial fibre misalignment. Starting from Argon's work the calculation of the critical kinking stress has been significantly improved incorporating friction and material nonlinearity in the models. Several authors have considered that misaligned fibres fail by the formation of a kink band when local matrix cracking occurs.

In the present approach, the compressive strength  $X^C$  is assumed to be a known material property that can be used in the LaRC03 matrix damage criterion to calculate the fibre misalignment angle that would cause matrix failure under uniaxial compression.

#### Calculation of Fibre Misalignment Angle

The imperfection in fiber alignment is idealized as a local region of waviness, as shown in *Fig. 13*. The ply stresses in the misalignment coordinate frame 'm' shown in *Fig. 13* are:

$$\begin{cases} \sigma_{11}^m = \cos^2 \varphi \sigma_{11} + \sin^2 \varphi \sigma_{22} + 2 \sin \varphi \cos \varphi \tau_{12} \\ \sigma_{22}^m = \sin^2 \varphi \sigma_{11} + \cos^2 \varphi \sigma_{22} - 2 \sin \varphi \cos \varphi \tau_{12} \\ \tau_{12}^m = -\sin \varphi \cos \varphi \sigma_{11} + \sin \varphi \cos \varphi \sigma_{22} + (\cos^2 \varphi - \sin^2 \varphi) \tau_{12} \end{cases} \quad (2.6.2 - 7)$$

So, to evaluate these new stresses is necessary to calculate the angle  $\varphi$ , which is the angle of rotation of material reference system from which is obtained the coordinate frame 'm'. with *Eq.(2.6.2-8)*:

$$\varphi = \varphi^0 + \varphi^R = \frac{|\tau_{12}| + (G_{12} - X^C)\varphi^C}{G_{12} + \sigma_{11} - \sigma_{22}} \quad (2.6.2 - 8)$$

with

- $\varphi^0 = \varphi^C \left(1 - \frac{X^C}{G_{12}}\right)$
- $\varphi^R = \frac{t_{12}^m}{G_{12}} = \frac{-\varphi\sigma_{11} + \varphi\sigma_{22} + |\tau_{12}|}{G_{12}}$ <sup>9</sup>
- $\varphi^C = \tan^{-1} \left( \frac{1 - \sqrt{1 - 4 \left(\frac{S_{is}^L}{X^C} + \eta^L\right) \left(\frac{S_{is}^L}{X^C}\right)}}{2 \left(\frac{S_{is}^L}{X^C} + \eta^L\right)} \right)$

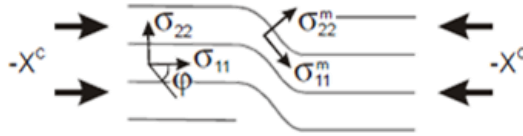


Figure 13 - Imperfection in fibre alignment idealized as local region of waviness.

#### Failure Index

Fibre compression failure by formation of a kink band was predicted by using the stresses from Eq(2.6.2-7) and the failure criterion for matrix tension or matrix compression. Hence, in the first case the criterion for fibre kinking becomes like this:

$$FI_{F_{compMtens}} = (1 - g) \left(\frac{\sigma_{22}^m}{Y_{is}^T}\right) + g \left(\frac{\sigma_{22}^m}{Y_{is}^T}\right)^2 + \left(\frac{\tau_{12}^m}{S_{is}^L}\right)^2 \leq 1 \quad (\text{LaRC03 - 4})$$

while for matrix compression is:

$$FI_{F_{compMcomp}} = \left\langle \frac{|\tau_{12}^m| + \eta^L \sigma_{22}^m}{S_{is}^L} \right\rangle \leq 1 \quad (\text{LaRC03 - 5})$$

#### 2.6.2.3 - Matrix Damage under Biaxial Compression

There is another possible failure of the matrix, in fact in the presence of high transverse compression combined with moderate fiber compression, matrix damage can occur without the formation of kink bands or damage to the fibers. This matrix damage mode was evaluated by using the stresses in the misaligned frame in the failure criterion in Eq.LaRC03-1, which gives:

<sup>9</sup> Using small angle approximations.

$$FI_M = \left( \frac{\tau_{eff}^{mT}}{S^T} \right)^2 + \left( \frac{\tau_{eff}^{mL}}{S_{is}^L} \right)^2 \leq 1 \quad (\text{LaRC03} - 6)$$

where the effective shear stress  $\tau_{eff}^{mT}$  and  $\tau_{eff}^{mL}$  are defined in terms of the in-plane stresses in the misalignment frame by following equations:

$$\begin{aligned} \tau_{eff}^{mT} &= \langle -\sigma_{22}^m \cos\alpha (\sin\alpha - \eta^T \cos\alpha) \rangle \\ \tau_{eff}^{mL} &= \langle \cos\alpha (|\tau_{12}^m| + \eta^L \sigma_{22}^m \cos\alpha) \rangle \end{aligned} \quad (2.6.2 - 9)$$

As for all matrix, compressive failures herein, the stresses  $\tau_{eff}^{mT}$  and  $\tau_{eff}^{mL}$  are functions of the fracture angle  $\alpha$ , which must be determined iteratively.

### 2.6.3 - LaRC04

In this paragraph will be described an extension of the LaRC03 plane stress criteria to account for general three-dimensional loading and for in-plane shear non-linearity.

It consists of six failure indexes expressions for laminated fiber-reinforced composites, denoted LaRC04<sup>10</sup>. As it has been already written the criteria are based on physical models for each failure mode and take into consideration non-linear matrix shear behavior. The model for matrix compressive failure is based on the Mohr-Coulomb criterion and it predicts the fracture angle. Fiber kinking is triggered by an initial fiber misalignment angle and by the rotation of the fibers during compressive loading. The plane of fiber kinking is predicted by the model. Predictions using LaRC04 correlated well with the experimental data, arguably better than most existing criteria. The good correlation seemed to be attributable to the physical soundness of the underlying failure models.

#### 2.6.3.1 - Matrix failure

##### 2.6.3.1.1 - Tensile Matrix failure

For this type of failure, the LaRC04 is different from LaRC03 because the components of the energy release rate for the crack geometry were determined by Dvorak and Laws for a linear orthotropic material. But, it was added an extension of their analysis for non-linear shear behaviour. So, three modes components are considered, but the mode II and III are combined in a shear mode,  $G_{SH} = G_{II} + G_{III}$ .

News corresponding components of the fracture toughness are associated to the components of the energy release rate, and they are given by:

---

<sup>10</sup> Ref. 15

- Transverse direction

$$G_{Ic}(T) = \frac{\pi a_0}{2} \Lambda_{22}^0 (Y_{is}^T)^2$$

$$G_{SHc}(T) = \frac{\pi a_0}{2} \chi(\gamma_{12|is}^u)$$

- Longitudinal direction

$$G_{Ic}(L) = \frac{\pi a_0}{4} \Lambda_{22}^0 (Y_{is}^T)^2$$

$$G_{SHc}(L) = \frac{\pi a_0}{4} \chi(\gamma_{12|is}^u)$$

(2.6.3 – 1)

where  $Y_{is}^T$  is the in-situ transverse tensile strength, and  $\gamma_{12|is}^u$  is the in/situ in-plane shear ultimate strain. These new expressions lead to the following expression for the material constant  $g$ :

$$g = \frac{\Lambda_{22}^0 (Y_{is}^T)^2}{\chi(\gamma_{12|is}^u)} \quad (2.6.3 - 2)$$

Finally, a failure index for matrix tension can be expressed in terms of the ply stresses and in-situ strengths and the following criterion is getting:

$$FI_{Mtens} = (1 - g) \frac{\sigma_{22}}{Y_{is}^T} + g \left( \frac{\sigma_{22}}{Y_{is}^T} \right)^2 + \frac{\Lambda_{23}^0 \tau_{23}^2 + \chi(\gamma_{12})}{\chi(\gamma_{12|is}^u)} = 1 \quad (\text{LaRC04} - 1)^{11}$$

The criterion presented in Eq. (LaRC04 -1) with linear and quadratic terms in  $\sigma_{22}$ , a quadratic term in  $\tau_{23}$  and a term on the in-plane shear internal energy,  $\chi(\gamma_{12})$  <sup>[14]</sup>.

As for LaRC03 criterion, there are different expressions for in-situ strengths for different geometries of the model:

---

<sup>11</sup> If  $g=1$  it is possible reverts to the linear version of the criterion proposed by Wu and Reuter for the propagation of delamination in laminated composites. Furthermore eq. Larc03-2 reverts to Hashin criterion. Furthermore, the non-linear term in Eq. (LaRC04-1) is also found to be similar to the strain-energy based criterion proposed by Sandhu, later used by Chang and Scott <sup>[17]</sup>.

Geometry	$Y_{is}^T$	$S_{is}^L$
Thin embedded plies	$\sqrt{\frac{8G_{Ic}(L)}{\pi t \Lambda_{22}^0}}$	$\sqrt{\frac{\sqrt{1 + \beta \frac{48G_{SHc}(L)}{\pi t} (G_{12})^2} - 1}{3\beta G_{12}}}$
Thick embedded plies <sup>13</sup>	$\sqrt{\frac{2G_{Ic}(T)}{\pi a_0 \Lambda_{22}^0}}$	$\sqrt{\frac{\sqrt{1 + \beta \left( \frac{12(S^L)^2}{G_{12}} + 18\beta(S^L)^4 \right) (G_{12})^2} - 1}{3\beta G_{12}}}$
Unidirectional Laminates	$Y^T$	$S^L$

Table 5 - In situ strengths LaRC04

In the absence of specific data, the toughness values  $G_{Ic}(L)$  and  $G_{SHc}(L)$  can be assumed to have the values measured by standard Fracture Mechanics tests, such as the DCB for mode I and the ENF test for mode II.

### 2.6.3.1.2 - Compressive Matrix failure

Matrix compression specimens fail by shear, which would suggest that the angle of the fracture surface with the through-the-thickness direction should be  $\alpha_0 = 45^\circ$  along the plane of the maximum shear stress. However, the experiments indicate that the angle of fracture under uniaxial compression is generally  $\alpha_0 = 53^\circ \pm 2^\circ$  for most technical composite materials. The fact that  $\alpha_0 > 45^\circ$  can be explained by the existence of a compressive stress acting on the potential fracture surfaces, and its associated friction. The magnitude of the compressive stress, and hence the friction stress, is maximum for a fracture surface with  $\alpha_0 = 0^\circ$  and decreases monotonically until  $\alpha_0 = 90^\circ$ , in which case the compressive (and friction) stress is zero. Although the shear stress is maximum for  $\alpha_0 = 45^\circ$ , the friction stress which opposes fracture, decreases with larger values of the angle  $\alpha_0$ . As a result, fracture is expected for values of  $\alpha_0$  larger than  $45^\circ$ , where a critical combination of shear and normal stress acts. <sup>[15]</sup>.

Like the criteria before experimental evidence on the fracture surface of specimens failing suggest that the Mohr-Coulomb criterion is applicable in this case. It is represented geometrically in Fig.6 and it postulates: “In a state of biaxial normal stress, fracture occurs for any Mohr’s circle that is tangent to the M-C fracture line”.

For a general loading situation shown in Fig. 14, the angle of the fracture plane with the through-the-thickness direction, denoted as  $\alpha$ , might assume a different value than the one for pure compression.

<sup>12</sup> For a linear shear law:  $S_{is}^L = \sqrt{\frac{8G_{12}G_{SHc}(L)}{\pi t}}$

<sup>13</sup> The in-situ strengths of thick embedded plies are independent of the ply thickness. In case of linear shear law, the expression become  $S_{is}^L = \sqrt{2} S^L$  and  $Y_{is}^T = 1.12\sqrt{2}Y^T$

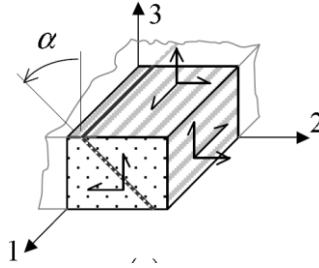


Figure 14 – Fracture plane for a 3D stress state

It depends on the particular combination of shear ( $\tau^T$  and  $\tau^L$ ) and normal ( $\sigma_n$ ) tractions for each value of  $\alpha$ . In plane-stress formulations they are obtained using transformation equations:

$$\begin{cases} \sigma_n = \frac{\sigma_{22}}{2} (1 + \cos(2\alpha)) \\ \tau^T = -\frac{\sigma_{22}}{2} \sin(2\alpha) \\ \tau^L = \tau_{12} \cos(\alpha) \end{cases} \quad (2.6.3 - 3)$$

While in a 3D formulation are given by:

$$\begin{cases} \sigma_n = \frac{\sigma_{22} + \sigma_{33}}{2} + \frac{\sigma_{22} - \sigma_{33}}{2} \cos(2\alpha) + \tau_{23} \sin(2\alpha) \\ \tau^T = -\frac{\sigma_{22} - \sigma_{33}}{2} \sin(2\alpha) + \tau_{23} \cos(2\alpha) \\ \tau^L = \tau_{12} \cos(\alpha) + \tau_{13} \sin(\alpha) \end{cases} \quad (2.6.3 - 4)$$

where  $\alpha \in ]-\pi, \pi[$ .

Then is possible to establish a relation between  $S^T$ ,  $Y^C$  and  $\alpha_0$  for a pure compression case:

$$S^T = Y^C \cos(\alpha_0) \left( \sin(\alpha_0) + \frac{\cos(\alpha_0)}{\tan(2\alpha_0)} \right) \quad (2.6.3 - 5)$$

where  $\alpha_0$  can be easily evaluated from compression test and  $S^T$  is the transverse (to the fibres) shear strength.

Moreover, form  $\alpha_0$  is possible to calculate the friction coefficient,  $\eta^T$ , by using the following relationship:

$$\tan(2\alpha_0) = -\frac{1}{\eta^T} \quad (2.6.3 - 6)$$

Motivated by the fact that the M-C criterion can be expressed by several forms, there were proposed different expressions of the failure index (Puck and Shürmann, LaRC02 or LaRC03), but finally it was demonstrated the LaRC03's expression overestimates the friction stresses, so that in LaRC04's theory has been proposed the following expression of the failure index:

$$FI_M = \left( \frac{\tau^T}{S^T - \eta^T \sigma_n} \right)^2 + \left( \frac{\tau^L}{S_{is}^L - \eta^L \sigma_n} \right)^2 \leq 1 \quad (LaRC04 - 2)$$

where:

$\eta_n^{T\sigma}$  and  $\eta_n^L \sigma_n$  are shear stresses due to friction.

To obtain  $\eta^L$  without experimental data it was suggested the relation:

$$\frac{\eta^L}{S^L} = \frac{\eta^T}{S^T} \quad (2.6.3 - 7)$$

### 2.6.3.2 - Fibre failure

#### 2.6.3.2.1 - Tensile fibre failure

The criterion adopted in LaRC04 for this type of failure is a non-interacting maximum allowable stress criterion, so the formula of failure index is simply:

$$FI_F = \frac{\sigma_{11}}{X^T} \leq 1 \quad (LaRC04 - 3)$$

#### 2.6.3.2.2 - Compressive fibre failure

While for matrix compression failure it is possible to represent correctly the failure with a relatively simple mechanical model, in this case, depending on the material, different failure modes are possible.

A briefly description of each follows:

- a) **Microbuckling**: This failure mode consists of the microbuckling of the fibres in the elastic matrix. Rosen was the first who proposed a first mechanical model for this failure mode (fibres like infinite beams in an elastic matrix and failure is attained when compressive load equals the buckling load). In this type of failure, the matrix shear properties and material imperfections play a relevant role.
- b) **Kinking**: It can be defined as the localized shear deformation of the matrix along a band. Sometimes it is considered as a consequence of microbuckling, while others authors consider it as a separate mode. The first author was Argon, for whom this failure is the result of matrix shear failure, prompted by an initial

fibre misalignment. So, the matrix elastic behaviour and initial material imperfections are very important.

- c) **Fibre failure:** It is a characteristic of fibre with low compressive strength, such as Aramid, but it is not predictable for carbon, glass or boron fibres.

For a state of the art review about microbuckling see *Ref.15*, now follows a more detailed description of the kinking failure mode.

#### 2.6.3.2.2.1 – Kinking Failure Mode

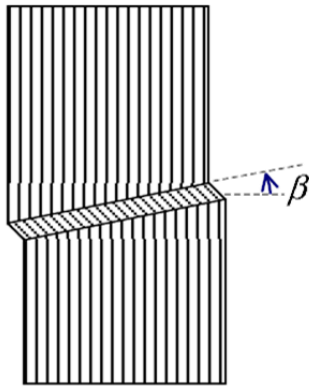


Figure 15 – Kinking band

Kinking failure is the most common failure mode observed after test in most high fibre-volume-fraction advanced composite materials. It is localized in a band in which the fibres have rotated by a large amount, and the matrix has undergone large shearing deformation [17]. A representation is shown in *Fig. 15*.

A lot of experimental tests have been carried to demonstrate that kinking failure is not a consequence of microbuckling. For example, if kinking is a result of it the one would expect the kink-band boundary to lie normal to the loading axis, so with an angle  $\beta = 0^\circ$ . However, in most cases  $\beta$  lie in the range of  $30^\circ$ . Other arguments were introduced by Chaplin, Effendi,

Schultheisz and Waas. A very important aspect for study kinking seems to be the presence of initial microstructural defects, such as fibre misalignment. A stream of researchers follows the hypothesis from Rosen according to which kink band failure is somehow the final result of the microbuckling of the fibres. On the other side, another stream follows Argon and argues that kink bands are triggered by localised matrix failure next to misaligned fibres. Argon was the first researcher to provide a model for kink-band formation. In his model was assumed an initial fibre misalignment, which leads to shearing stresses between the fibres. A first relation between the compressive failure stress  $X^C$ , the matrix in-plane shear failure stress,  $S^L$ , and the initial fibre misalignment angle  $\varphi^0$  results from his studies:

$$X^C = \frac{S^L}{\varphi^0} \quad (2.6.3 - 8)$$

This was later extended by Budiansky to:

$$X^C = \frac{S^L}{\varphi^0 + \gamma^u} \quad (2.6.3 - 9)$$

where  $\gamma^u$  is the shear strain at failure.

In the following paragraphs, will be presented main characteristics of the 2D and 3D models of this failure.

#### 2.6.3.2.2.1.1 – 2D Kinking Model

Consider an unidirectional composite with misaligned region that is compressed (Fig.16).

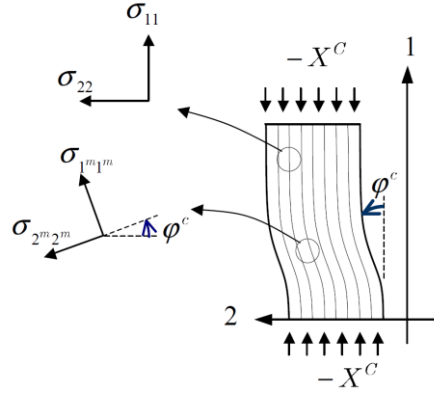


Figure 16 - Fibre misalignment frame

Stresses can be transformed into the misalignment frame using:

$$\begin{cases} \sigma_{1^m 1^m} = \frac{\sigma_{11} + \sigma_{22}}{2} + \frac{\sigma_{11} - \sigma_{22}}{2} \cos(2\varphi) + \tau_{12} \sin(2\varphi) \\ \sigma_{2^m 2^m} = \frac{\sigma_{11} + \sigma_{22}}{2} - \frac{\sigma_{11} - \sigma_{22}}{2} \cos(2\varphi) - \tau_{12} \sin(2\varphi) \\ \tau_{1^m 2^m} = -\frac{\sigma_{11} - \sigma_{22}}{2} \sin(2\varphi) + \tau_{12} \cos(2\varphi) \end{cases} \quad (2.6.3 - 10)$$

That becomes for failure under pure compression:

$$\begin{cases} \sigma_{1^m 1^m}^c = -X^C \cos^2(\varphi) \\ \sigma_{2^m 2^m}^c = X^C \sin^2(\varphi) \\ \tau_{1^m 2^m}^c = X^C \sin(\varphi) \cos(\varphi) \end{cases} \quad (2.6.3 - 11)$$

This new stress state can now be used to check for fibre kinking, however a different approach is adopted if material has a linear shear behaviour or non-linear. Indeed, in the last case kinking can result either form matrix failure or instability, due to the loss of (shear) stiffness for a larger shear strain values. On the other side, for a linear material there is no need to check the instability. It is sufficient replacing the stress state in the misalignment coordinate frame in a matrix failure criterion and it leads directly to the expression for the value of the misalignment angle  $\varphi$  at failure for a pure compression case,  $\varphi^c$ .

A briefly part with the majors' formulas will follow, but for a more detailed argumentation see *Ref.15*.

Case 1 - Kinking for pure compression as the result of matrix failure

Using LaRC04 matrix compression failure criterion, *Eq. LaRC04-2*, the expression of the misalignment angle  $\varphi$  at failure for a pure compression case ( $\varphi^c$ ) is:

$$\varphi^c = \arctan \left( \frac{1 - \sqrt{1 - 4 \left( \frac{S^L}{X^c} + \eta^L \right) \left( \frac{S^L}{X^c} \right)}}{2 \left( \frac{S^L}{X^c} + \eta^L \right)} \right) \quad (2.6.3 - 12)$$

In general, it is the sum of an initial misalignment ( $\varphi^0$ ) with the rotation due to loading, so:

$$\varphi^0 = \varphi^c - \gamma_{1^c 2^m}^c \quad (2.6.3 - 13)$$

Whereas from the constitutive law the shear stress is obtained as a function of shear strain:

$$\tau_{1^c 2^m} = f_{CL}(\gamma_{1^c 2^m}^c) \quad (2.6.3 - 14)$$

That for pure axial compressive failure becomes:

$$\tau_{1^c 2^m} = \frac{1}{2} \sin(2\varphi^c) X^c \quad (2.6.3 - 15)$$

It can be possible to obtain the relations summarized in *Tab.6*

Non-linear behaviour of the material
$\gamma_{1^c 2^m}^c = f_{CL}^{-1} \left( \frac{1}{2} \sin(2\varphi^c) \right) X^c$
Linear behaviour of the material
$\gamma_{1^c 2^m}^c = \frac{\sin(2\varphi^c) X^c}{2G_{12}}$

**Table 6 - Shear strain possible expressions**

It is very useful to plot the relationship between the shear strain vs. shear stress material law (Left Hand Side - LHS) such as the shear stress resulting from the compressive longitudinal loading in a rotate coordinate system (Right Hand Side-RHS), the result is *Fig.17*. The point of intersection defines the strain in the misalignment frame. In case of material non-linear behaviour, there could be more than one, so that the equilibrium position, which defines the orientation of the misaligned frame, corresponds to the first because it is that with lowest energy.

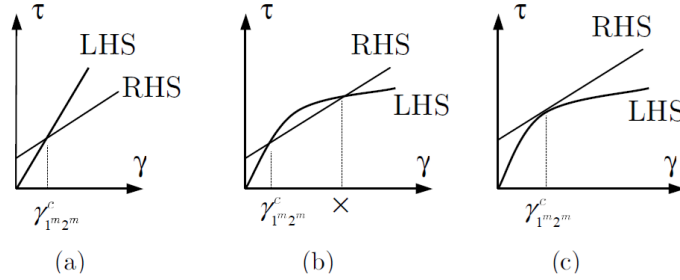


**Figure 17 - Left and Right hand side of Eq. (96), for a material with a (a) linear shear behaviour, (b) non-linear shear behaviour, and failure by matrix cracking, and (c) non-linear shear behaviour, and failure by instability**

The case in *Fig.17(c)* represents the second mechanism of failure, for which the matrix compression failure criterion is not verified yet, that is the elastic instability of matrix.

Case 2 - Kinking for pure compression as the results of the instability

In this case a little increase in the compressive load results in the two curves that do not touch each other, in fact RHS curve shifts up. So, physically this means that there is not an equilibrium position and a catastrophic failure, due to an unstable rotation of fibres. In this case the corresponding values of  $\varphi^0$  and  $\gamma_{1^m 2^m}^c$  can be obtained from the following system:

$$\begin{cases} f_{CL}(\gamma_{1^m 2^m}^c) = \frac{X^c}{2} \sin[2(\varphi^0 + \gamma_{1^m 2^m}^c)] \\ \left. \frac{\partial f_{CL}(\gamma_{1^m 2^m})}{\partial \gamma_{1^m 2^m}} \right|_{\gamma_{1^m 2^m}^c} = X^c \cos[2(\varphi^0 + \gamma_{1^m 2^m}^c)] \end{cases} \quad (2.6.3 - 16)$$

For a more detailed discussion about the solution of the system see *Ref. 15*, either way,  $\varphi^0$ ,  $\gamma_{1^m 2^m}^c$  and  $\varphi^c$  are always defined.

Knowing the initial misalignment allows the definition of the misalignment angle for a generic plane stress situation,  $\varphi$ , by the equation:

$$\varphi = \frac{\tau_{12}}{|\tau_{12}|} (\varphi^0 + \gamma_{1^m 2^m}) \quad (2.6.3 - 17)$$

Note that,  $|\tau_{12}|$  was used instead because it is the easiest way to consider simultaneously the possibility of an initial misalignment  $\pm\varphi^0$ .

In this equation, the only unknown variable is  $\gamma_{1^m 2^m}$ , that for linear behavior was given by Davila's formula:

$$\gamma_{1^m 2^m} = \frac{\varphi^0 G_{12} + |\tau_{12}|}{G_{12} + \sigma_{11} - \sigma_{22}} - \varphi^0 \quad (2.6.3 - 18)$$

#### 2.5.3.2.2.1.2 - 3D Kinking Model

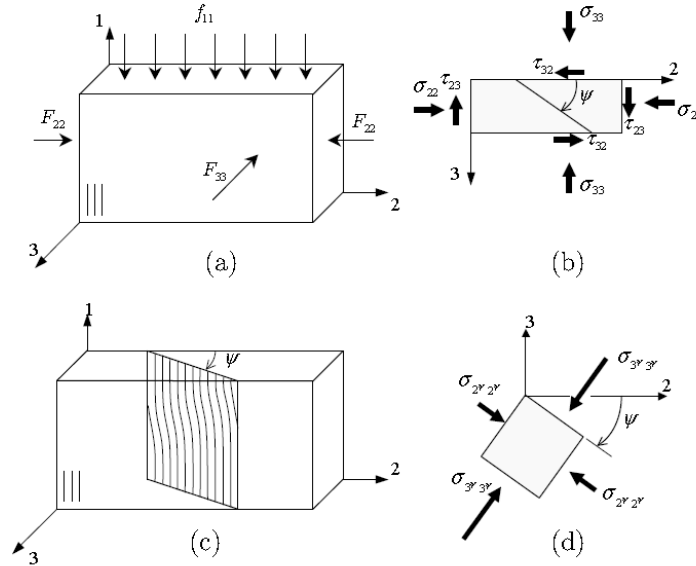


Figure 18 - 3D kinking model

The 2D model assumes that kinking happens in the plane of the lamina, however there is a significant evidence that support the importance of 3D analysis. the model that follows generalizes the previous one for a generic 3D stress state.

Consider an unidirectional lamina under compressive stress as shown in *Fig. 18(a)*. The stresses acting on the (2; 3) plane are shown in *Fig. 18(b)*. While a 2D kinking model assumes that the angle  $\psi$  in *Figs. 18(c) and (d)* is equal to zero, on the contrary in 3D case the kink plane is at an angle  $\psi$  with the 2 axes.

The actual value of the angle  $\psi$  depends on the particular stress state, but also a particular distribution of fibre initial misalignment could influence it<sup>14</sup>. The local stresses in the (2; 3) plane can be found as a function of  $\psi$  through the use of transformation equations:

$$\left\{ \begin{array}{l} \sigma_{2\psi 2\psi} = \frac{\sigma_{22} + \sigma_{33}}{2} + \frac{\sigma_{22} - \sigma_{33}}{2} \cos(2\psi) + \tau_{23} \sin(2\psi) \\ \sigma_{3\psi 3\psi} = \sigma_{22} + \sigma_{33} - \sigma_{2\psi 2\psi} \\ \tau_{12\psi} = \tau_{12} \cos(\psi) + \tau_{13} \sin(\psi) \\ \tau_{2\psi 3\psi} = 0 \\ \tau_{3\psi 1} = \tau_{31} \cos(\psi) - \tau_{12} \sin(\psi) \end{array} \right. \quad (2.6.3 - 19)$$

<sup>14</sup> If the composite is constrained so that it cannot move laterally, then the kink plane would have an angle  $\psi = 90^\circ$ . In general,  $\psi$  will have a value between  $0^\circ$  and  $180^\circ$ .

For a potential kinking plane oriented at an angle  $\psi$ , a negative stress  $\sigma_3\psi_3\psi$  will act as to close microcracks in the matrix for alternative kinking planes, while a positive  $\sigma_2\psi_2\psi$  will act as to open microcracks thus favouring kinking in that plane. Therefore, the kinking plane is expected to be created at the orientation that maximizes  $\sigma_2\psi_2\psi$  and minimizes  $\sigma_3\psi_3\psi$ , which coincides with the local principal directions. Another argument is that the reduced shear stiffness in the kink band would result in fibres rotating in different directions, in case  $\tau_2\psi_3\psi$  was nonzero, however, experimental observations support the contention that kink bands lie in a plane. Hence, with the assumption that the kink plane happens at an angle such that  $\tau_2\psi_3\psi = 0$ , the value of the angle  $\psi$  that defines the kink plane is given by:

$$\tan(2\psi) = \frac{2\tau_{23}}{\sigma_{22} - \sigma_{33}} \quad (2.6.3 - 20)$$

After defining the kink plane, the stresses are then rotated to the misalignment frame. This misalignment frame is defined first determining  $\gamma_{1^m 2^m}$  solving iteratively the Eq. 105 in Ref.15, if the equation has no solution, then failure will take place by instability.

After obtaining it, the angle  $\varphi$  is obtained from:

$$\varphi = \frac{\tau_{12}\psi}{|\tau_{12}\psi|} (\varphi^0 + \gamma_{1^m 2^m}) \quad (2.6.3 - 21)$$

Finally, if  $\gamma_{1^m 2^m}$  exists, matrix failure is checked next. The first step it is to writing stresses in misalignment frame as:

$$\left\{ \begin{array}{l} \sigma_{1^m 1^m} = \frac{\sigma_{11} + \sigma_2\psi_2\psi}{2} + \frac{\sigma_{11} - \sigma_2\psi_2\psi}{2} \cos(2\varphi) + \tau_{12}\psi \sin(2\varphi) \\ \sigma_{2^m 2^m} = \sigma_{11} + \sigma_2\psi_2\psi - \sigma_{1^m 1^m} \\ \tau_{1^m 2^m} = -\frac{\sigma_{11} - \sigma_2\psi_2\psi}{2} \sin(2\varphi) + \tau_{12}\psi \cos(2\varphi) \\ \tau_{2^m 3\psi} = \tau_2\psi_3\psi \cos(\varphi) - \tau_{3\psi 1} \sin(\varphi) \\ \tau_{3\psi 1^m} = \tau_{3\psi 1}\psi \cos(\varphi) \end{array} \right. \quad (2.6.3 - 22)$$

The LaRC04 criteria for matrix tension failure, and matrix compression failure, can be applied in the misalignment frame to predict failure. The type of failure predicted is matrix failure, and this might or not promote subsequent fibre kinking. It might be trivial in some cases to predict that subsequent fibre kinking takes place like for pure compression in the fibre direction, but the same is not true for all load combinations<sup>[15]</sup>. For  $\sigma_{2^m 2^m} < 0$ , it seems reasonable to assume that failure is by kink-band formation only if Eq. (LaRC04-2) is verified with  $\alpha = 0$ . Otherwise, the failure is considered to lead to matrix failure, without kink-band formation. Thus, kink-band formation with  $\sigma_{2^m 2^m} < 0$  is predicted with the criterion:

$$FI_F = \frac{|\tau_{1^m 2^m}|}{S_{is}^L - \eta^L \sigma_{2^m 2^m}} \leq 1 \quad (LaRC04 - 4)$$

while matrix failure under biaxial compression ( $\sigma_{11} < -Y^C$ ) is predicted by

$$FI_M = \left( \frac{\tau^{Tm}}{S^T - \eta^T \sigma_n^m} \right)^2 + \left( \frac{\tau^{Lm}}{S^L - \eta^L \sigma_m^m} \right)^2 \leq 1 \quad (LaRC04 - 5)$$

with

$$\begin{cases} \sigma_n^m = \frac{\sigma_{2^m 2^m} + \sigma_{3\psi 3\psi}}{2} + \frac{\sigma_{2^m 2^m} - \sigma_{3\psi 3\psi}}{2} \cos(2\alpha) + \tau_{2^m 3\psi} \sin(2\alpha) \\ \tau^{Tm} = -\frac{\sigma_{2^m 2^m} - \sigma_{3\psi 3\psi}}{2} \sin(2\alpha) + \tau_{2^m 3\psi} \cos(2\alpha) \\ \tau^{Lm} = \tau_{1^m 2^m} \cos(\alpha) + \tau_{3\psi 1^m} \sin(\alpha) \end{cases} \quad (2.6. -23)$$

where the angle  $\alpha$ , which is comprised in the interval  $]0, \pi[$ , is obtained by trying a small number of tentative angles.

For  $\sigma_{2^m 2^m} \geq 0$ , it seems more difficult to agree with a criterion for eventual fibre-kinking after matrix failure, in the absence of experimental data. Possible solutions to identify the conditions triggering fibre-kinking are the use of a threshold value for  $\sigma_{11}$ ; without further support from experimental data  $\frac{X^C}{2}$  is taken. Thus, for  $\sigma_{2^m 2^m} \geq 0$ , and from *Eq.LaRC04-1*, the criterion for matrix tensile failure under longitudinal compression (with eventual fiber-kinking,  $\sigma_{11} < \frac{X^C}{2}$ ) is:

$$F_{M/F} = (1 - g) \frac{\sigma_{2^m 2^m}}{Y_{is}^T} + g \left( \frac{\sigma_{2^m 2^m}}{Y_{is}^T} \right)^2 + \frac{\Lambda_{23}^0 \tau_{2^m 3\psi}^2 + \chi(\gamma_{1^m 2^m})}{\chi(\gamma_{12|is}^u)} \leq 1 \quad (2.6.3 - 24)$$

#### 2.6.4 - LaRC05

Further development of LaRC criteria is LaRC05<sup>15</sup>, which was developed during World-Wide Failure Exercise (WWFE-II). The philosophy behind the approach is that failure models and resulting criteria ought to include as much as possible of the physics associated with the failure process at the micromechanical level, while still allowing for solutions to be computed for laminae and laminates.

---

<sup>15</sup> For more details the reader can see Ref.20.

## 2.6.4.1 - Failure model at the ply level

### 2.6.4.1.1 - Matrix Failure

The strengths associated with matrix dominated failure in a composite should not be expected to be material properties. They are structural properties, dependent on the thickness of the ply, and on the neighboring plies in the laminate. Indeed, under the same stress state (averaged over ply thickness), the conditions for the propagation of micro-cracks are much more favorable for the case of a UD laminate than for a thin ply in a multi-axial laminate neighbored by  $0^\circ$  plies. The thickness of the ply and the presence of neighboring plies change the boundary conditions of the fracture mechanics problem for crack growth.

Consider the different types of plies presented in *Fig.19*, which include an equivalent slit crack. The equivalent slit crack is an equivalent crack of a well defined shape and orientation which purposes to represent the existing microcracks in the ply, resulting from manufacturing.

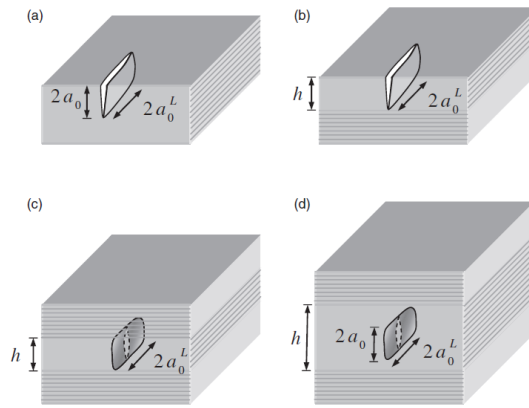


**Figure 19 - Slit crack considered for in-situ effects. (a) Ply in a UD laminate; (b) thin outer ply; (c) thin embedded ply and (d) thick**

Matrix-dominated failure in composites has similarities to that of pure polymer. This would indicate that criteria analogous to Raghava's would be amongst the most suitable to predict matrix failure in a composite. However, to predict the consequences of failure in composites, becomes extremely important knowing the fracture angle. Then, is used an adaptation of Mohr-Coulomb's failure criterion for UD composite plies, like already explained previous paragraph. So, the matrix failure index is defined as:

$$FI_M = \left( \frac{\tau_T}{S_T^{is} - \eta_T \sigma_N} \right)^2 + \left( \frac{\tau_L}{S_L^{is} - \eta_L \sigma_N} \right)^2 + \left( \frac{\langle \sigma_N \rangle_+}{Y_T^{is}} \right)^2 \quad (LaRC05 - 1)$$

with failure being predicted when  $FI_M = 1$

The terms in *Eq.(LaRC05-1)* are:

- $\sigma_N, \tau_L$  and  $\tau_T$  are the traction components in the (potential) fracture plane, see *Fig.15*, and are obtained by stress transformation:

$$\begin{cases} \sigma_N = \frac{\sigma_2 + \sigma_3}{2} + \frac{\sigma_2 - \sigma_3}{2} \cos(2\alpha) + \tau_{23} \sin(2\alpha) \\ \tau_T = -\frac{\sigma_2 - \sigma_3}{2} \sin(2\alpha) + \tau_{23} \cos(2\alpha) \\ \tau_L = \tau_{12} \cos(\alpha) + \tau_{31} \sin(\alpha) \end{cases} \quad (2.6.4 - 1)$$

where  $\alpha$  is the angle that maximizes  $FI_M$  and is obtained numerically by evaluating the function at selected angles in the interval  $0^\circ \leq \alpha < 180^\circ$ .

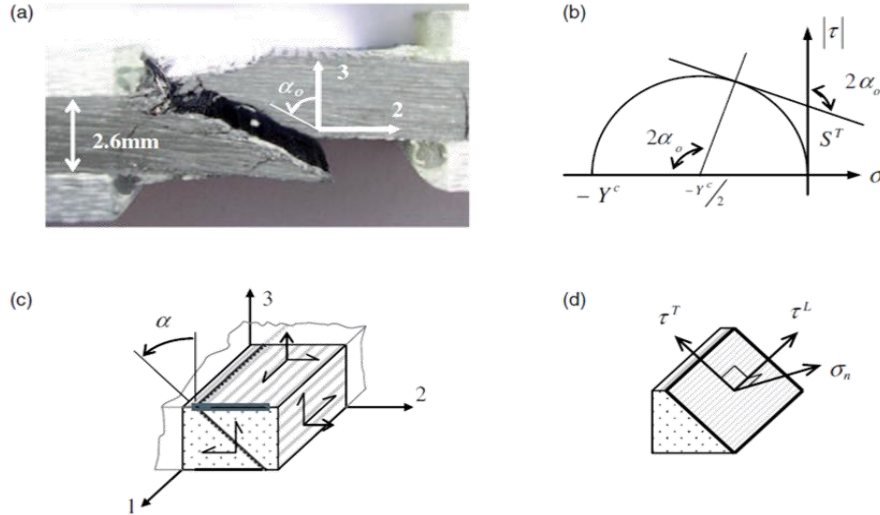


Figure 20 - Traction components acting on the matrix fracture plane

- The strengths  $Y_T^{is}$ ,  $S_L^{is}$  and  $S_T^{is}$  are the in-situ transverse tensile strength, longitudinal shear strength and transverse shear strengths, respectively. These strengths are in-situ because they depend on the thickness of the ply and on the location of the ply in the laminate (inner or outer ply). The different expressions for case in Fig.19 are reported in fig.21.

Where  $G_{Ic}$ ,  $G_{IIc}^L$  and  $G_{IIc}^T$  are the mode I and mode II (longitudinal and transverse) fracture toughness, respectively, Y is a geometry-dependent factor, m is equal to either 2, for unstable propagation in the transverse direction, or 4, for unstable propagation in the longitudinal direction. While, the functions  $\xi(\sigma)$  represent the area under the strain versus stress curve up to the point  $(\varepsilon, \sigma)$ . The detailed expressions are Eq. 13, 14 in Ref.19.

	Transverse tensile strength		Longitudinal shear strength		Transverse shear strength	
	Linear	Nonlinear	Linear	Nonlinear	Linear	Nonlinear
UD		$Y_T$		$S_L$		$S_T = Y_C \cos(\alpha_0) \left( \sin(\alpha_0) + \frac{\cos(\alpha_0)}{\tan(2\alpha_0)} \right)$
Thick embedded	$1.12\sqrt{2}Y_T$	$\xi_2^{-1}(1.12^2 2\xi(Y_T))$	$\sqrt{2}S_L$	$\xi_L^{-1}(2\xi(S_L))$	$\sqrt{2}S_T$	$\xi_T^{-1}(2\xi(S_T))$
Thin embedded	$\sqrt{8G_{IC}^L/\pi h\Lambda}$	$\xi_2^{-1}(2G_{IC}^L/\pi h)$	$\sqrt{8G_{IIc}^L G_{12}/\pi h}$	$\xi_L^{-1}(4G_{IIc}^L/\pi h)$	$\sqrt{8G_{IIc}^L G_{12}/\pi h}$	$\xi_T^{-1}(4G_{IIc}^L/\pi h')$
Thin outer	$\sqrt{4G_{IC}^T/\pi h\Lambda}$	$\xi_2^{-1}(G_{IC}^T/\pi h)$	$\sqrt{4G_{IIc}^T G_{12}/\pi h}$	$\xi_L^{-1}(2G_{IIc}^T/\pi h)$	$\sqrt{8G_{IIc}^T G_{12}/\pi h}$	$\xi_T^{-1}(2G_{IIc}^T/\pi h')$

<sup>a</sup>with  $\Lambda = 2\left(\frac{1}{E_T} - \frac{\nu_T^2}{E_L}\right)$  and  $h' = h/\cos\alpha_0$ .

**Figure 21 - Formulas for in-situ strengths LaRC05**

The slope or friction coefficients  $\eta_T$  and  $\eta_L$  in equation are introduced to account for the effect of pressure on the failure response. Their effect is that of increasing the respective shear strengths in the presence of a compressive normal traction and reducing the respective shear strengths in the presence of a tensile normal traction. The slope or friction coefficient  $\eta_T$  is obtained from the pure transverse compression test as a function of  $\alpha_0$  (Eq. 2.5.3 - 2), like in LaRC04. This is the particular value of  $\alpha$  for pure transverse compression, it is a material property that can be measured experimentally. Several sources have observed that the fracture angle for either glass or carbon composites is typically in the range 51°-55°.

$$\eta_T = -\frac{1}{\tan(2\alpha_0)} \quad (2.6.4 - 2)$$

while the slope or friction coefficient  $\eta_L$  is an independent material property that needs to be measured experimentally, however in LaRC04 criteria an analytic relation with  $\eta_T$  is proposed as in LaRC03 Eq. 2.6.2 - 6.

- The last term in the criterion represents the contribution from the positive normal traction ( $\langle\sigma_N\rangle_+$ ) in opening the cracks. In fact, the McCauley brackets  $\langle\cdot\rangle_+$  are defined as  $\langle x \rangle_+ = \max\{0, x\}$ . Therefore, this criterion is intended to be applicable for both tensile and compressive matrix failure.

#### 2.6.4.1.2 - Fibre Kinking Failure

The physics of axial compressive failure has been already discussed in paragraph about LaRC04, then, starting from those concepts some new are explained in this paragraph. The micrographs in Fig. 22 show different stages of kink-band formation in a T300/913 specimen. Matrix splitting in between the fibres can be identified in Fig. 22(b) and it is the result of the high shear stresses introduced by failure in the neighbouring plies. In general, the high localised shear stresses can also be introduced by manufacturing defects, such as fibre misalignments. The splitting promotes further bending of the fibres, which in turn results in more splitting, Fig. 22(c). The bent fibres eventually break due to the combination of bending and compressive stresses, first at one end and then at the other, finally resulting in a kink band, Fig. 22(d).

Experimental observations, as shown in Fig. 23, suggest that kink bands are preceded by matrix failure and that microbuckling is not necessarily the triggering factor for failure. Following the previous observations, fibre kinking is assumed to

result from shear-dominated matrix failure in a misaligned frame, under significant longitudinal compression. However, if the longitudinal compression is not significant, the shear-dominated matrix failure on the misaligned frame results in fibre splitting but not necessarily in fibre kinking [19].

Experimental data for combined longitudinal compression and in plane shear suggests that fibre kinking only takes place for an absolute value of longitudinal compression greater than  $X^C/2$ . However, for longitudinal compression combined with transverse tension, experimental results indicate that no kink bands are formed if the magnitude of the longitudinal compression is lower than  $X^C$ .

The criteria proposed for fibre kinking and for splitting use the same failure index equation written as:

$$FI_{KINK} = FI_{SPLIT} = \left( \frac{\tau_{23}^m}{S_T^{is} - \eta_T \sigma_2^m} \right)^2 + \left( \frac{\tau_{12}^m}{S_L^{is} - \eta_L \sigma_2^m} \right)^2 + \left( \frac{\langle \sigma_2^m \rangle_+}{Y_T^{is}} \right)^2 \quad (LaRC05 - 2)$$

The two failure modes are then distinguished based on the magnitude of longitudinal compression with  $\sigma_1 \leq -\frac{X^C}{2}$  indicating fibre kinking and  $\sigma_1 \geq -\frac{X^C}{2}$  signifying fibre splitting. This distinction is relevant for the propagation of failure.

For a better understanding and visualization of the phenomena in *Fig.23* is presented the physical model for kink-band formation. So, stress rotation equations are for rotation to the kink-band plane  $\psi$ :

$$\begin{cases} \sigma_2^\psi = \cos^2 \psi \sigma_2 + \sin^2 \psi \sigma_3 + 2 \sin \psi \cos \psi \tau_{23} \\ \tau_{12}^\psi = \tau_{12} \cos \psi + \tau_{31} \sin \psi \\ \tau_{23}^\psi = -\sin \psi \cos \psi \sigma_2 + \sin \psi \cos \psi \sigma_3 + (\cos^2 \psi - \sin^2 \psi) \tau_{23} \\ \tau_{31}^\psi = \tau_{31} \cos \psi - \tau_{12} \sin \psi \end{cases} \quad (2.6.4 - 3)$$

and for the subsequent rotation to the misalignment frame:

$$\begin{cases} \sigma_2^m = \sin^2 \varphi \sigma_1 + \cos^2 \varphi \sigma_2^\psi - 2 \sin \varphi \cos \varphi \tau_{12}^\psi \\ \tau_{12}^m = -\sin \varphi \cos \varphi \sigma_1 + \sin \varphi \cos \varphi \sigma_2^\psi + (\cos^2 \varphi - \sin^2 \varphi) \tau_{12}^\psi \\ \tau_{23}^m = \tau_{23}^\psi \cos \varphi - \tau_{31}^\psi \sin \varphi \end{cases} \quad (2.6.4 - 4)$$

where:

- $\psi$  is the angle of the kink band, it is found numerically in the range  $[0, \pi[$  so as to maximise the failure index of *Eq. LaRC05-2*.
- $\varphi$  is the misalignment angle. It is the sum of the initial misalignment angle,  $\varphi^0$ , produced by manufacturing defect, and the shear strain  $\gamma_{m^0}$  expressed in a coordinate system aligned with the manufacturing defect.

$$\varphi = \text{sign}(\tau_{12}^\psi)\varphi^0 + \gamma_{m^0} \quad (2.5.3 - 5)$$

The strain  $\gamma_{m^0}$  is a function of the corresponding shear stress,  $\tau_{m^0}$ , so  $\gamma_{m^0} = \gamma(\tau_{m^0})$ , while, the initial misalignment angle  $\varphi^0$  is a material property which can be obtained from the longitudinal compressive strength solving the following iterative equation:

$$\varphi^0 = \varphi^c - \gamma\left(\frac{1}{2}\sin(2\varphi^0)X_c\right) \quad (2.5.3 - 6)$$

with  $\varphi^c$  given by the same relation used in LaRC04,

$$\varphi^c = \arctan\left(\frac{1 - \sqrt{1 - 4\left(\frac{S^L}{X^C} + \eta^L\right)\left(\frac{S^L}{X^C}\right)}}{2\left(\frac{S^L}{X^C} + \eta^L\right)}\right) \quad (2.5.3 - 7)$$

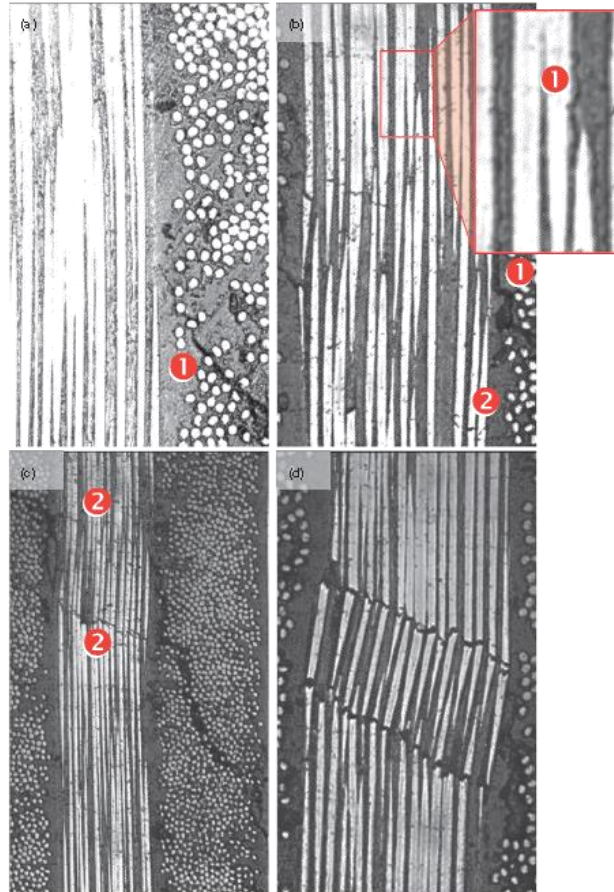


Figure 22 - Sequence of events during kink-band formation. The laminate is being loaded in compression in the vertical direction. (a) Misalignment introduced by a matrix crack in an adjacent layer. (b) Matrix-fibre splitting exists throughout (see zoom); the first fibre failures are indicated. (c) Further fibre failure. (d) Final kink band. Legend. 1 Matrix cracking; 2 Fibre failure

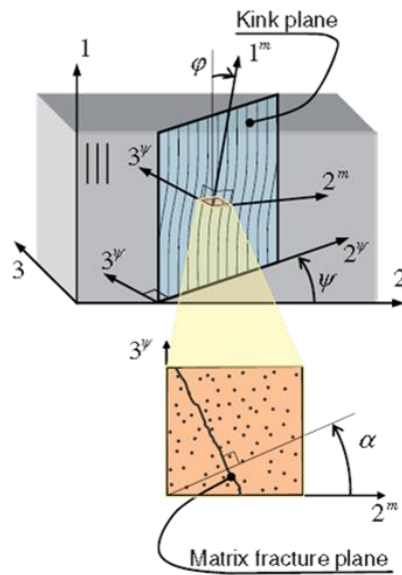


Figure 23 - Physical model for kink-band formation.

#### 2.6.4.1.3 - Fibre Tensile Failure

Similarly, to LaRC04, the maximum stress failure criterion is used to predict this failure mode, indeed, it has been shown to correlate well with existing experimental data:

$$FI_{FT} = \frac{\langle \sigma_1 \rangle_+}{X_T} \quad (LaRC05 - 3)$$

## Chapter 3 – The API

In the first paragraphs of this chapter will be described the computational framework, so the main software used to write the API. Then will follow a presentation of the functions of the API, which was written in Visual Basic language using libraries of Excel and Femap functions. By using the implemented software the user can evaluate the failure index (*FI*) of the modelled object using Hoffman's formulas for 2D problems and LaRC05 formulas. Beside others margin of safety about sandwich plate are evaluable. A detailed description of the code itself is available in *Ref. 23*.

### 3.1 - Computational framework

What is an API? In computer programming it stands for *application programming interface*. APIs represent an open interface of a software and a set of commands, that libraries, software or platforms can use to interact with a program.

In this way, they allow to expand the functionality of a program. In fact, for a developer providing a set of APIs of its software means giving the opportunity to others to interact with its platform and, above all, to extend the functions and features of the basic structure of the platform. In other words, APIs are a great way to promote a program by giving others a way to interact with. The Facebook API, giving a concrete example, have enabled developers and third parties to create thousands of applications and services that access the data offered by the social network: just share your Facebook account to buy, for example, tickets a travel agency or complete the purchase from an e-commerce site.

This last factor is in the business world more important, because it represents a strategic component of digital transformation. Furthermore, by automating some procedures, the Application Programming Interfaces allow the programmer to avoid rewriting routine, avoiding redundancies and unnecessary code replication, which translates in a saving of time and money.

In general an API may be for a web-based system, operating system, database system, computer hardware or software library. An API specification can take many forms, but often includes specifications for routines, data structures, object classes, variables or remote calls. And the separation of the API from its implementation can allow programs written in one language to use a library written in another. Then, the design of an API has significant impact on its usability. Thus, it attempts to provide only the tools a user would expect. The design of programming interfaces represents an important part of software architecture, the organization of a complex piece of software.

Software programming in all effects is a language and, as such, it is characterized by a syntax (which consists of a series of rules) and a style of code writing that can change depending on the programmer. In fact, a developer can adopt different writing methods depending on his skills, his experiences and his habits.

In this case, to create the application two software were used and linked each others:

- Siemens Femap

- Visual Studio

In the graphic interface of the first software the API would be launched and would run, while using the second program it was possible to write the code in VISUAL BASIC family languages.

### **3.1.1 - Femap**

Femap is an advanced engineering simulation software program by Siemens PLM Software that creates finite element analysis models of complex engineering products ("pre-processing") and systems, and displays solution results ("post-processing") that allows mechanical engineers to interpret analysis results. In general it is used by engineering organizations and consultants to model complex products, systems and processes including satellites, aircraft, defense electronics, heavy construction equipment, lift cranes, marine vessels and process equipment.

Femap can virtually model components, assemblies or systems and determine the behavioural response for a given operating environment. Therefore, typically it is used in the design process to reduce costly prototyping and testing, evaluate differing designs and materials, and for structural optimization to reduce weight.

Product simulation applications include basic strength analysis, frequency and transient dynamic simulation, system-level performance evaluation and advanced response, fluid flow and multi-physics engineering analysis for simulation of functional performance.

Further in Femap an Integrated BASIC API Programming Environment was implemented, in this way it offers a full-featured BASIC development environment in a separate window. Directly from the Femap user interface, you can access the OLE/COM object-oriented Femap application programming interface (API) that provides direct access to all Femap objects and functionality. The BASIC engine is fully OLE/COM compliant and can interface with Femap as well as any OLE/COM compliant program such as Word or Excel. These powerful customization capabilities allow a complete access to Femap full functionality through standard nonproprietary programming languages.

In *Fig.24* is reported. the optional FEMAP API editing window. Although the window appears to be part of your FEMAP session, it is not. It is merely a code editing tool. In fact it is important to repeat that the API script you write is not part of FEMAP, but is a standalone program that is interacting with FEMAP.

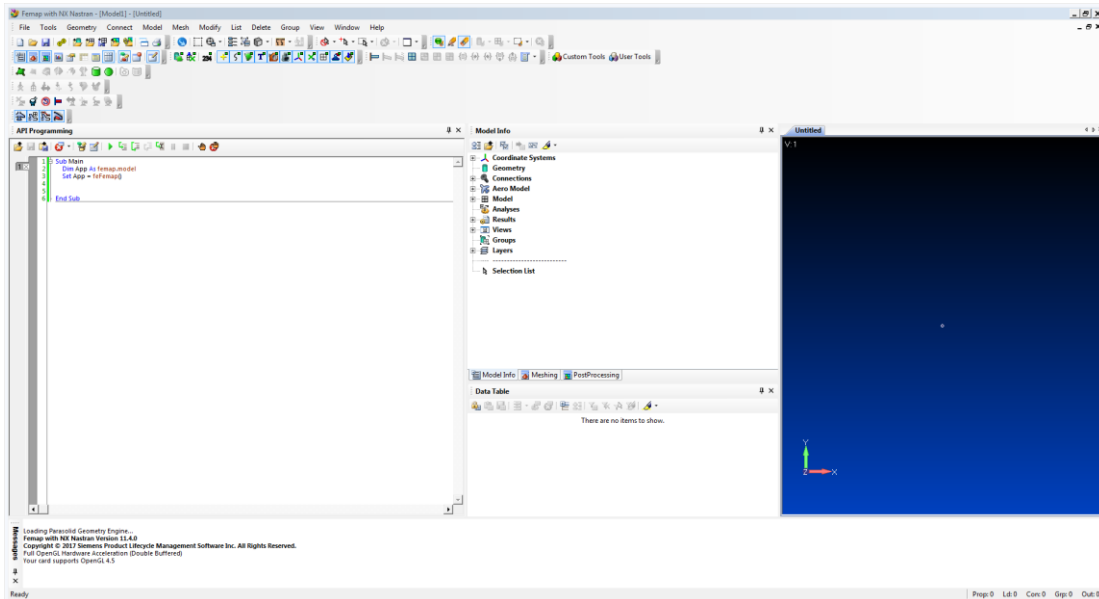


Figure 24 -Femap API editing window

### 3.1.2 - Visual Basic Language

In order to write the code was used visual basic language in Microsoft Visual Studio, a briefly description of them follows.

- a) *Visual Basic*: it is a third-generation event-driven programming language and integrated development environment (IDE) from Microsoft for its Component Object Model (COM) programming model first released in 1991 and declared legacy during 2008. Microsoft intended Visual Basic to be relatively easy to learn and use. Visual Basic was derived from BASIC, a user-friendly programming language designed for beginners, and it enables the rapid application development (RAD) of graphical user interface (GUI) applications, access to databases using Data Access Objects, Remote Data Objects, or ActiveX Data Objects, and creation of ActiveX controls and objects.
- b) *Microsoft Visual Studio*: it is an integrated development environment (IDE) from Microsoft. It is used to develop computer programs, as well as web sites, web apps, web services and mobile apps. Visual Studio uses Microsoft software development platforms such as Windows API, Windows Forms, Windows Presentation Foundation, Windows Store and Microsoft Silverlight. It can produce both native code and managed code.

### 3.2 - API: Flowchart

At the beginning of the programming it was necessary to understand all the functions, which the API should execute. Then, it was very important to figure out all the relations between them and what data they should read from the model. Finally, the last question was how the different output should be displayed to the user. To facilitate these phases the flowchart below in *Fig.25* was created using an free tool online.

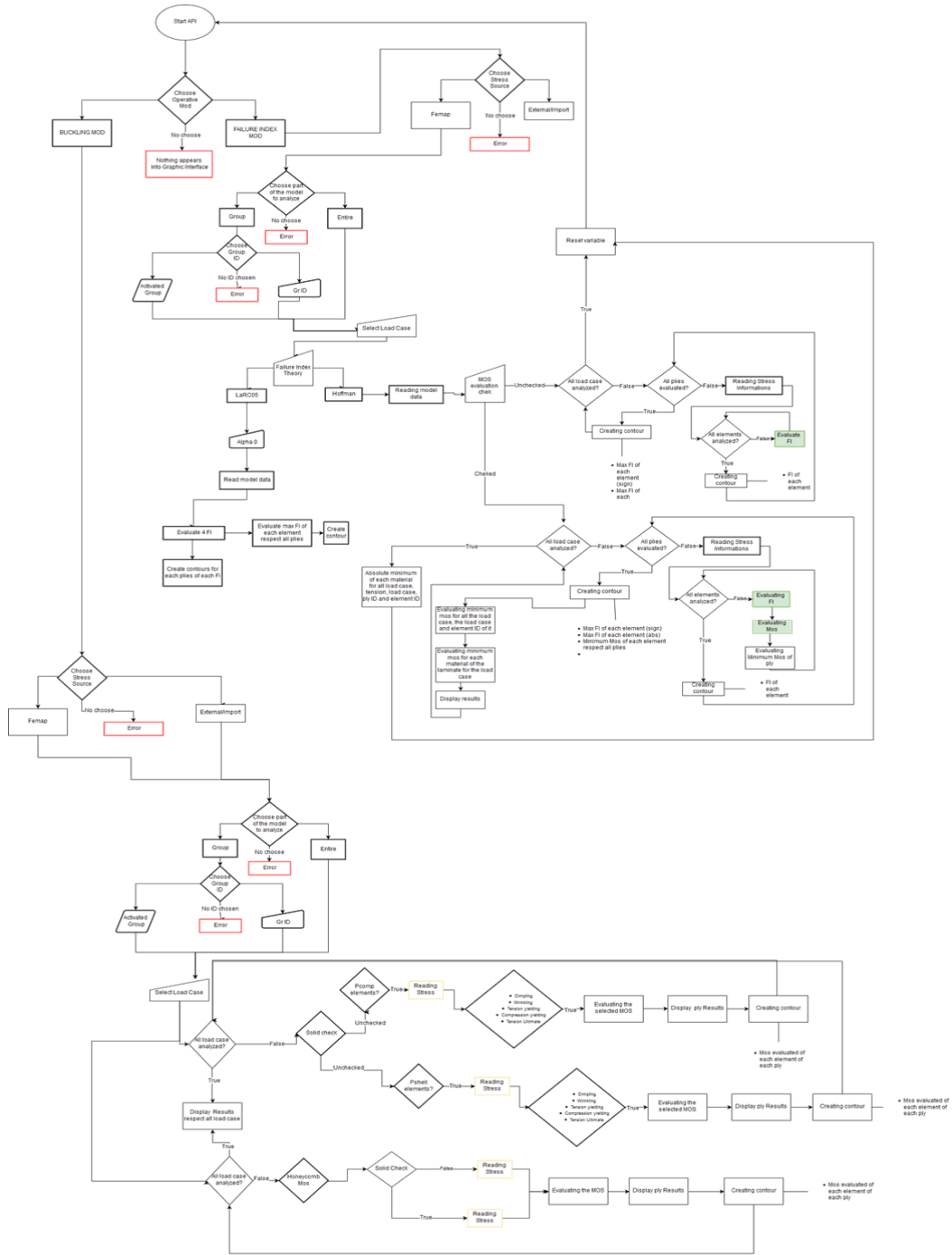


Figure 25 – API basic flowchart

### 3.3 API: Functions and GUIs

The strength of the API is an user friendly graphic interface, GUI, that allows to choose between the different activities. It was thought to reduce at minimum the risk of error by user's utilization. The user can work with API using popup bar on the window or the menu on the top side of the GUI.

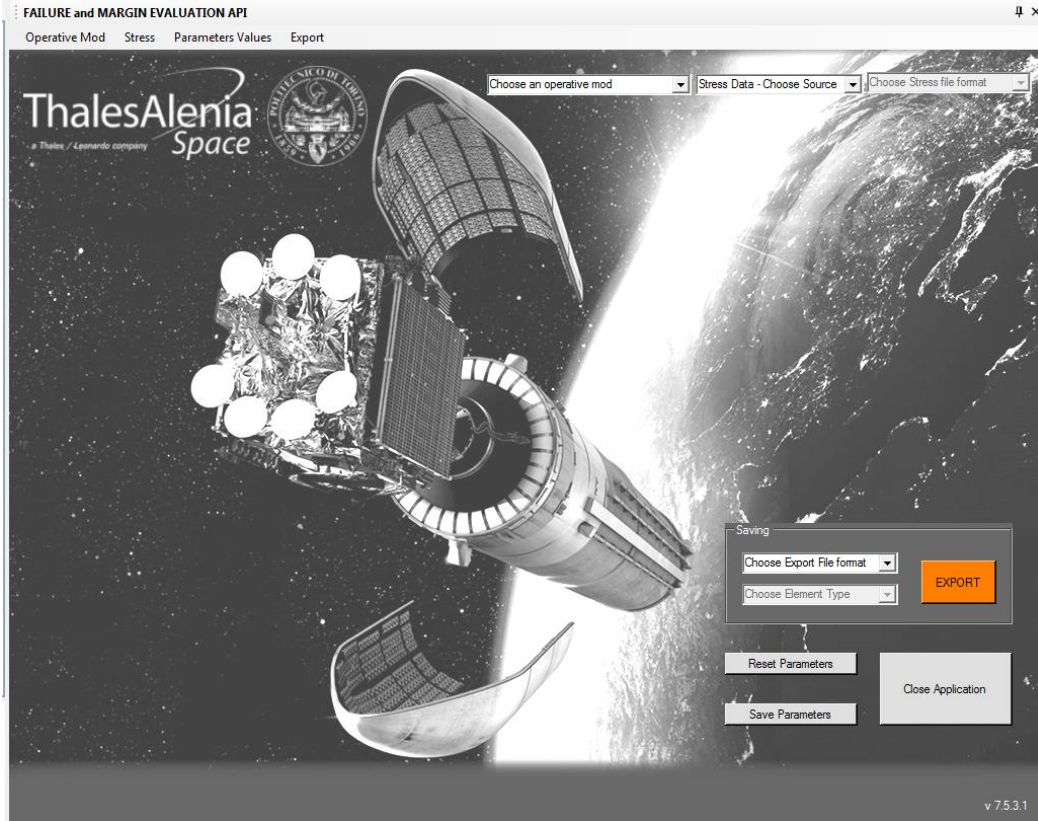


Figure 26 - Starting Graphic User Interface, GUI

With the API it is possible to evaluate failure index with different theories:

- Hoffman,
- LaRC05.

Or to calculate many margin of safety for sandwich panels:

- basing on Hoffman's failure index in case of composites laminates as skins,
- about sandwich panels structures with metallic skins.

In both case the user can choose the source of stresses to use. Indeed, they can be read directly from Femap output vector, that was read by Nastran output file, or they are imported by an external file.

These are the first choices that the user must take when he will start to use the API, if one of them is forgotten an error message on 'window message' of Femap will appeared.

#### 3.3.1 - Failure Index Operative Mod

In this operative mode the user must select which theory to use firstly, then a new window appears and customer must select if the entire model or a part, a group in Femap, will be analyzed.

Finally, for Hoffman's theory the code is able to calculate the associated margin of safety, in this case in the new window the user must insert the different factor of safety.

The API returns the contours for each single ply of the failure indexes of each element. Another plot is created with the maximum values of FI of the elements respect all the plies.

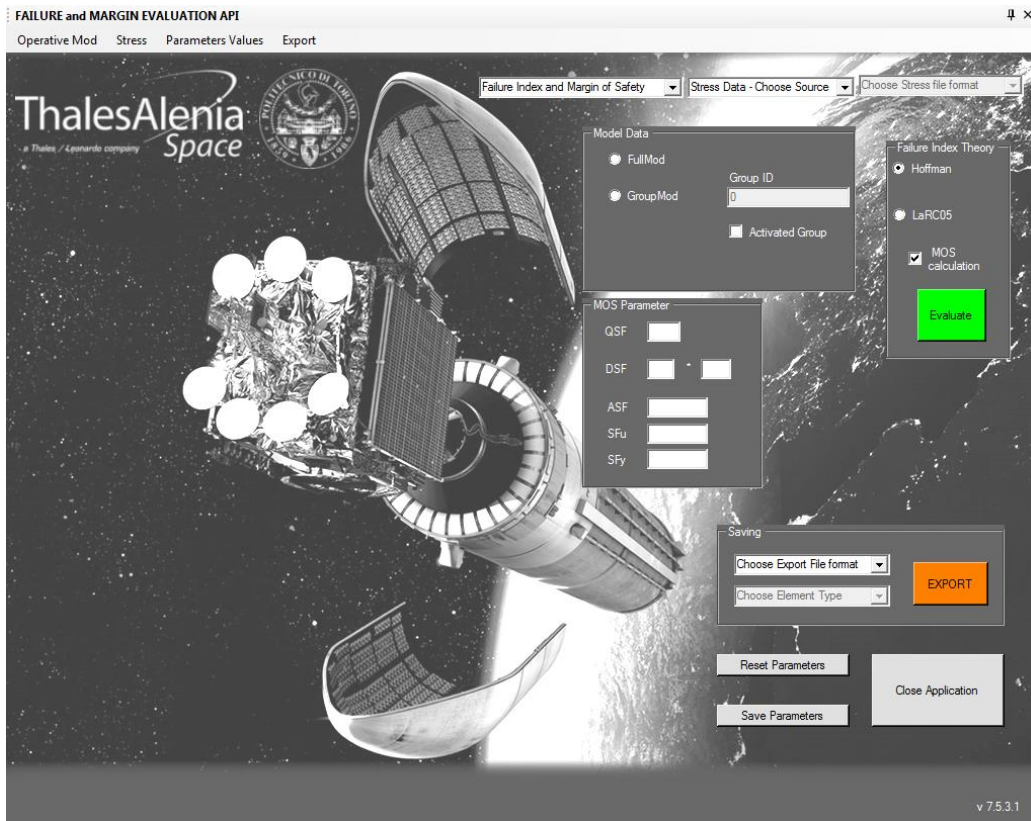


Figure 27 - GUI for Failure Index Operative Mode

### 3.3.2 - Sandwich Panel – Margin of Safety

“Sandwich Panel – Margin of safety” operative mode allows to evaluate different margins of safety, MoS, that company must evaluate for the reports of the analysis. It is divided in the calculation of MoS about skins, in particular metallic skin, and MOS of the honeycomb.

For metallic skin the user can select the different MoS below:

- *Dimpling buckling,*
- *Wrinkling buckling,*
- *Tensile Yielding*
- *Compression Yielding*
- *Tensile Ultimate*

While for the honeycomb is possible to evaluate MOS in the case it is meshed with a laminate element or solid elements.

For company's needed beyond the value of the margin of safety (MOS) the application find other useful information about the conditions of minimum MOS:

- Load case,
- Element ID, basing on Femap model numeration,
- Stress used in the calculation of the formula of margin of safety.

When a margin of safety is selected the related window will be open, and the required parameter will must be manually inserted.

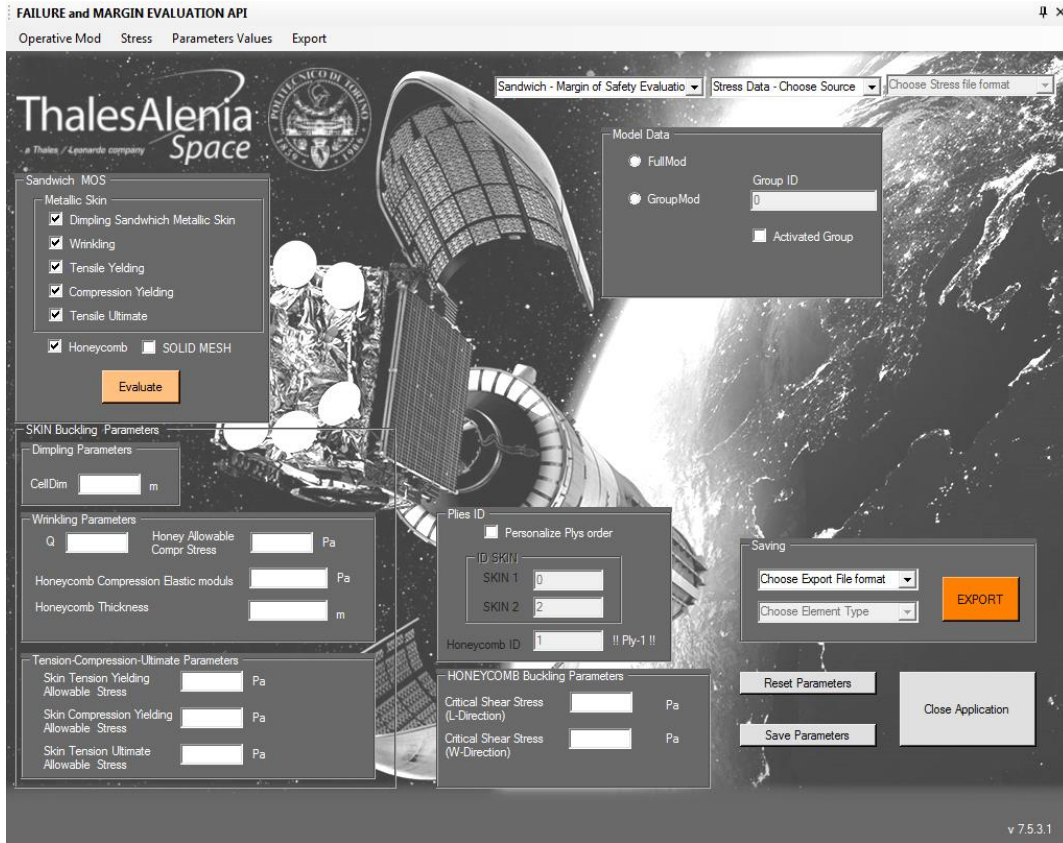


Figure 28 - GUI for Sandwich Panel Operative Mode

Similarly, to the previous function many plots have been created by the API.

## Chapter 4 - API: Validation

During all the time spent to write the code, it was necessary a parallel validation of all its parts, and, also the result given by the API were compared with what expected by others tools. Hence, it was possible to be sure that the code worked in the correctly way in all its functions.

To do this activity basic model were created from time to time and the analyzed using MSC Nastran. At the beginning it was very important to control many times debugging line for line that the API was reading the correct properties of the model and the resulting stresses from analysis.

### 4.1 - Validation of functions to evaluate Hoffman failure index and MOS

At the beginning in order to support on many aspects the validation of the functions of the API that calculate Hoffman failure index, the excel file “*Hoffman Failure Index*” was created to compare the results. It is based on different buttons, which allow to run macro written in *Visual Basic for Application*. These implement the equations reported in chapter 2.4. Then simple models were created to be analyzed. Thus, the values of Hoffman FI obtained with *Femap-Nastran* were compared with that of Excel and of the API. Finally, to verify that all concerning MOS calculation was correct, the external Excel workbook was used again comparing it with the API.

In the figure below it is possible to see an example of how must be compiled the graphic interface in this operative mode.



Figure 29 - Hoffman failure index GUI instructions

### 4.1.1 - Description of the model

The current example is a 4-ply cantilever beam with a  $[0/45/-45/0]$  ply lay-up clamped at one end and subjected to a vertical deflection  $U_z = 5 \text{ mm}$  at the free end. The model representation of the structure has been shown in *Fig. 30* along with the applied boundary conditions, and its schematic representation has been shown in *Fig.31*.

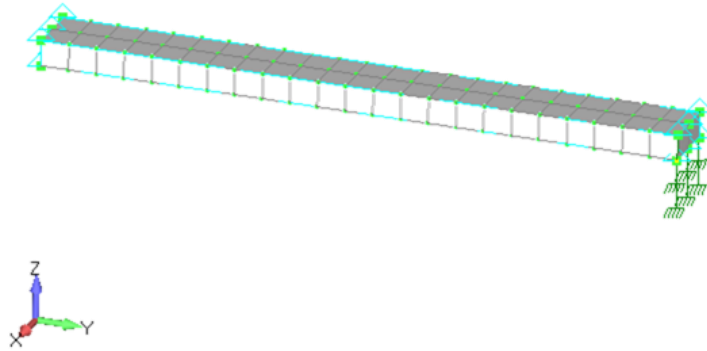


Figure 30- Validation test 1: 4-ply cantilever beam - Model

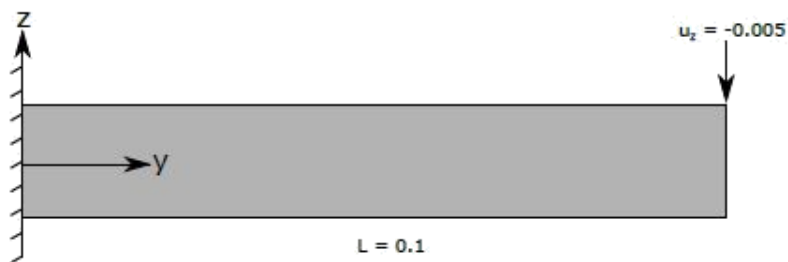


Figure 31 - Validation test 1: 4-ply cantilever beam - Schematic representation

### Material properties

The T300/PR319 material system has been considered for the current example, and its modelled material properties are listed in *Fig. 32*.

```

Material 1 - T300/PR319
  Type 2D ORTHOTROPIC Color 55 Layer 1 #Prop/Ply 4
  Density 0. Damping 0. Ref Temp 0.
  Tsai-Wu 0.
STIFFNESS E1 1.29E+11 G12 1330000000. Nu12 0.318
           E2 5600000000. G1z 0.
           G2z 0.
STRENGTH Tension1 1378000000. Compress1 950000000. Shear 970000000.
          Tension2 40000000. Compress2 125000000.
THERMAL Alpha11 0. K11 0. K12 0.
          Alpha22 0. K22 0. K13 0.
          K33 0. K23 0.
          Spec Heat 0.
OPTICAL Front Off Reverse Off
  
```

Figure 32- T300/PR319 material properties

### 4.1.2 - Numerical Results of the analysis and comparison

The analysis of the model was made by using NX NASTRAN and the displacement

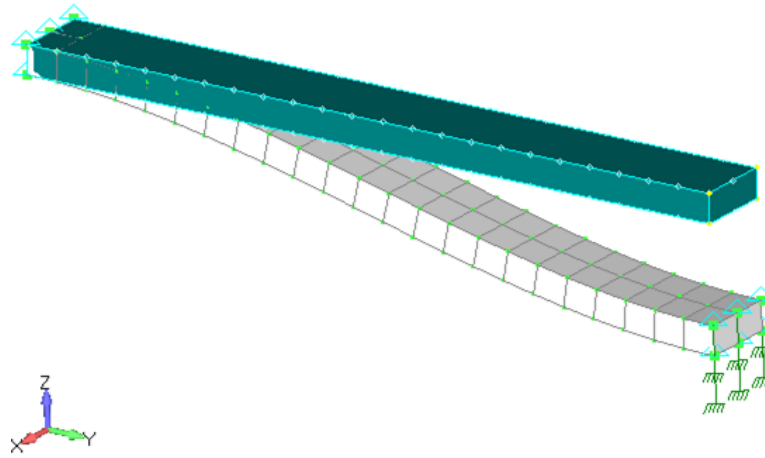


Figure 33 - Validation test 1: 4-ply cantilever beam - Total translation

state of the model, which is represented in *Fig.33*, results from it. During the analysis, FEM failure index value for each element of the mesh of each ply was evaluated using Hoffman failure theory<sup>16</sup>. The complete table with numerical values of all failure indexes is not provided for sake of conciseness, but only the first seventeen were compared and reported in this work.

ID	CSys ID	2..NX NASTRAN Case 1, 1000090..Lam Ply1 Fib Fail Index	2..NX NASTRAN Case 1, 1000290..Lam Ply2 Fib Fail Index	2..NX NASTRAN Case 1, 1000490..Lam Ply3 Fib Fail Index	2..NX NASTRAN Case 1, 1000690..Lam Ply4 Fib Fail Index
143	0	0,0512659	0,154298	0,520356	1,507798
144	0	0,0952849	0,189354	0,571518	1,524612
145	0	0,168732	0,16258	0,462516	1,34201
146	0	0,161146	0,193587	0,447797	1,380726
147	0	0,132973	0,137461	0,420567	1,216402
148	0	0,12976	0,153295	0,364512	1,181299
149	0	0,105791	0,108369	0,349728	1,024934
150	0	0,0984259	0,12709	0,330851	1,040104
151	0	0,0966985	0,0886702	0,303722	0,871556
152	0	0,0954624	0,110423	0,263528	0,856791
153	0	0,0822653	0,0690992	0,24823	0,709366
154	0	0,0761878	0,0906122	0,218991	0,713465
155	0	0,0677876	0,0506308	0,203909	0,571166
156	0	0,0652062	0,0745763	0,167555	0,564257
157	0	0,0546667	0,0346506	0,158575	0,43408
158	0	0,0499362	0,0590477	0,125425	0,43396
159	0	0,0407885	0,0196614	0,119219	0,312242
160	0	0,0375503	0,0458864	0,0833641	0,308595

Figure 34 - Validation test 1: 4-ply cantilever beam - Hoffman failure indexes evaluated using Nastran

<sup>16</sup> See chapter 2 for more theoretical details.

FAILURE INDEX HOFFMAN				TO EVALUATE FI INDEX HOFFMAN			
Element N°	Ply 1	Element N°	Ply 2	Element N°	Ply 3	Element N°	Ply 4
1	0,051265896	1	0,1542985	1	0,520355748	1	1,507798
2	0,095284863	2	0,189354167	2	0,571518179	2	1,524612
3	0,168731816	3	0,162580263	3	0,462515926	3	1,34201
4	0,161145597	4	0,193586529	4	0,447796863	4	1,380726
5	0,132972607	5	0,137461086	5	0,420566678	5	1,216402
6	0,129759911	6	0,153295365	6	0,364512023	6	1,181299
7	0,105791365	7	0,10836858	7	0,349727541	7	1,024934
8	0,098425885	8	0,12708983	8	0,330850986	8	1,040104
9	0,096698539	9	0,088670211	9	0,303721866	9	0,871556
10	0,095462412	10	0,110423244	10	0,263528479	10	0,856792
11	0,082265306	11	0,069099187	11	0,248229885	11	0,709366
12	0,076187781	12	0,090612161	12	0,218990915	12	0,713465
13	0,067787611	13	0,050630759	13	0,203909203	13	0,571166
14	0,065206177	14	0,074576363	14	0,167555436	14	0,564257
15	0,054666727	15	0,03465065	15	0,158575247	15	0,43408
16	0,049936251	16	0,059047743	16	0,125425219	16	0,43396
17	0,040788471	17	0,019661371	17	0,119219046	17	0,312242

Figure 35 - Validation test 1 : 4-ply cantilever beam - Hoffman failure indexes evaluated using Excel file

The agreement between API values and those from MSC Nastran was confirmed by Fig.36 and Fig 37.

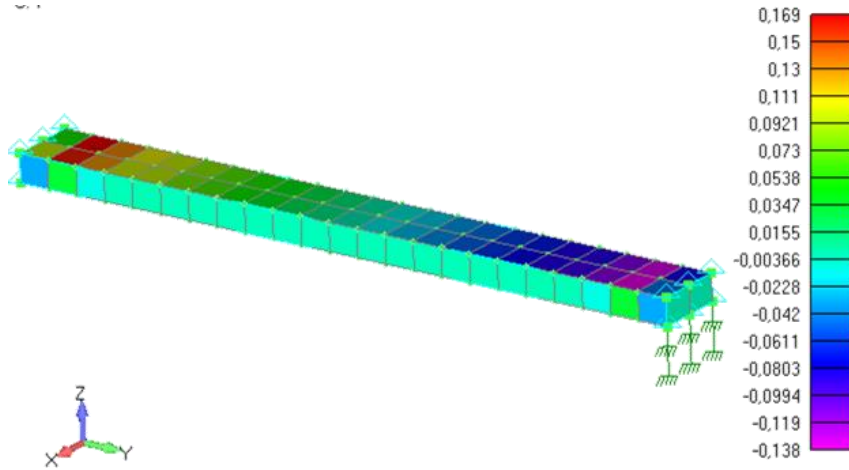


Figure 36- Validation test 1: 4-ply cantilever beam - Ply 1 API Hoffman failure indexes distribution

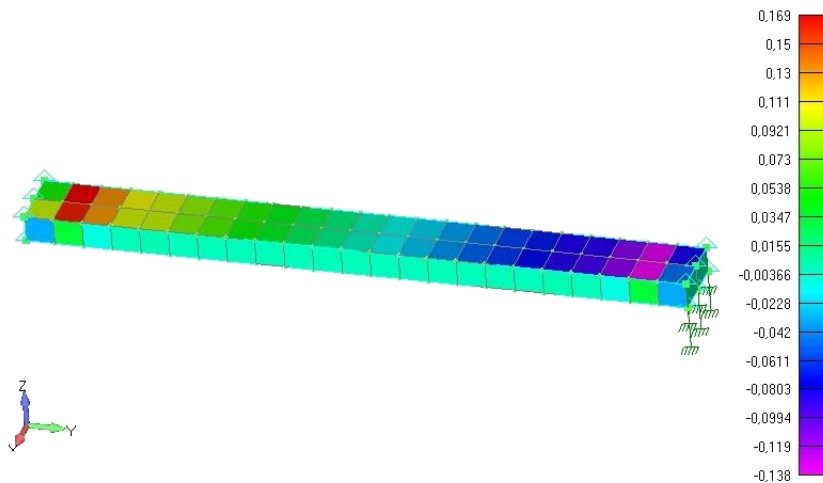


Figure 37 - Validation test 1: 4-ply cantilever beam - Ply 1 Nastran Hoffman failure indexes distribution

Another control that validates these calculations was realized about the maximum value of failure index. As it can see in Tab.7 that results obtained with the two methods were equals with at least a  $10^{-9}$  precision.

Max FI / Source	Ply 1	Ply 2	Ply3	Ply 4
Excel file	0,168731816	0,193586529	0,571518179	1,524612035
Api Femap	0,168731816	0,193586529	0,571518179	1,524612035

Table 7 - Validation test 1 : 4-ply cantilever beam -Maximum Hoffman failure index comparison

And in Fig.38 the contour, with data about maximum FI respect all plies for each element, was illustrated.

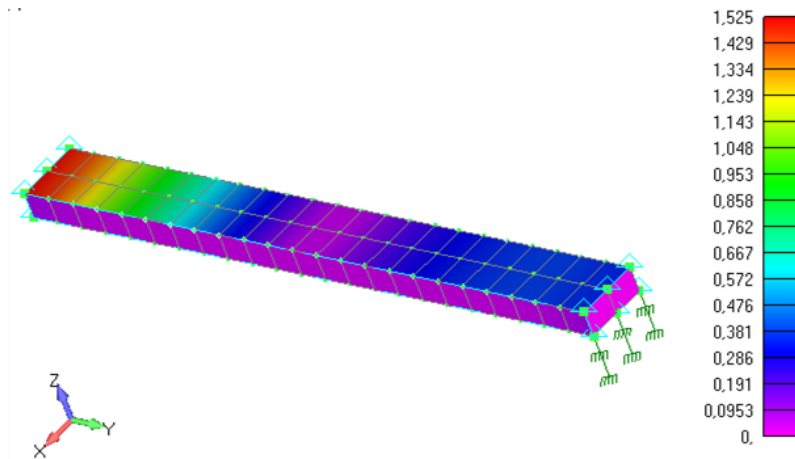


Figure 38 - Validation test 1: 4-ply cantilever beam - Ply 1 API Hoffman failure indexes distribution

Then as already written, to verify that API results about Hoffman margins of safety calculation were correct, they were compared with them obtained with the excel file. Like example the results for ply 1 were shown below in Fig. 39 and Tab.8.

The image below is the window message of Femap, where the API print final results after its execution:

```

FULL MODEL MOD
FINISHED READING DATA OF THE ANALYSIS MODEL
STARTING FAILURE INDEX EVALUATION HOFFMAN 2D
Analysis Study: 1, has 1 Results Sets
-----CASE STUDY 1-----
Minimum MOS of ply1(FULL MODEL): 2,13877637066977
Minimum MOS of ply2(FULL MODEL): 0,930105106864839
Minimum MOS of ply3(FULL MODEL): 0,0315471954907547
Minimum MOS of ply4(FULL MODEL): -0,488402703608061
Minimum MOS of Laminate (FULL MODEL): -0,488402703608061
Minimum MOS of Material: 1 (FULL MODEL): -0,488402703608061
IN PLY: 4
In the element ID : 144
FINISHED FAILURE INDEX EVALUATION - HOFFMAN 2D

```

Figure 39 - Validation test 1: 4-ply cantilever beam - Margin of Safety API results

While Tab 7. reports the value of MoS and terms using in its formula obtained in Excel, however to avoid an excessive length of the table for some elements of ply 1 were only given:

Element	a	b	SR	MOS
1	0,004174376	0,07039108710	9,193768	8,193768
2	0,010991326	0,128571112	5,340024	4,340024
3	0,031690824	0,219125082	3,138776	<b>2,138776</b>
4	0,028594128	0,210442311	3,28533	2,28533
5	0,020253345	0,17598765	3,916736	2,916736
6	0,019172942	0,17214902	4,014232	3,014232
7	0,013324349	0,141963925	4,842818	3,842818

Table 8 - Value of MoS and terms resulted from Excel

It is possible to see that the minimum value for ply one in two cases were exactly the same.

In the end, the function about the way in which should be used imported stresses was tested also. Slightly a difference between values was found. It was probably induced by a variation in decimal precision when stresses were imported in excel and then in Femap. In *Fig. 40* they were shown:

```

FULL MODEL MOD

FINISHED READING DATA OF THE ANALYSIS MODEL

STARTING FAILURE INDEX EVALUATION HOFFMAN 2D

Analysis Study: 1, has 1 Results Sets

-----CASE STUDY 1-----
Opening File H:\Backup\Documenti\UNIVERSITA\MAGISTRALE\Tes\Modelli test\4PlyCantileverBeam\Stresses 4plyCantileverBeam.xlsx...
Minimum MOS of ply1(FULL MODEL): 2,15614086376433
Minimum MOS of ply2(FULL MODEL): 0,958019709319799
Minimum MOS of ply3(FULL MODEL): 0,0469574169570532
Minimum MOS of ply4(FULL MODEL): -0,488249758382096

Minimum MOS of Laminate (FULL MODEL): -0,488249758382096

Minimum MOS of Material: 1 (FULL MODEL): -0,488249758382096
IN PLY: 4
In the element ID : 144

FINISHED FAILURE INDEX EVALUATION - HOFFMAN 2D

```

Figure 40 - Validation test 1 : 4-ply cantilever beam - Margin of Safety API results with imported stresses

## 4.2 – Failure indexes with LaRC05 theory validation of results.

There were not commercial codes that evaluated LaRC05 failure indexes. So, it was necessary to use an alternative method to validate the written code. It has been created an Excel file (“*FAILURE INDEX CALCULATION-LARC05.xlsx*”), where failure indexes of each element for a ply is evaluated automatically. The file needs the data entry about material constants, the value of  $\alpha_0$  and the stress state of the model.

During all time spent to create the API there have been a lot of validations of each single part of the code. For example it was controlled that the API took the correct stresses from Femap. Now, to verify the algorithms to calculate FI, are illustrated results for ply 2 of the same laminate of section 4.1.

### 4.2.1 - Fiber tension

In this case it was possible to compare API outputs with an additional case study, that has been reported in *Ref.24* which is analysed using the academic code *MUL2*. The failure index has been calculated in the middle plane of the beam. Both results have the same order of magnitude and they present a similar distribution along the longitudinal axis of the beam. The little difference in numerical values it would be caused by the different stress state evaluated by Nastran or *MUL2* and the used mesh.

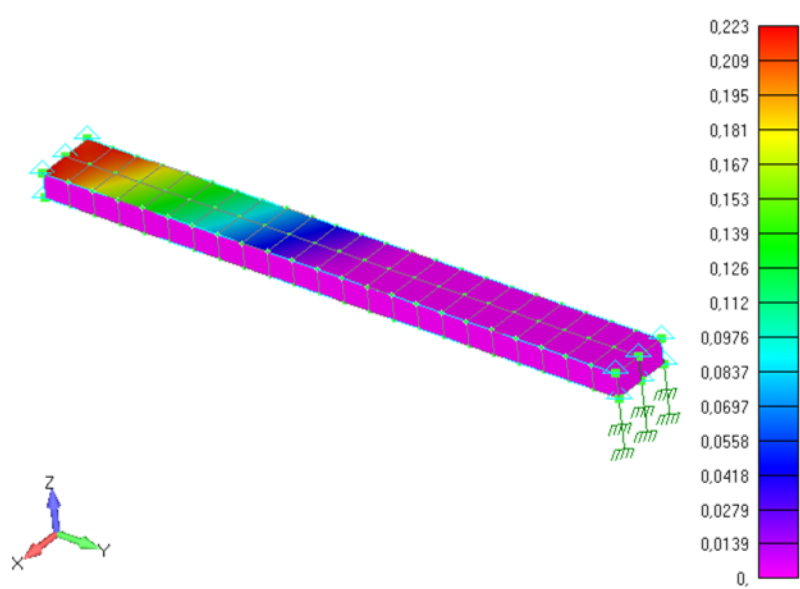


Figure 41 - Validation test 2: Contour plot of the Failure Index for fibre failure under tension, API

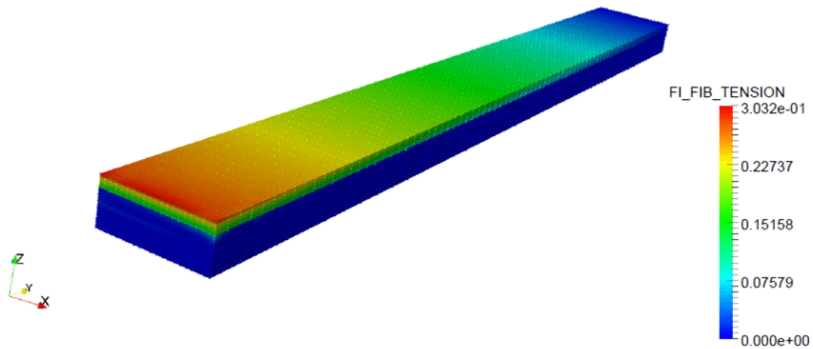


Figure 42 - Validation test 2: Contour plot of the Failure Index for fibre failure under tension, MUL2

In *Tab.9* is presented the comparison between numerical values of failure index. A perfect correlation has been reached.

Element ID	FI tension mode API	FI tension mode Excel
143	0,214615	0.214615
144	0,223190	0.223190
145	<b>0,224451</b>	<b>0.224451</b>
146	0,187702	0.187702
147	0,198441	0.198441
148	0,16408	0.164080
250	0,148524	0.148524
251	0,173358	0.173358
252	0,16408	0.164080
253	0,198441	0.198441
254	0,187702	0.187702

Table 9 - Comparison of Failure Indexes for fibre failure under tension

In *Tab.9* the bolding value is the maximum failure index, as it was illustrated in *Fig.43*. In this way it was controlled that the API creating the correct contours from new output vectors.

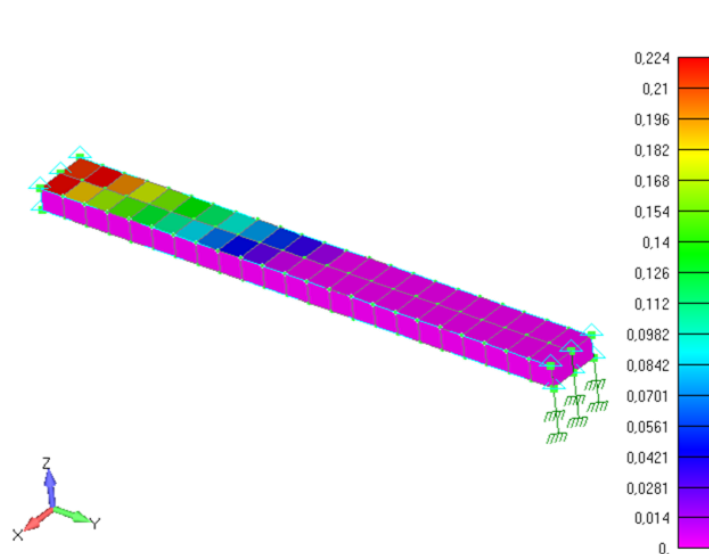


Figure 43 - Validation test 2: Contour plot of the Failure Index for fibre failure under tension, API (not elements averaging)

Further, a last control has been realized comparing the distribution of stresses  $\sigma_x$  in *Fig.44* with the distribution of failure indexes. The reader can see that they are analogous, like it would be predictable basing on the formula *LaRC05-3*. In fact, where are reached maximum stresses, near the fixed -ended, there are maximum failure indexes.

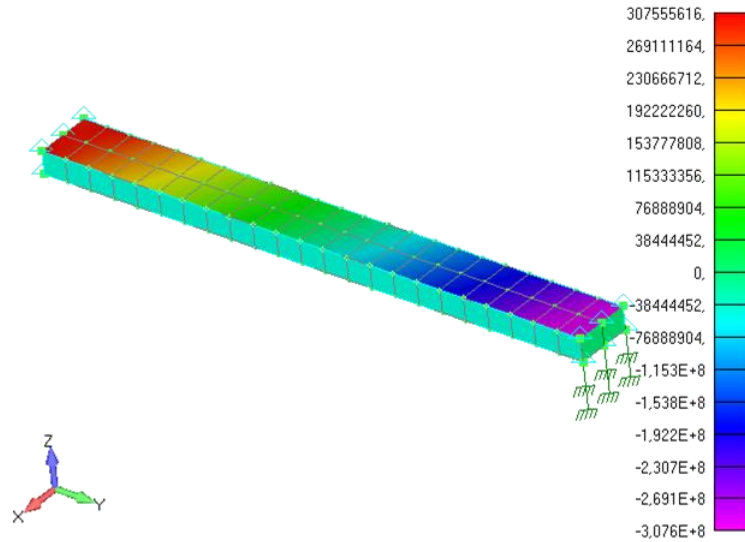


Figure 44 - Validation test 2: Contour plot of the X normal stress, ply 2

Finally, it was verified the valuation of the overall maximum FI of each element. The following contour plot is obtained.

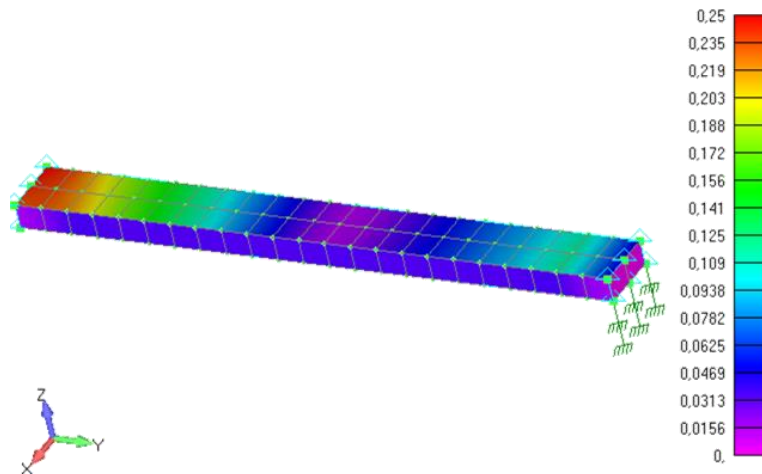


Figure 45 - Validation test 2: Contour plot of the maximum Failure Index for fibre failure under tension for each element of the mesh.

#### 4.2.2 - Matrix failure

The matrix failure of the laminate has been calculated for different angles  $\alpha^{17}$ , to avoid useless repetitions of images, the case  $\alpha = 0^\circ$  is just reported in *Fig.46*. However, all cases have been considered in numerical results presentation in *Tab.10-11*.

<sup>17</sup>  $\alpha = 0^\circ, 15^\circ, 30^\circ, 45^\circ, 60^\circ, 75^\circ, 90^\circ, 105^\circ, 120^\circ, 135^\circ, 150^\circ, 165^\circ$ .

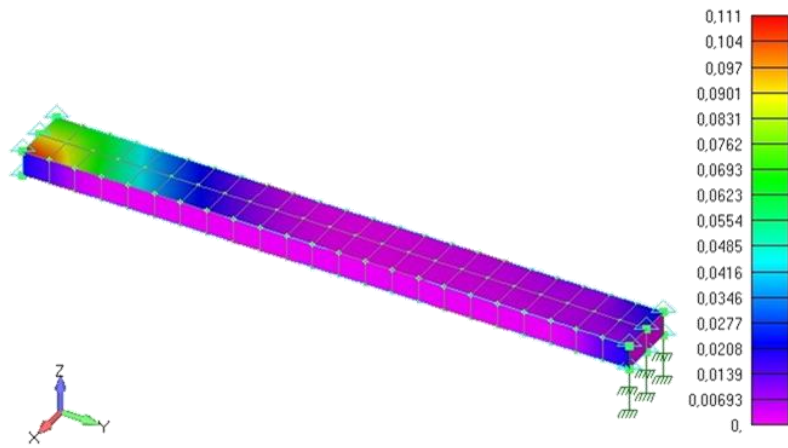


Figure 46 - Contour plot of the Failure Index for matrix failure,  $\alpha = 0^\circ$

API:

Element ID	0°	15°	30°	45°	60°	75°	90°	105°	120°	135°	150°	165°
143	0.0660 4	0.0508 7	0.0315 1	0.0145 1	0.0039 5	0.0000 8	0.0037 0	0.0141 3	0.0311 5	0.0505 8	0.0658 8	0.0716 7
144	<b>0.1108</b> 4	0.0739 2	0.0392 4	0.0158 7	0.0016 4	0.0056 8	0.0240 2	0.0519 9	0.0896 6	0.1230 7	0.1399 5	0.1355 4
145	0.0675 8	0.0675 7	0.0571 5	0.0398 6	0.0216 0	0.0078 4	0.0010 4	0.0012 0	0.0082 1	0.0219 0	0.0400 0	0.0572 1
146	0.0973 9	0.0741 4	0.0452 1	0.0204 9	0.0056 3	0.0005 1	0.0067 3	0.0229 8	0.0490 1	0.0779 1	0.0996 2	0.1068 5
147	0.0567 6	0.0604 9	0.0545 8	0.0410 5	0.0246 5	0.0107 9	0.0026 5	0.0003 8	0.0043 1	0.0139 1	0.0286 0	0.0447 0
148	0.0664 2	0.0537 4	0.0354 7	0.0178 7	0.0057 1	0.0003 9	0.0020 2	0.0105 4	0.0258 0	0.0445 9	0.0609 2	0.0691 2
250	0.0560 3	0.0645 8	0.0628 2	0.0513 4	0.0342 1	0.0176 2	0.0064 2	0.0006 9	0.0020 5	0.0097 2	0.0229 0	0.0402 0
251	0.0393 6	0.0353 6	0.0265 4	0.0159 8	0.0070 0	0.0015 5	0.0000 7	0.0025 9	0.0091 4	0.0188 9	0.0293 6	0.0370 9
252	0.0664 2	0.0691 2	0.0609 2	0.0445 9	0.0258 0	0.0105 4	0.0020 2	0.0003 9	0.0057 1	0.0178 7	0.0354 7	0.0537 4
253	0.0567 6	0.0447 0	0.0286 0	0.0139 1	0.0043 1	0.0003 8	0.0026 5	0.0107 9	0.0246 5	0.0410 5	0.0545 8	0.0604 9
254	0.0973 9	0.1068 5	0.0996 2	0.0779 1	0.0490 1	0.0229 8	0.0067 3	0.0005 1	0.0056 3	0.0204 9	0.0452 1	0.0741 4

Table 10 - Comparison of Failure Indexes for matrix failure, API

Excel:

Element ID	0°	15°	30°	45°	60°	75°	90°	105°	120°	135°	150°	165°
143	0.0660 4	0.0508 7	0.0315 1	0.0145 1	0.0039 5	0.0000 8	0.0037 0	0.0141 3	0.0311 5	0.0505 8	0.0658 8	0.0716 7
144	0.1108 4	0.0739 2	0.0392 4	0.0158 7	0.0016 4	0.0056 8	0.0240 2	0.0519 9	0.0896 6	0.1230 7	0.1399 5	0.1355 4
145	0.0675 8	0.0675 7	0.0571 5	0.0398 6	0.0216 0	0.0078 4	0.0010 4	0.0012 0	0.0082 1	0.0219 0	0.0400 0	0.0572 1
146	0.0973 9	0.0741 4	0.0452 1	0.0204 9	0.0056 3	0.0005 1	0.0067 3	0.0229 8	0.0490 1	0.0779 1	0.0996 2	0.1068 5
147	0.0567 6	0.0604 9	0.0545 8	0.0410 5	0.0246 5	0.0107 9	0.0026 5	0.0003 8	0.0043 1	0.0139 1	0.0286 0	0.0447 0
148	0.0664 2	0.0537 4	0.0354 7	0.0178 7	0.0057 1	0.0003 9	0.0020 2	0.0105 4	0.0258 0	0.0445 9	0.0609 2	0.0691 2
250	0.0560 3	0.0645 8	0.0628 2	0.0513 4	0.0342 1	0.0176 2	0.0064 2	0.0006 9	0.0020 5	0.0097 2	0.0229 0	0.0402 0
251	0.0393 6	0.0353 6	0.0265 4	0.0159 8	0.0070 0	0.0015 5	0.0000 7	0.0025 9	0.0091 4	0.0188 9	0.0293 6	0.0370 9
252	0.0664 2	0.0691 2	0.0609 2	0.0445 9	0.0258 0	0.0105 4	0.0020 2	0.0003 9	0.0057 1	0.0178 7	0.0354 7	0.0537 4
253	0.0567 6	0.0447 0	0.0286 0	0.0139 1	0.0043 1	0.0003 8	0.0026 5	0.0107 9	0.0246 5	0.0410 5	0.0545 8	0.0604 9
254	0.0973 9	0.1068 5	0.0996 2	0.0779 1	0.0490 1	0.0229 8	0.0067 3	0.0005 1	0.0056 3	0.0204 9	0.0452 1	0.0741 4

Table 11 - Comparison of Failure Indexes for matrix failure, Excel

### 4.2.3 - Kinking failure

For the kinking failure of the structure have been obtained a good agreement of results between API and Excel, as it has been shown in *Tab.12*.

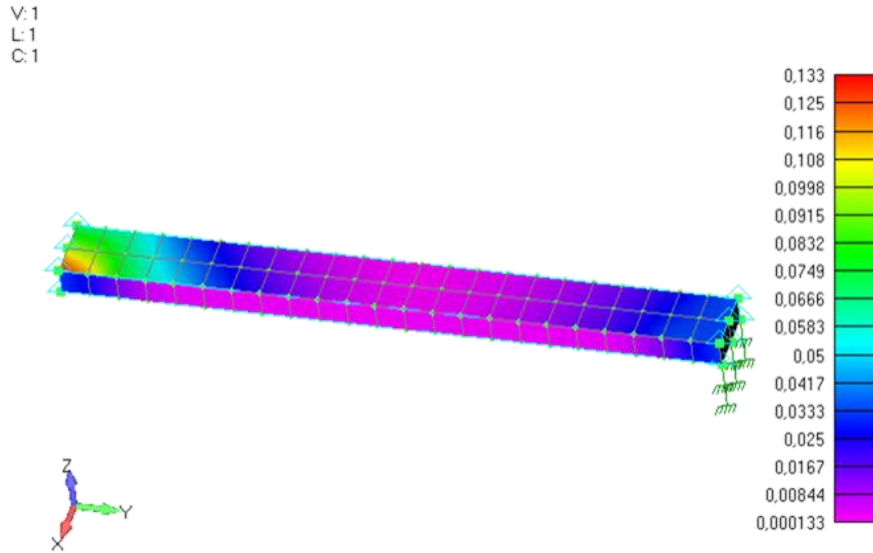


Figure 47 - Contour plot of the Failure Index for kinking failure mode

Element ID	FI tension mode API	FI tension mode Excel
143	0.067409	0.067409
144	<b>0.132997</b>	<b>0.131957</b>
145	0.063656	0.063615
146	0.098234	0.097921
147	0.055709	0.055742
148	0.063641	0.062987
250	0.0595642	0.0593553
251	0.0364779	0.0364761
252	0.0636411	0.0635637
253	0.0557091	0.0556161
254	0.0982335	0.0979206

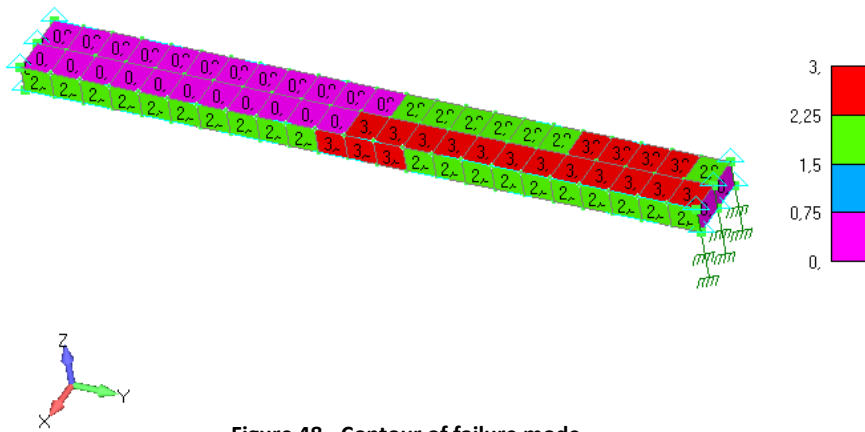
Table 12 - Comparison of Failure Indexes for kinking failure, API

#### 4.2.4 - Failure mode

The last aspect of the API verified is the contour of failure mode. It allows to know for which mode of failure each element collapses. The numbers have the following meaning:

- 0 = Fibre Tension Mode
- 2 = Matrix Failure
- 3 = Kink Mode

An example of contour is *Fig.48*.



## 4.3 – Validation of calculation of margin of safety for sandwich panel

To validate each subroutine of the code, that evaluates many MoS for sandwich panels, the results obtained with the API were compared with those of many excel files. Those last were currently used by engineers for company's programs. The matching was perfect to nine decimal places.

The models analyzed are components of a real structure, so, their stress state and the boundary conditions of each are not reported because Nastran analysis was launched for the entire structure, but for calculation of margins the parts were grouped.

### 4.3.1 Panel with metallic skins

#### 4.3.1.1 - Description of the model

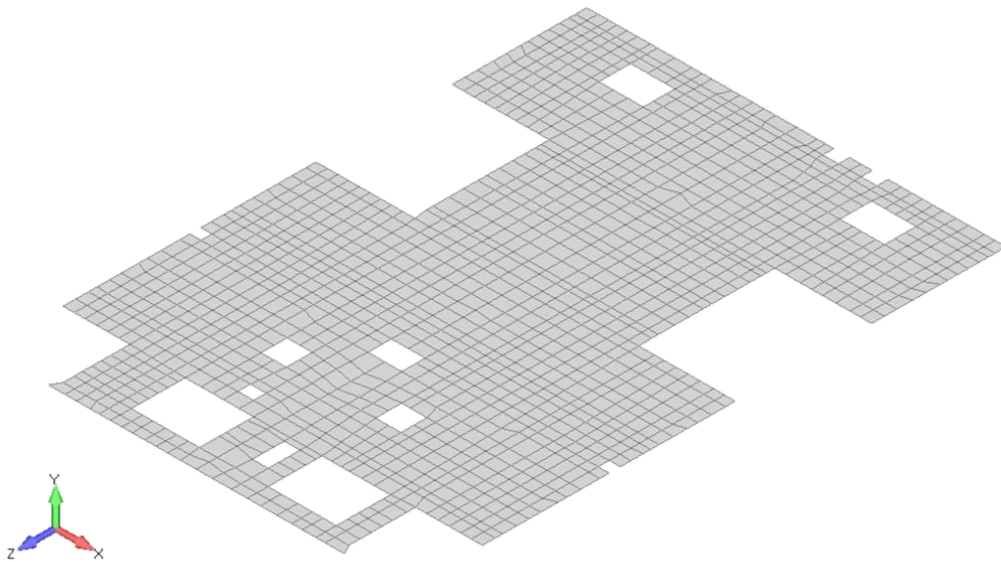


Figure 49 - Validation test: Sandwich Panel with metallic skins - Model4

The example shown in *Fig. 49* is a sandwich panel with a [0/90/0] ply lay-up.

In the full structure it has the following mesh data:

- Property 223001 - LAMINATE PLATE Property
- N° elements: 1389

## Layup and materials data

The sandwich panel was modelled as a laminate with three plies, the first and the last one are the skins while the second ply is the honeycomb. The respective thickness were reported in *Fig.50*.

```

Failure Theory  HOFF      Bond Shear Allowable 20000000.
Ref Temp      20.        Damping Coef 0.
NS Mass/Area  0.        Bottom Surf OFF 0.
Layup 57 -
Ply 1 Material 501      Thickness 0.000635      Angle 0.
Ply 2 Material 650      Thickness 0.02533       Angle 90.
Ply 3 Material 501      Thickness 0.000635      Angle 0.
    
```

**Figure 50 - Validation test: Sandwich Panel with metallic skins - Layup**

The metallic skins are made in *Al-2024 T81*, that was modelled in Femap like an orthotropic material 2D with the following characteristics in *Fig.51*:

While the honeycomb is made with *3/16-5056-0.001*, that has characteristics in *Fig.52*

```

Material 501 - 2D ORTHOTROPIC Material
Type 2D ORTHOTROPIC Color 55 Layer 1 #Prop/Ply 80
Density 2768. Damping 0. Ref Temp 20.
Tsai-Wu 0.
STIFFNESS E1 72340000000. G12 275800000000. Nu12 0.33
           E2 72340000000. G1z 0.
           G2z 0.
STRENGTH Tension1 1.E+15 Compress1 1.E+15 Shear 1.E+15
          Tension2 1.E+15 Compress2 1.E+15
THERMAL Alpha11 0.000023 K11 0. K12 0.
          Alpha22 0.000023 K22 0. K13 0.
          K33 0. K23 0.
          Spec Heat 0.
OPTICAL Front Off Reverse Off
    
```

**Figure 51 - Validation test: Sandwich Panel with metallic skins - Al-2024 T81 Data**

```

Material 650 - 2D ORTHOTROPIC Material
Type 2D ORTHOTROPIC Color 55 Layer 1 #Prop/Ply 8
Density 50. Damping 0. Ref Temp 20.
Tsai-Wu 0.
STIFFNESS E1 1000. G12 0.001 Nu12 0.001
           E2 1000. G1z 310000000.
           G2z 138000000.
STRENGTH Tension1 1.E+15 Compress1 1.E+15 Shear 1.E+15
          Tension2 1.E+15 Compress2 1.E+15
THERMAL Alpha11 0.000023 K11 0. K12 0.
          Alpha22 0.000023 K22 0. K13 0.
          K33 0. K23 0.
          Spec Heat 0.
OPTICAL Front Off Reverse Off
    
```

**Figure 52 - Validation test: Sandwich Panel with metallic skins - 3/16-5056-0.001 Data**

### 4.3.1.2 - Numerical Results of the analysis and comparison

For this example were considered ten different load cases for the structure and were obtained the following results in *Tabs. 13-14-15*:

### Upper skin – Results

Margin of Safety	File Excel	API	Case Set	Element ID	Max compression principal stress [Pa]	Max Von Mises stress [Pa]
<b>Dimpling</b>	<b>0.85</b>	<b>0.85</b>	3	224607	96896704	
<b>Wrinkling</b>	<b>-0.99</b>	<b>-0.99</b>	3	224607	96896704	
<b>Tensile yielding</b>	<b>0.50</b>	<b>0.50</b>	5	224607		1.7E+08
<b>Compression yielding</b>	<b>0.50</b>	<b>0.50</b>	5	224607		1.7E+08
<b>Tensile ultimate</b>	<b>0.52</b>	<b>0.52</b>	5	224607		1.7E+08

### Bottom skin - Results

Margin of Safety	File Excel	API	Case Set	Element ID	Max compression principal stress [Pa]	Max Von Mises stress [Pa]
<b>Dimpling</b>	<b>1.2</b>	<b>1.2</b>	3	224230	81614800	
<b>Wrinkling</b>	<b>-0.99</b>	<b>-0.99</b>	3	224230	81614800	
<b>Tensile yielding</b>	<b>0.70</b>	<b>0.70</b>	5	224607		1.49E+08
<b>Compression yielding</b>	<b>0.70</b>	<b>0.70</b>	5	224607		1.49E+08
<b>Tensile ultimate</b>	<b>0.73</b>	<b>0.73</b>	5	224607		1.49E+08

### Honeycomb – Results

Margin of Safety	File Excel	API	Case Set	Element ID	Max compression principal stress [Pa]	Max Von Mises stress [Pa]
<b>Ultimate, L-direction</b>	<b>2.37</b>	<b>2.37</b>	2	224449	229211	
<b>Ultimate, W-direction</b>	<b>0.69</b>	<b>0.69</b>	5	223203		252135
<b>L-W</b>	<b>0.67</b>	<b>0.67</b>	2		229211	- 220571
<b>W-L</b>	<b>0.54</b>	<b>0.54</b>	5		204795	252135

## 4.3.2 Panel with composite laminate skins

### 4.3.2.1 - Description of the model

The current example is a sandwich panel with two composite multilayered plates as skins.

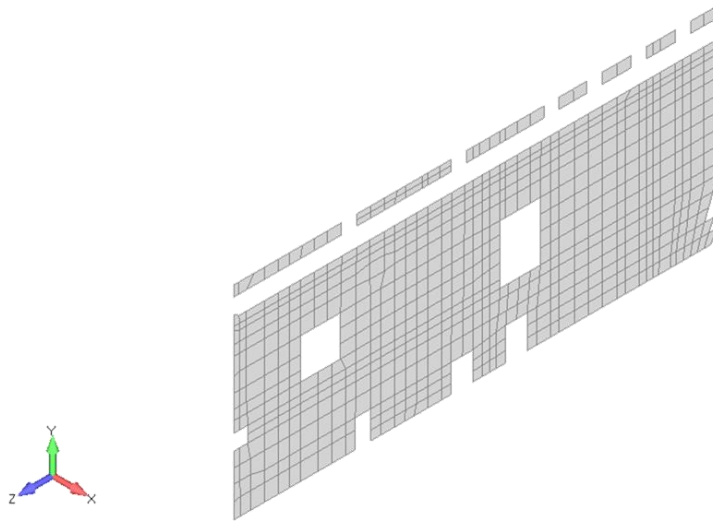


Figure 53 - Validation test: Sandwich Panel with composite laminate skins - Model

Respect the entire model it is defined by the ‘Property 71001 - LAMINATE PLATE Property’ and it is meshed using 659 elements.

#### Layup and material data

In this case the layup was more complex than before, indeed, the skins were made of two type of composite laminate named:

- Fabric,
- M55J<sup>18</sup>,

and there were many plies

---

<sup>18</sup> M55J is the name of carbon fibre, however in this context it is the name of the entire laminate plate made of it.

The reader can see the complete layup in *fig.54*.

```

Property 71001 - LAMINATE PLATE Property
Type LAMINATE PLATE Color 110 Layer 1 Material 0 #Elem 661
Laminate Option As Specified
Failure Theory HOFF Bond Shear Allowable 58000000.
Ref Temp 20. Damping Coef 0.
NS Mass/Area 0. Bottom Surf OFF 0.
Layup 41 -
Ply 1 Material 600 Thickness 0.000137 Angle 0.
Ply 2 Material 601 Thickness 0.000127 Angle 0.
Ply 3 Material 601 Thickness 0.000127 Angle -45.
Ply 4 Material 601 Thickness 0.000127 Angle 90.
Ply 5 Material 601 Thickness 0.000127 Angle 90.
Ply 6 Material 601 Thickness 0.000127 Angle 45.
Ply 7 Material 601 Thickness 0.000127 Angle 0.
Ply 8 Material 601 Thickness 0.000127 Angle 0.
Ply 9 Material 601 Thickness 0.000127 Angle 45.
Ply 10 Material 601 Thickness 0.000127 Angle 90.
Ply 11 Material 601 Thickness 0.000127 Angle 90.
Ply 12 Material 601 Thickness 0.000127 Angle -45.
Ply 13 Material 601 Thickness 0.000127 Angle 0.
Ply 14 Material 600 Thickness 0.000137 Angle 0.
Ply 15 Material 654 Thickness 0.0243 Angle 90.
Ply 16 Material 600 Thickness 0.000137 Angle 0.
Ply 17 Material 601 Thickness 0.000127 Angle 0.
Ply 18 Material 601 Thickness 0.000127 Angle -45.
Ply 19 Material 601 Thickness 0.000127 Angle 90.
Ply 20 Material 601 Thickness 0.000127 Angle 90.
Ply 21 Material 601 Thickness 0.000127 Angle 45.
Ply 22 Material 601 Thickness 0.000127 Angle 0.
Ply 23 Material 601 Thickness 0.000127 Angle 0.
Ply 24 Material 601 Thickness 0.000127 Angle 45.
Ply 25 Material 601 Thickness 0.000127 Angle 90.
Ply 26 Material 601 Thickness 0.000127 Angle 90.
Ply 27 Material 601 Thickness 0.000127 Angle -45.
Ply 28 Material 601 Thickness 0.000127 Angle 0.
Ply 29 Material 600 Thickness 0.000137 Angle 0.

```

Figure 54 - Validation test: Sandwich Panel with composite laminate skins - Layup

Fabric:

```

Material 600 - 2D ORTHOTROPIC Material
  Type 2D ORTHOTROPIC Color 55 Layer 1 #Prop/Ply 252
    Density 1800. Damping 0. Ref Temp 20.
    Tsai-Wu 0.
STIFFNESS E1 55000000000. G12 55000000000. Nu12 0.31
           E2 55000000000. G1z 0.
           G2z 0.
STRENGTH Tension1 690000000. Compress1 371000000. Shear 107000000.
          Tension2 580000000. Compress2 334000000.
THERMAL Alpha11 -2.35E-6 K11 0. K12 0.
          Alpha22 -2.25E-6 K22 0. K13 0.
           K33 0. K23 0.
          Spec Heat 0.
OPTICAL Front Off Reverse Off
  
```

Figure 55 - Validation test: Sandwich Panel with composite laminate skins - Fabric Data

M55J

```

Material 601 - 2D ORTHOTROPIC Material
  Type 2D ORTHOTROPIC Color 55 Layer 1 #Prop/Ply 1670
    Density 1618. Damping 0. Ref Temp 20.
    Tsai-Wu 0.
STIFFNESS E1 3.11E+11 G12 4000000000. Nu12 0.22
           E2 60000000000. G1z 3500000000.
           G2z 3500000000.
STRENGTH Tension1 1776000000. Compress1 714000000. Shear 56000000.
          Tension2 299000000. Compress2 947000000.
THERMAL Alpha11 -1.E-6 K11 0. K12 0.
          Alpha22 0.0000358 K22 0. K13 0.
           K33 0. K23 0.
          Spec Heat 0.
OPTICAL Front Off Reverse Off
  
```

Figure 56 - Validation test: Sandwich Panel with composite laminate skins - M55J Data

3/16-5056-0.001

```

Material 654 - 2D ORTHOTROPIC Material
  Type 2D ORTHOTROPIC Color 55 Layer 1 #Prop/Ply 14
    Density 50. Damping 0. Ref Temp 20.
    Tsai-Wu 0.
STIFFNESS E1 1000. G12 0.001 Nu12 0.001
           E2 1000. G1z 310000000.
           G2z 138000000.
STRENGTH Tension1 1.E+15 Compress1 1.E+15 Shear 1.E+15
          Tension2 1.E+15 Compress2 1.E+15
THERMAL Alpha11 0.000023 K11 0. K12 0.
          Alpha22 0.000023 K22 0. K13 0.
           K33 0. K23 0.
          Spec Heat 0.
OPTICAL Front Off Reverse Off
  
```

Figure 57- Validation test: Sandwich Panel with composite laminate skins - 3/16-5056-0.001 Data

#### 4.3.2.2 - Numerical Results of the analysis and comparison

For this example have been considered two load cases and a good match was generally found. However, an important difference was crosschecked in minimum margin of safety evaluation.

## Failure index

In this sub-section the correlation of failure indexes is reported in *Tab.16*, however all plies and elements were not indicated to limit table dimension. The results match with  $10^{-9}$  decimal precision.

<i>Element ID/Ply</i>		<i>File Excel</i>				<i>Api</i>		
<b>7400</b> <b>1</b>	0,00 03	0,05 98	0,04 22	0,00 03	0,00 03	0,05 98	0,04 22	0,00 03
<b>7400</b> <b>2</b>	0,00 33	0,05 67	0,04 79	0,00 33	0,00 33	0,05 67	0,04 79	0,00 33
<b>7400</b> <b>3</b>	0,00 36	0,05 85	0,04 64	0,00 37	0,00 36	0,05 85	0,04 64	0,00 37
<b>7400</b> <b>4</b>	0,00 39	0,05 61	0,04 90	0,00 38	0,00 39	0,05 61	0,04 90	0,00 38
<b>7400</b> <b>5</b>	0,00 45	0,05 61	0,04 94	0,00 45	0,00 45	0,05 61	0,04 94	0,00 45
<b>7400</b> <b>6</b>	0,00 73	0,04 87	0,05 90	0,00 72	0,00 73	0,04 87	0,05 90	0,00 72
<b>7400</b> <b>7</b>	0,00 50	0,05 98	0,04 62	0,00 51	0,00 50	0,05 98	0,04 62	0,00 51

Table 16 - Validation test: Sandwich Panel with composite laminate skins - Failure Index comparison

In *Fig.58* a distribution of failure index for ply 13 was reported.

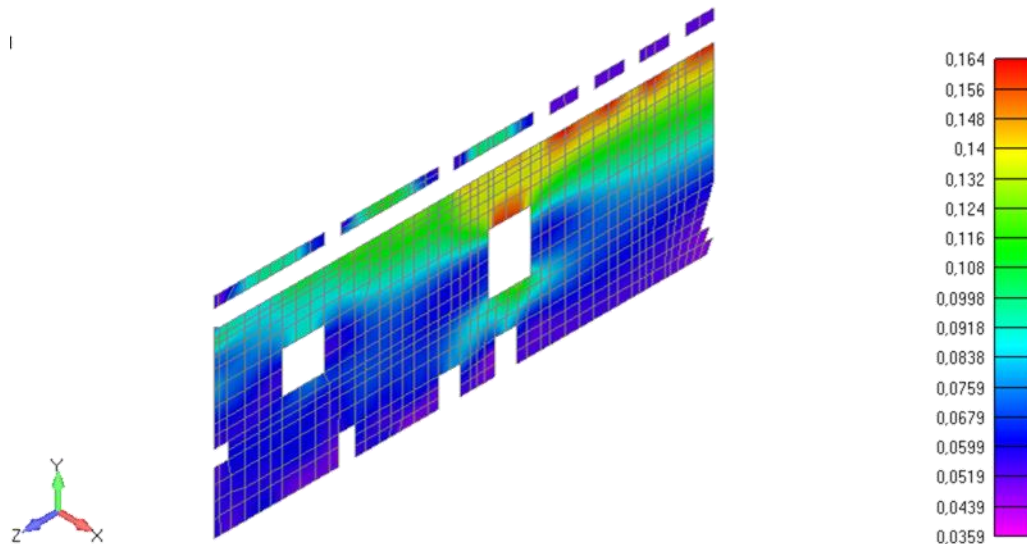


Figure 58 - Validation test: Sandwich Panel with composite laminate skins - Lam ply 13 Hoffman failure

## Margin of Safety

The Hoffman MoS of the single element of each ply evaluated with API and excel were the same value. Anyway, the final minimum values deduced were not the same,

because before the research of the minimum margin was only related to a condition of maximum or minimum component of stress. However, it was verified that a combination of all the three components of stress, which were not a maximum or minimum, can provide a lower value of MoS.

Herein, in the table, which was exported using the API, the absolute minimum value of margins of safety for this model were noted. They are relative to all plies and all load case selected. Besides, the stress state that provides it and where it was verified were insert together the minimum value for each material in *Tab.17*.

	Value	Load Case	Ply ID	Element ID	Sigma X [Pa]	Sigma Y [Pa]	Sigma XY [Pa]
Compressive Minimum Hoffman's MOS	<b>0,5588</b>	2	3	74015	-1,3E+08	10430600	101947
<b>HOFFMAN'MOS for each material in the laminate</b>							
Material ID	Value	Load Case	Ply ID	Element ID	Sigma X [Pa]	Sigma Y [Pa]	Sigma XY [Pa]
600	7,3680	2	29	74888	-2,9E+07	-1,1E+07	2535880
601	0,5588	2	3	74015	-1,3E+08	10430600	101947
654	6,8E+14	2	15	74008	1	1	0

**Table 17 - Validation test: Sandwich Panel with composite laminate skins - Minimum MoS by API**

While the data acquired from excel file are presented below in *Tab.18*.

Material ID	Element ID	Load Case	Ply ID	Sigma X [MPa]	Sigma Y [MPa]	Sigma XY [MPa]	Value
601	74019	2	3	-155,606	9,5575	0,3760	<b>0,5719</b>

Table 18 - Validation test: Sandwich Panel with composite laminate skins - Minimum MoS by Excel

Thus, the error committed was estimated as:

$$\text{Error: } |Value\ API - Value\ Excel| * 100 = |0,558797419 - 0,571892074| * 100 = \mathbf{1,3095\%}$$

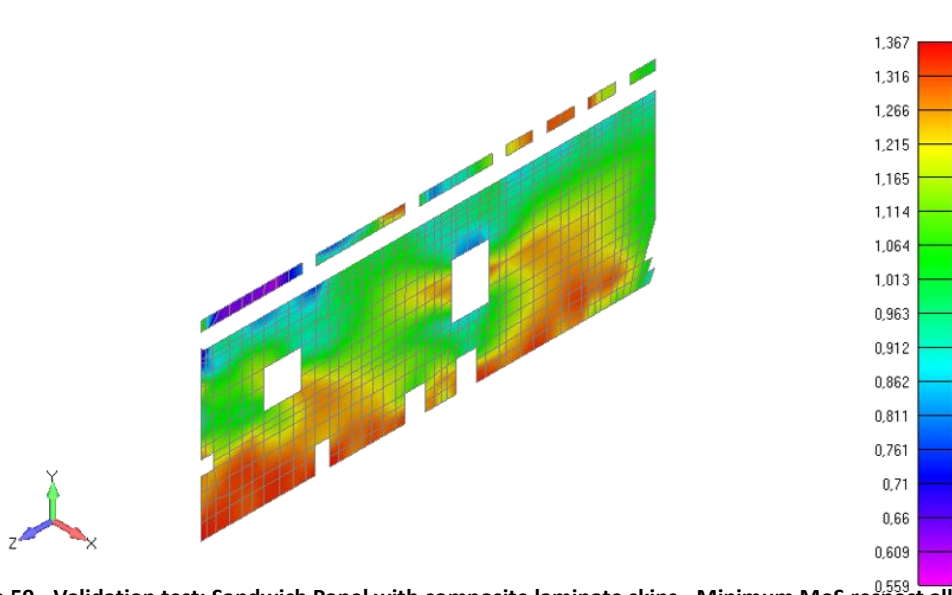


Figure 59 - Validation test: Sandwich Panel with composite laminate skins - Minimum MoS respect all plies contour

### 4.3.3 - Honeycomb meshed with solid elements

#### 4.3.3.1 - Description of the model

The case study presented in following section was only the model of honeycomb component of a sandwich panel. It was used to validate the routine to evaluate MoS in case of a structure meshed with solid elements.

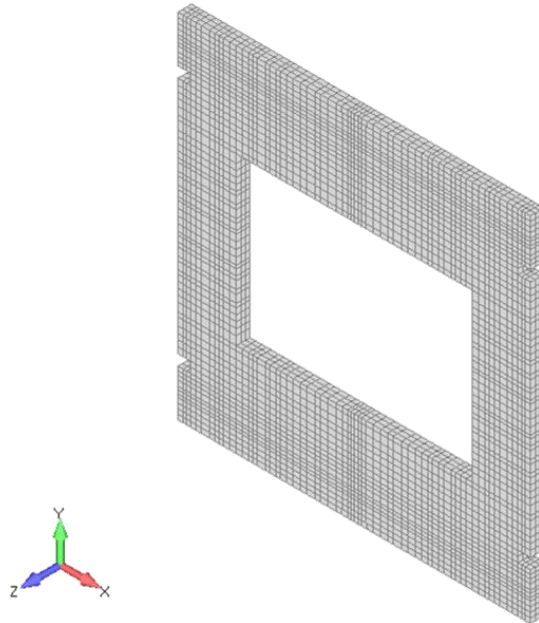


Figure 60 - Validation test: Honeycomb meshed with solid elements - Model

Its details respect the full model were:

- Property 10002 – SOLID Property
- N° elements: 8844

Layup and material data

In Femap was modelled with an anisotropic material 3D, that had the properties indicated in *Fig. 61*

```
Material 655 - 3D ANISOTROPIC Material
Type 3D ANISOTROPIC Color 55 Layer 1 #Prop/Ply 6
Density 91. Damping 0. Ref Temp 20.
STIFFNESS G11 448000000. G22 448000000. G33 1862000000.
G44 1000. G55 248000000. G66 648000000.
G12 448000000. G13 268800000. G14 0.
G15 0. G16 0. G23 268800000.
G24 0. G25 0. G26 0.
G34 0. G35 0. G36 0.
G45 0. G46 0. G56 0.
THERMAL Alpha11 0.00000164 Alpha22 0.000023 Alpha33 0.000023
Alpha12 0. Alpha13 0. Alpha23 0.
K11 0. K22 0. K33 0.
K12 0. K13 0. K23 0.
Spec Heat 0.
OPTICAL Front Off Reverse Off
```

Figure 61 - Validation test: Honeycomb meshed with solid elements - Material data

#### 4.3.3.2 - Numerical Results of the analysis and comparison

In this test only four load cases were considered in the analysis. The results obtained with API were compared with that estimated by Thales Alenia Space and they matching with  $10^{-8}$  precision. They were illustrated in *Tab.19*:

Margin of Safety	File Excel	API	Case Set	Element ID	Max compression principal stress [Pa]	Max Von Mises stress [Pa]
Ultimate, L-direction	0,92	0,92	2	10291	1244836	
Ultimate, W-direction	0,87	0,87	2	22397		738272
L-W (Max Txz & Consistent Tyz)	0,66	0,66	2		1244836	-419845
W-L (Max Tyz & Consistent Txz)	0,76	0,76	2		-442865	738272

Table 19 - Validation test: Honeycomb meshed with solid elements - API Results

	Mos	LC	YZ [Mpa]	XZ [Mpa]
Margin of Safety (Ultimate, L-direction)	0.93			
Margin of Safety (Ultimate, W-direction)	0.87			
Margin of Safety W-L (Max Txz & Consistent Tyz)	0.66	2	-419844.80	1244836.00
Margin of Safety W-L (Max Tyz & Consistent Txz)	0.77	2	738271.70	-442864.60

Figure 62 - Validation test: Honeycomb meshed with solid elements - Excel Results

## Chapter 5 - Common issues when using failure criteria and critical discussion

In the first part of this chapter will be illustrated a briefly comparison between failure indexes obtained from classical criteria and LaRC03 and LaRC04. The data will be presented in the stress planes. The case study considered are the same analysed in *Ref.14* and *Ref.15*.

Then a deeper attention was spent to shown the difference from Hoffman criterion results and that calculated basing on LaRC05 theory. Both will be evaluated using the API.

### 5.1 - Comparison of failure indexes between classical and LaRCs criteria

#### 5.1.1 - Unidirectional 0° E-glass/MY750 epoxy

The first example reported is a 0° E-glass/MY750 epoxy lamina. It has been subjected to a biaxial compression.

In *Figs.63-65* are shown failure envelope in the  $(\sigma_{11} - \sigma_{22})$  plane of all the failure modes represented by the six LaRC03 and LaRC04 criteria. They has been compared with Puck's analysis results, since which showed the best correlation with experimental results in the WWFE. In the figures, there is good agreement between LaRC and Puck in all quadrants except biaxial compression, where the former predict an increase of the axial compressive strength with increasing transverse compression. Testing for biaxial loads presents a number of complexities, and experimental results are rare. However, Waas and Schultheisz report a number of references in which multiaxial compression was studied by superposing a hydrostatic pressure in addition to the compressive axial loading. It has been observed that for all materials considered, there is a significant increase in compressive axial strength with increasing pressure.

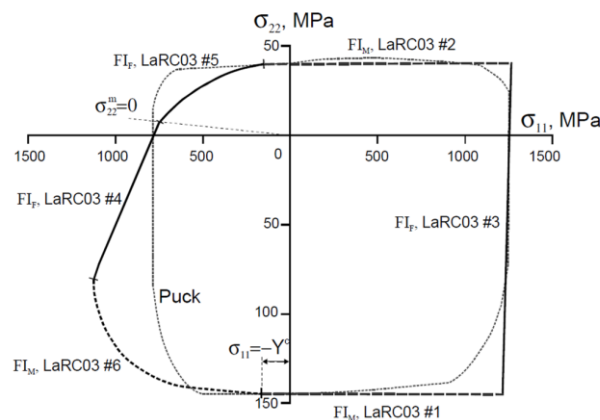
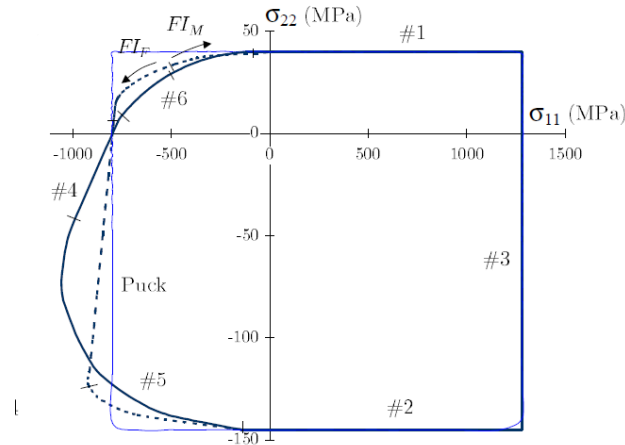


Figure 63 - Biaxial  $\sigma_{11} - \sigma_{22}$  failure envelope of 0° E-glass/MY750 epoxy lamina (LaRC03).

In the case of LaRC04, from 3D kinking model two possible values of the kinking angle were achieved,  $\psi = 0^\circ$  and  $\psi = 90^\circ$ . Thus meaning that the kink plane can either be in the plane of the lamina, or in the through-the-thickness direction.

Assuming first that the kink band develops in the plane of the lamina, either due to the micromechanics of the material or imposed by the testing, the failure envelope comes as in *Fig.64*. Moreover if it is assumed that the kink band is formed in the through-the-thickness direction, the envelope shown in *Fig.65(a)* is predicted. Finally if the orientation of the kink plane is unrestricted, the envelope in *Fig.65(b)* is



obtained.

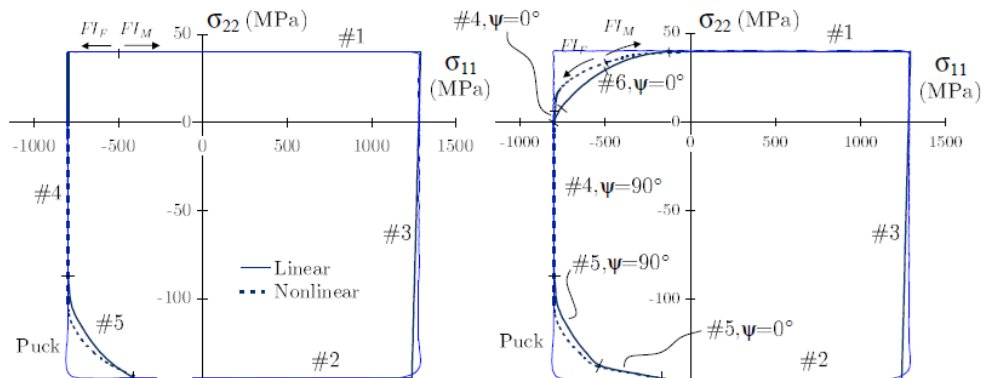


Figure 64 - Biaxial ( $\sigma_{11} - \sigma_{22}$ ) failure envelope of  $0^\circ$  E-glass/MY750 epoxy lamina, assuming a kink band in the plane of the lamina (LaRC04).

Figure 65 - Biaxial ( $\sigma_{11} - \sigma_{22}$ ) failure envelope of  $0^\circ$  E-glass/MY750 epoxy lamina (a) assuming through-the-thickness kinking; (b) assuming that there are no restrictions to the kinking plane(LaRC04).

### 5.1.2 - Unidirectional composite E-Glass/LY556

The following case study is a unidirectional composite E-Glass/LY556. In the figures below it can be observed that within the range of  $\sigma_{22} \geq 0$ , all the quadratic failure criteria and LaRCs correlate very well.

In the case of LaRC03 has been represented also results worked out using the Maximum Stress criterion, but since it does not prescribe interactions between stress components, its failure envelope is rectangular.

In both images an interesting behavior develops when  $\sigma_{22}$  becomes compressive. Indeed, Hashin's 1973 criterion gives an elliptical envelope with diminishing  $\tau_{12}$  as the absolute value of compressive  $\sigma_{22}$  increases, while the experimental data shows a definite trend of shear strength increase as  $\sigma_{22}$  goes into compression. The envelope for Hashin's 1980 criteria provides a modest improvement in accuracy. But only

Sun, LaRC03-1, LaRC04-2 and Puck criteria capture the shear strength increase at the initial stage of compressive  $\sigma_{22}$ .

Puck's envelope appears to be the most accurate, but it relies on fitting parameters based on the same test data. The LaRC03 curve assumed  $\alpha_0 = 53^\circ$ , and no other empirical or fitting parameter. In the case of matrix tension, Puck's predicted failure envelope is nearly identical to LaRC03-2. On the contrary LaRC04-2 curve fits very well with which of Puck.

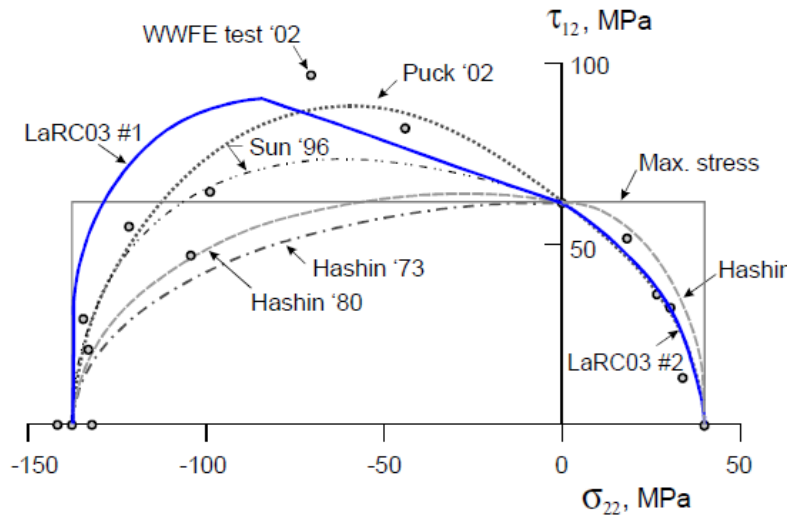


Figure 66 - Failure envelopes and WWFE test data for unidirectional composite E-Glass/LY556 (LaRC03).

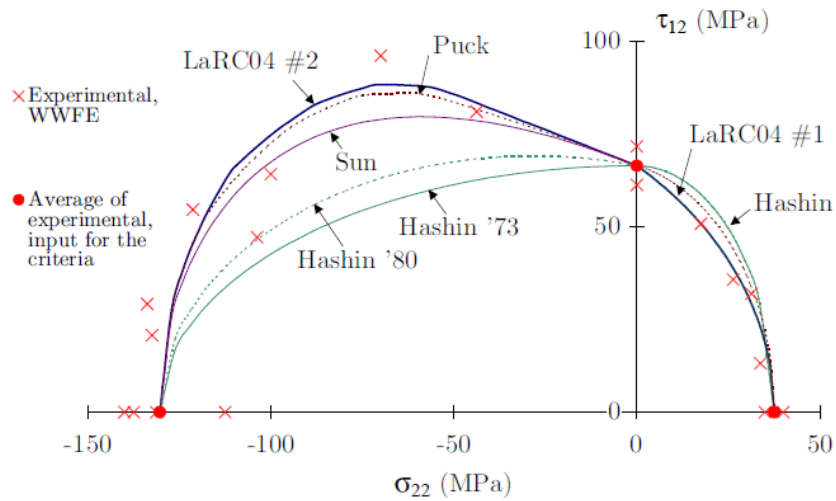


Figure 67 - Failure envelopes and WWFE test data for unidirectional composite E-Glass/LY556 (LaRC04).

### 5.1.3 - Cross-ply laminates

The last study reported in this document is on cross-ply laminates changing lamination angle.

The compression failure of  $[\pm\theta]_s$  laminates in AS4/3502 was studied by Shuart, he found that for  $\theta < 15^\circ$ , the dominant failure mode in these laminates is interlaminar shearing; for  $15^\circ < \theta < 50^\circ$ , it is in-plane matrix shearing; and for  $\theta > 50^\circ$ , it is matrix compression.

Fibre scissoring due to matrix material nonlinearity caused the switch in failure mode from in-plane matrix shearing to matrix compression failure at larger lamination angles. The fracture angle in pure transverse compression is considered to be

$$\alpha_0 = 53^\circ.$$

By this study it was found out that Hashin criteria is not very adequate. In fact for  $\theta < 20^\circ$ , the it result in an overprediction of the failure load because the criterion does not account for the effect of inplane shear on fibre failure. Also for lamination angles near  $70^\circ$ , the failure load was an underpredicted because the criteria do not account for the increase in shear strength caused by transverse compression.

While, all of these effects are represented by both LaRC criteria, which results in a good correlation between the calculated and experimental values (Shuart).

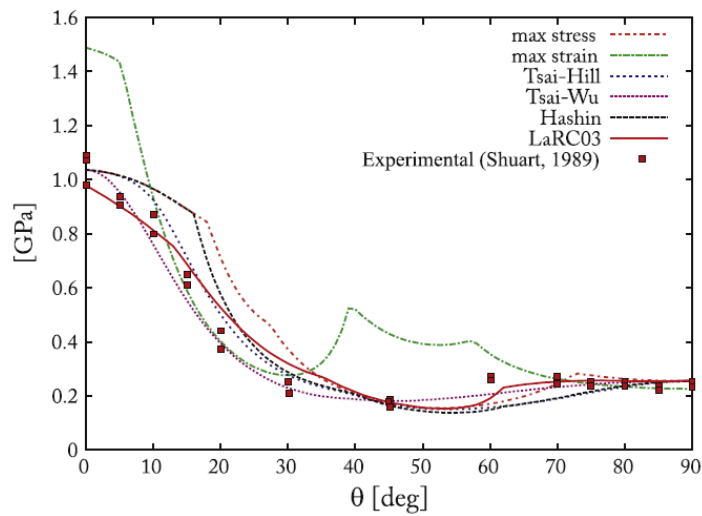


Figure 68 - Compressive strength as a function of ply orientation for  $[\pm\theta]_s$  AS4/3502 laminates (LaRC03).

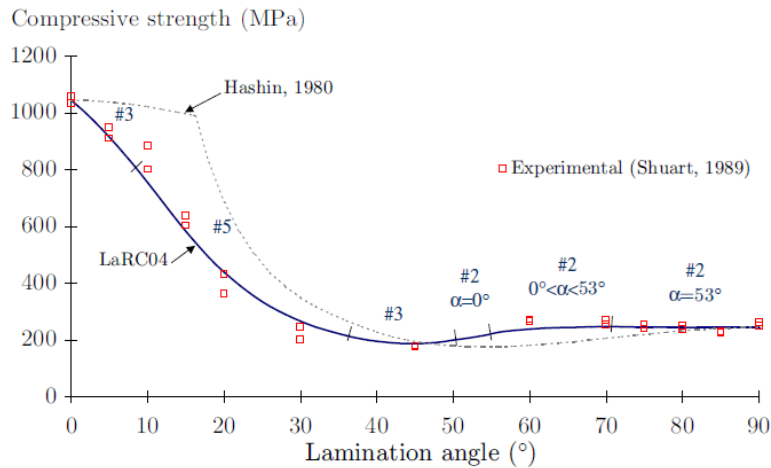


Figure 69 - Compressive strength as a function of ply orientation for  $[\pm\theta]_s$  AS4/3502 laminates (LaRC04).

## 5.2 - LaRC05 vs. Hoffman results

The difference between the results Hoffman's failure index criterion and LaRC05 criteria will be presented in this paragraph. To do this juxtaposition was used the API on models already analyzed for the validation. So, the reader can find detailed information about models in chapter 4.

### 5.2.1 - Example 1

The current example is the sandwich panel with two composite multilayered plates as skins of paragraph 4.3.2. To do the comparison will be reported some images of failure index contours.

In Figs.70-73 have been shown the values of failure index of each element of the mesh. As example it has been taken ply 1 and ply 13.

The load case considered is the 'MSC/NASTRAN Case 1'.

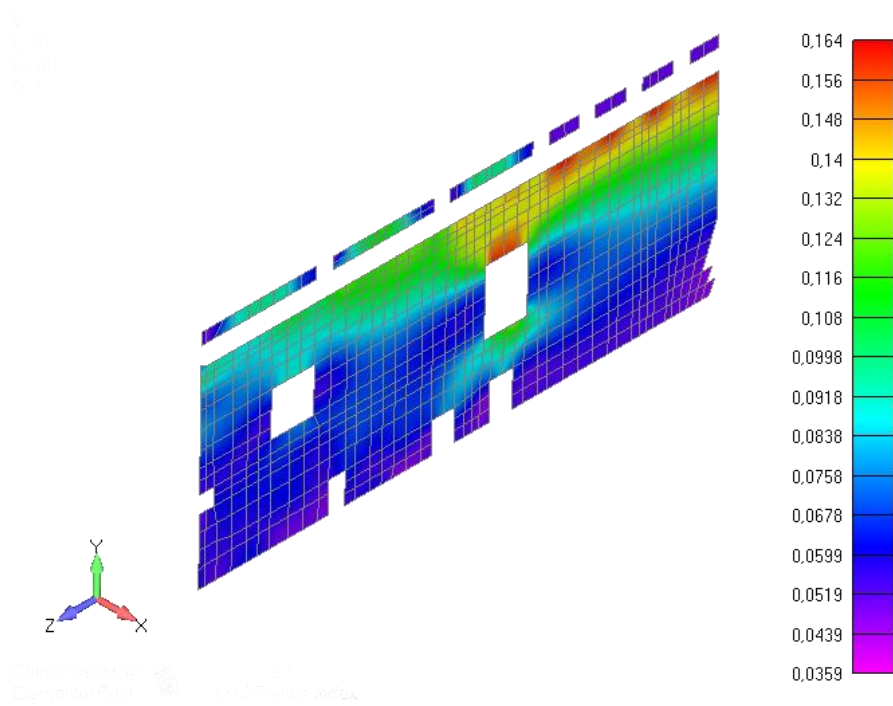


Figure 70 - Contour of Hoffman's failure indexes, Ply 13

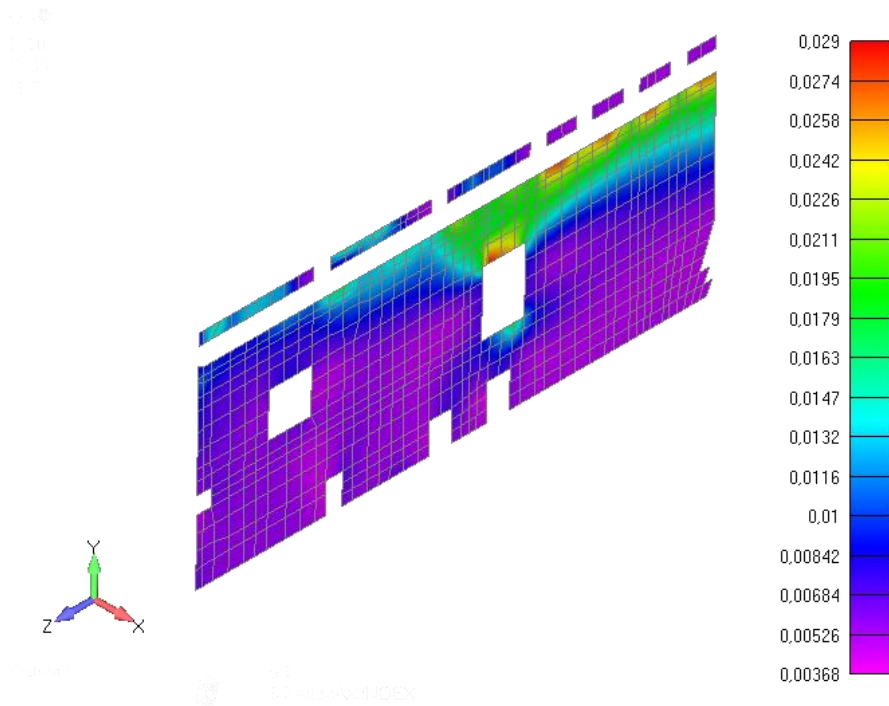


Figure 71 - Contour of LaRC05's failure indexes, Ply 13

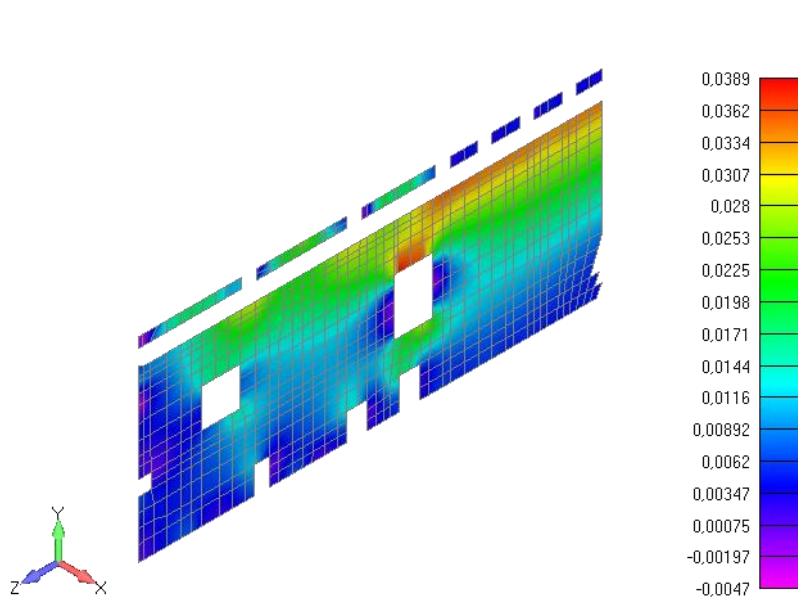


Figure 72 - Contour of Hoffman's failure indexes, Ply 1

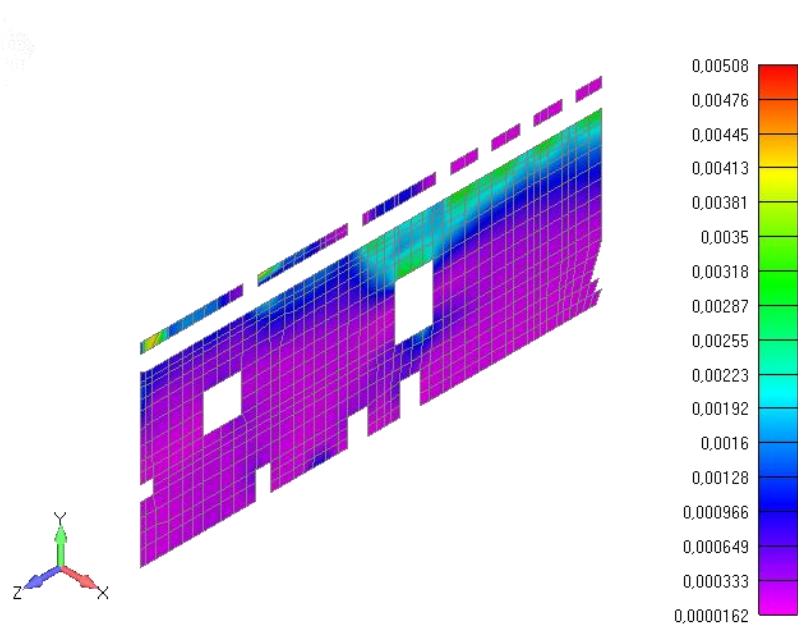


Figure 73 - Contour of LaRC05's failure indexes, Ply 1

Then has been illustrated the results of an other load case, which is 'MSC/NASTRAN Case 4'

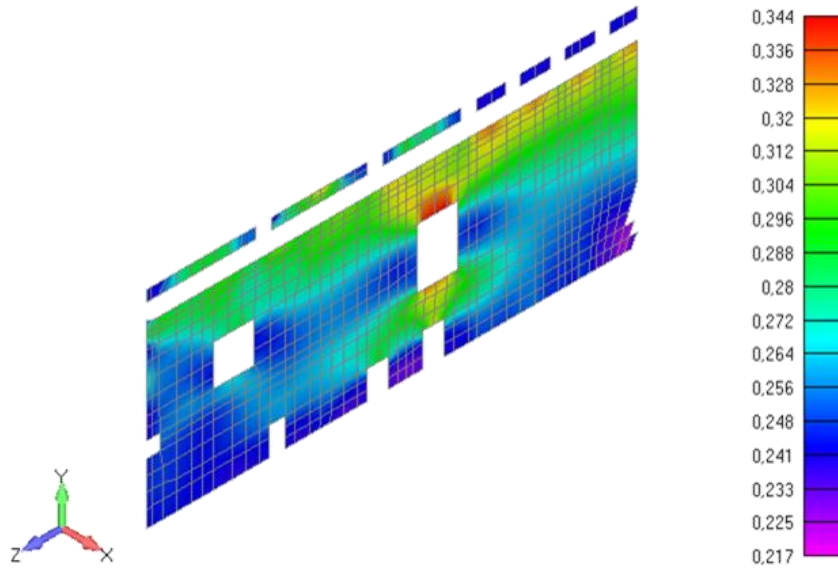


Figure 74 - Contour of Hoffman's failure indexes, Ply 13

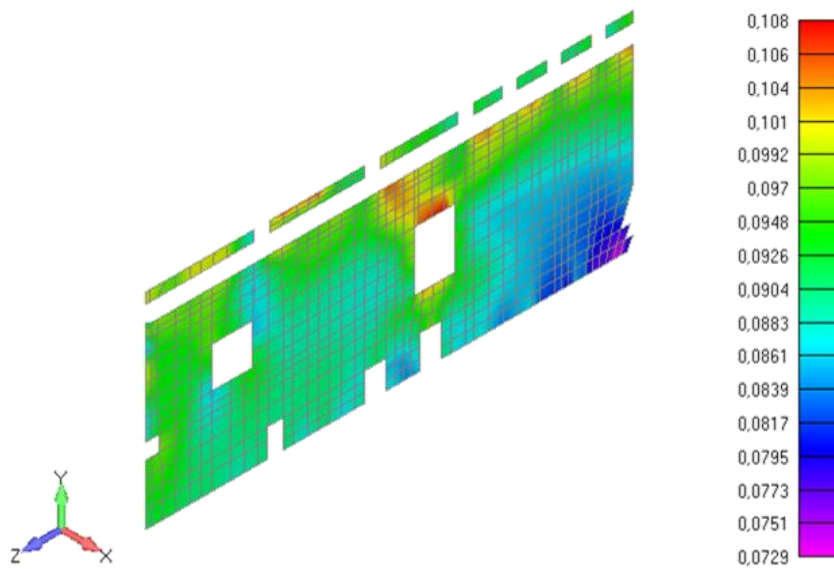


Figure 75 - Contour of LaRC05's failure indexes, Ply 13

In all case illustrated it is possible observing that the two distributions of failure index are similar, but there is a great difference in the values. This difference could be generated by the fact that LaRC05 criteria is based on a more accuracy physically description of the failure phenomena, so it is less conservative then Hoffman criteria.

For each case has been committed a discrepancy,  $\Delta$ , equal to:

$$\Delta_1 = \frac{|FI_{maxLaRC05} - FI_{maxHoff}|}{|FI_{maxHoff}|} * 100 = \frac{|-0.135|}{|0.164|} * 100 = 82.31\%$$

$$\Delta_2 = \frac{|FI_{maxLaRC05} - FI_{maxHoff}|}{|FI_{maxHoff}|} * 100 = \frac{|-0.03382|}{|0.0389|} * 100 = 86.94\%$$

$$\Delta_3 = \frac{|FI_{maxLaRC05} - FI_{maxHoff}|}{|FI_{maxHoff}|} * 100 = \frac{|-0.236|}{|0.344|} * 100 = 68.60\%$$

### 5.2.2 - Example 2

The current example is the 4-ply cantilever beam of paragraph 4.1. Herein will be presented the numerical results obtained for NX NASTRAN Case1 for ply 1.

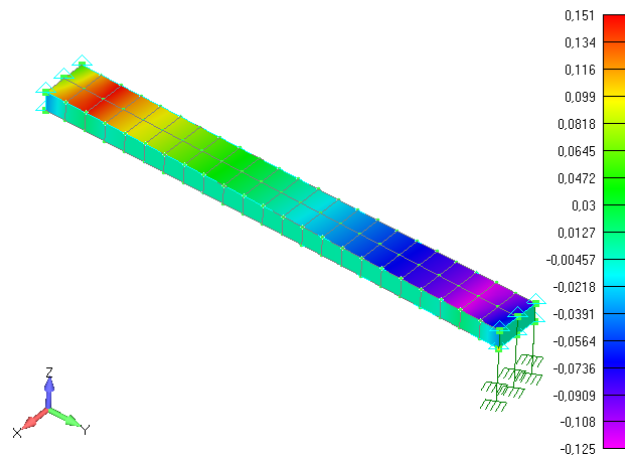


Figure 76 - Contour of Hoffman's failure indexes, Ply 1

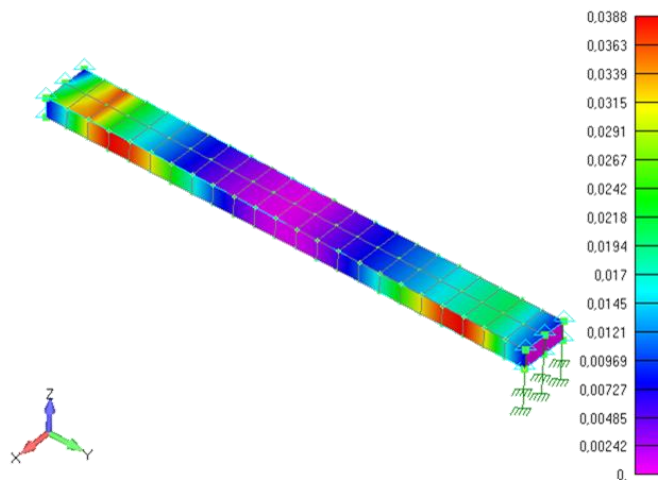


Figure 77 - Contour of LaRC05's failure indexes, Ply 1

$$\Delta = \frac{|FI_{max_{LaRC05}} - FI_{max_{Hoff}}|}{|FI_{max_{Hoff}}|} * 100 = \frac{|-0.1122|}{|0.151|} * 100 = 74.30\%$$

Concluding this chapter it is clear from these comparisons that new failure theories would allow to include more complex phenomena in the study of fracture. So it would be possible to reduce the conservative technical margins, therefore to make more light structure and save money. Considering that the maximum values of failure index were obtained near constraints and edges, it is, however, necessary that further analysis and comparisons be carried out during a more general and large investigation. Moreover, if an accurate stress field for each ply of laminate was included a more accurate prediction of failure would be evaluated.

## Chapter 6 - Numerical results on a real case study

After spending a lot of time to validate the API and be sure that it provides correct results it has been used to a real project. In particular, it has been tested on a sun tracker.

The main items of the structure are shown in figures from *Fig. 78* to *Fig. 79*.

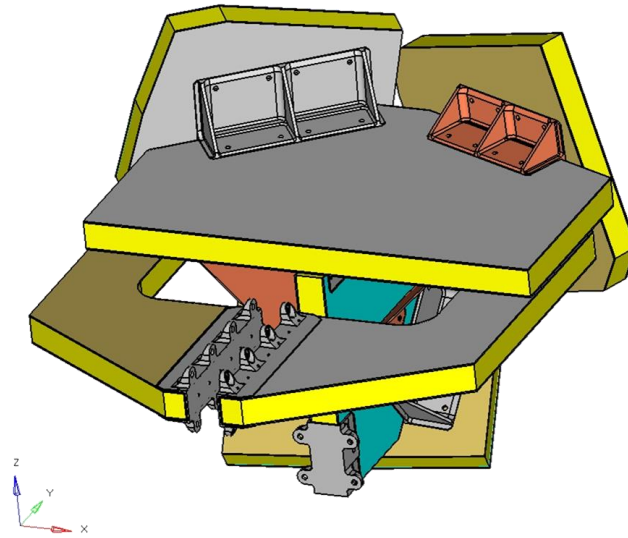


Figure 78 - Overview top side

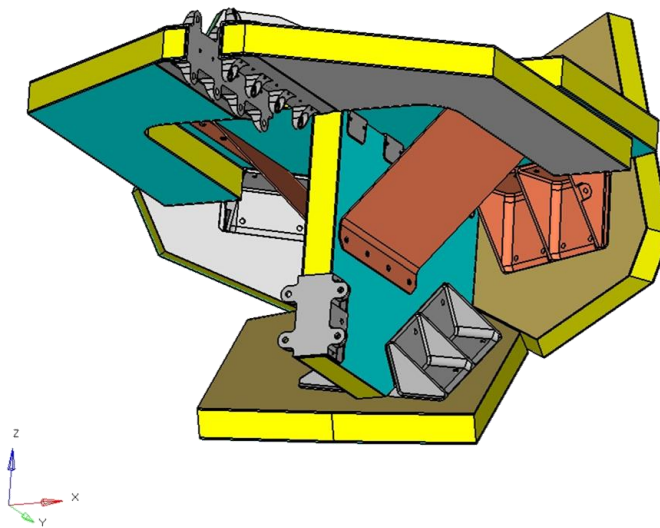
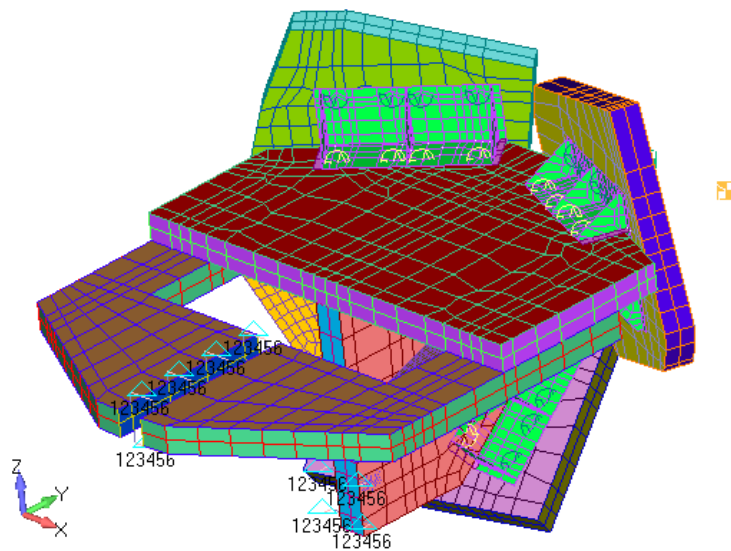
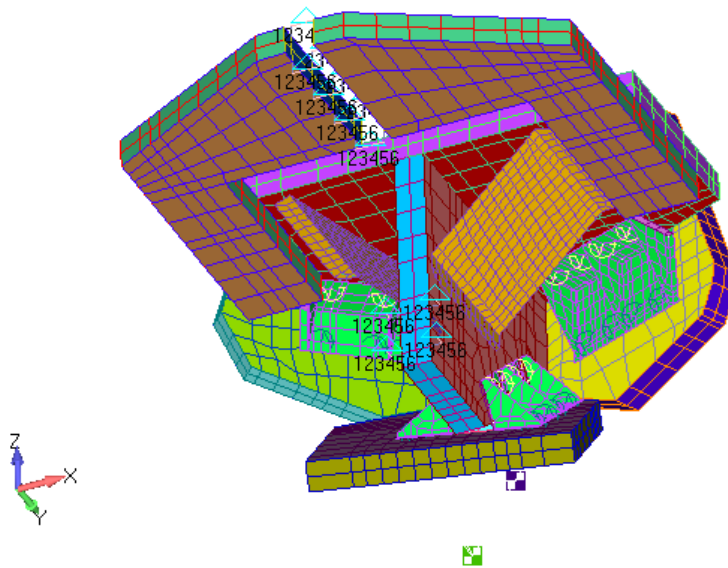


Figure 79 - Overview bottom side



**Figure 80 - Overview top side)**

According to this design a detailed FEM has been developed for the mechanical analysis and an overview has been illustrated in *Fig.81*. The final STT FEM mass is 5 Kg including fasteners.



**Figure 81 - FEM constraints**

## 6.1 - Sandwich Panels

The STT Structure is constituted by sandwich panels with CFRP skins and aluminum honeycomb cores. The CFRP prepreg used for the lamination of the panels are unidirectional M55J/M18 and fabric T300/M18.

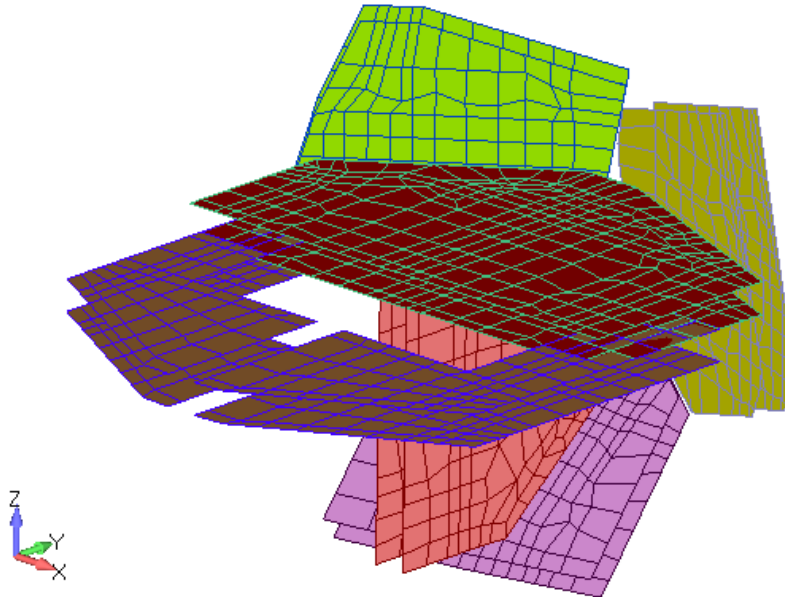


Figure 82 - FEM skins

The honeycomb properties are listed in table below (*Tab.20*) and distributed in the panels as shown in *Fig. 83*

Min. plate shear								
	Designation	Density	Min. Compressive		"L" direction		"W" direction	
			Strength	Modulus	Strength	Modulus	Strength	Modulus
		[kg/m <sup>3</sup> ]	[MPa]	[MPa]	[MPa]	[MPa]	[MPa]	[MPa]
1	3/16 5056 0.002	91.3	5.06	1861	3.3	648	1.9	248
2	3/16 5056 0.001	49.6 6	1.79	669	1.38	310	0.76	138

Table 20 - STT sandwich panels honeycombs

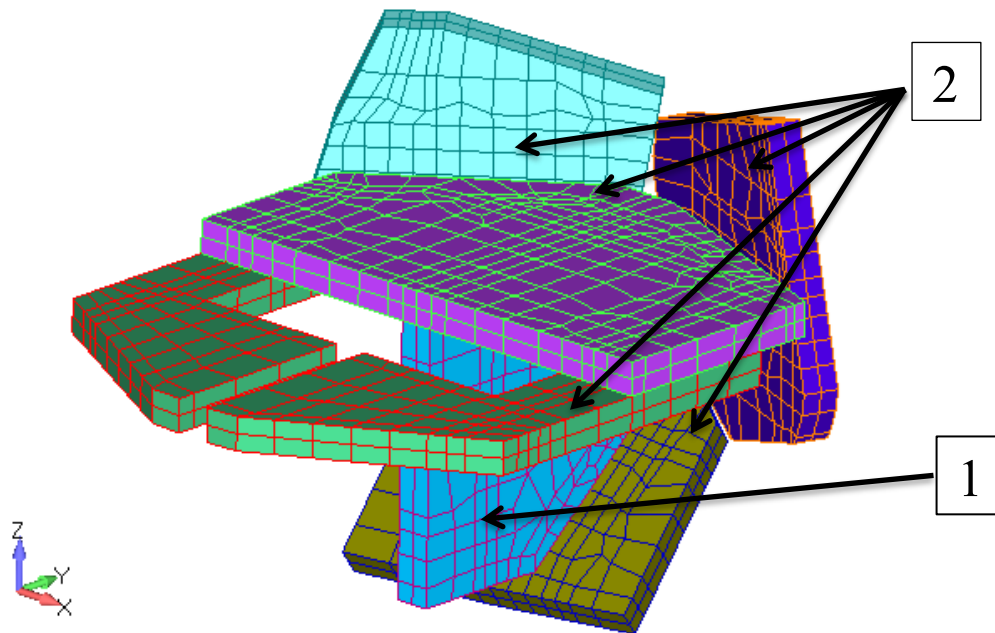


Figure 83 - Honeycombs distribution

### 6.1.1 - Skin Analysis

In this paragraph is reported the CFRP skins analysis under mechanical load application.

Figure 84 shows the minimum margin of safety detected by analysis.

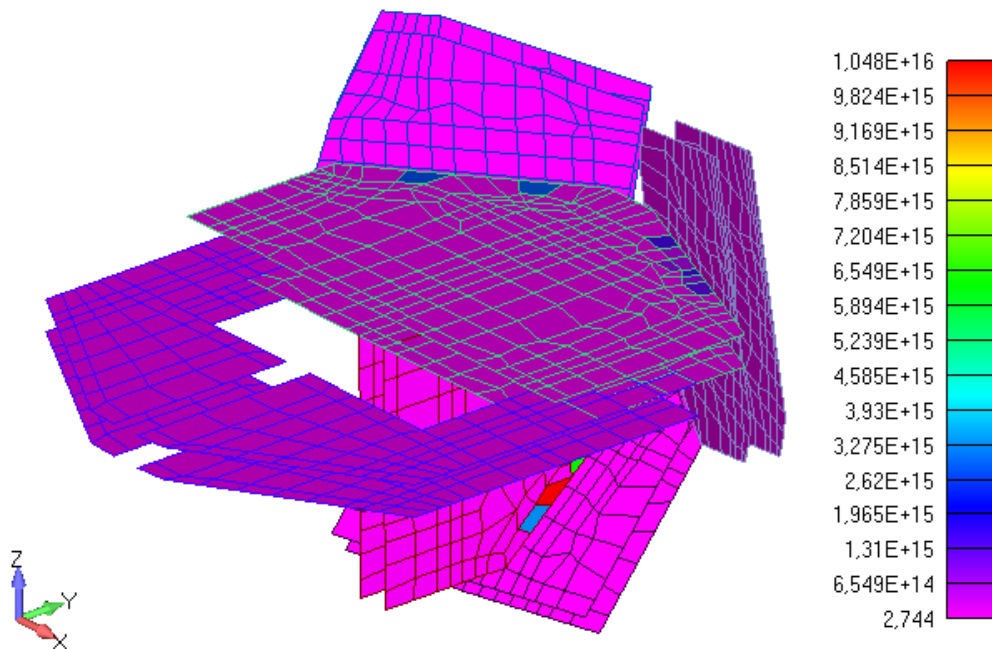


Figure 84 - CFRP skins minimum MOS

This minimum MoS relative to all plies and all load case selected has been computed in accordance with the stress reported in *Tab.21*

	Value	Load Case	Ply ID	Element ID	Sigma X [Pa]	Sigma Y [Pa]	Sigma XY [Pa]
<b>Compressive Minimum Hoffman's MOS (API)</b>	2,74	1	12	21777 1	- 13895 0384	- 145931 .6	13178 27

<b>HOFFMAN'MOS for each material in the laminate (API)</b>							
Material ID	Value	Load Case	Ply ID	Element ID	Sigma X [Pa]	Sigma Y [Pa]	Sigma XY [Pa]
<b>(T300) 600</b>	8,20	1	14	21777 1	- 86875 85	- 23400 688	28709 78
<b>(M55J /M18) 601</b>	2,74	1	12	21777 1	- 13895 0384	- 14593 1.6	13178 27

Table 21 - CFRP skins maxima stresses computed and MoS of the skins

### 6.1.2 - Honeycomb Analysis

The two types of honeycomb have been verified applying the interaction formula.

The margin of safety is computed as follows:

$$MoS = \frac{RF}{SF_u} - 1$$

SF<sub>u</sub> is the applied safety factor.

RF is the reserve factor computed with the following formula:

$$RF = \frac{1}{\sqrt{\left(\frac{\tau_w}{\tau_{allowW}}\right)^2 + \left(\frac{\tau_L}{\tau_{allowL}}\right)^2}}$$

Honeycomb type 1:

<b>HONEYCOMB</b>					
<b>MOS</b>	<b>Value</b>	<b>Case Set</b>	<b>Element ID</b>	<b>Tau XZ [Pa]</b>	<b>Tau Yz [Pa]</b>
<b>Ultimate, L-direction</b>	0,518612	2	218659	660890,6	
<b>Ultimate, W-direction</b>	0,608602	2	218569		343607,3
<b>W-L (Max Txz &amp; Consistent Tyz)</b>	0,505641	2		660890,6	47878,96
<b>W-L (Max Tyz &amp; Consistent Txz)</b>	0,262248	2		492888,2	343607,3

Table 22 - MoS of honeycomb type 1

Honeycomb type 2:

<b>HONEYCOMB</b>					
<b>MOS</b>	<b>Value</b>	<b>Case Set</b>	<b>Element ID</b>	<b>Tau XZ [Pa]</b>	<b>Tau Yz [Pa]</b>
<b>Ultimate, L-direction</b>	0,493361	1	218198	672065,4	
<b>Ultimate, W-direction</b>	0,953562	5	215293		282933
<b>W-L (Max Txz &amp; Consistent Tyz)</b>	0,492627	1		672065,4	11612,62
<b>W-L (Max Tyz &amp; Consistent Txz)</b>	0,836183	5		-186609	282933

Table 23 - MoS of honeycomb type 2

## Chapter 7 - Concluding remarks

The progress in the use of composites materials is greatly influenced by the capability of expecting and understanding their failure mode. Many different theories have been thought and developed for this purpose. However, some of these are not enough accurate since they are based on assumptions true for metallic structures or on a reduced knowledge of failure phenomena.

At the current state of the art the NASA Langley Research Center worked out a series of criteria, which obtained a significant correlation with real example. These were known as LaRC criteria, and the last criterion developed is the LaRC05.

A SW tool has been developed during the work developed in order to calculate the failure index of layered composite structures according to LaRC05 criterion, starting from the stress field calculated by a finite element code. In addition, this tool allows the user to calculate the failure index also by referring to the classical Hoffman criterion (which is commonly applied in the aerospace Industry). Particular care has been devoted to the computational efficiency of the code and to furnish automatic reporting capabilities.

The tool implemented is an API which has been embedded into Femap Siemens SW custom tools. FEMAP is a SW commonly used in order to post process FE results. The API has been written in Visual Basic language by referring to some Excel and Femap libraries. Then, an user friendly graphical interface has been associated to the API.

A number of case-studies have been referred to in order to achieve a proper validation of the implemented code and they are illustrated along this work. In order to double-check the implementation, a preexisting real structure, whose results were already available, has been considered as well. Moreover, for the same structure, the differences in results produced by passing from Hoffman to LaRC05 criterion have been identified and discussed. A number of additional comparisons have thus been produced between the results obtained by applying the above two criteria.

Possible future developments could explore the sensitivity of the failure indexes calculated to a progressively more accurate stress field (e.g. the stress-field calculated with finite elements formulated with higher order/hierarchical kinematic expansion). The outcomes could be further discussed by referring to some test-results.

## References

- [1] NALI P, CARRERA E. A NUMERICAL ASSESSMENT ON TWO-DIMENSIONAL FAILURE CRITERIA FOR COMPOSITE LAYERED STRUCTURES COMPOSITES: PART B (2011)
- [2] MATERIAL SOLUTIONS POLYMER COMPOSITES.
- [3] HOFFMAN O. THE BRITTLE STRENGTH OF ORTHOTROPIC MATERIALS. J COMPOS MATER 1967;1(2):200–6.
- [4] TSAI SW, HAHN HT. FAILURE ANALYSIS OF COMPOSITE MATERIALS. IN: WINTER ANNUAL MEETING OF ASME; 1975. P. 73–96.
- [5] REDDY JN. MECHANICS OF LAMINATED COMPOSITE PLATES AND SHELLS, THEORY AND ANALYSIS. 1ST ED. BOCA RATON (FL): CRC PRESS; 1997.
- [6] HILL R. THEORY OF MECHANICAL PROPERTIES OF FIBER-STRENGTHENED MATERIALS. III. SELF-CONSISTENT MODEL. J MECH PHYS SOLIDS 1965;13:189–98.
- [7] TSAI SW. STRENGTH THEORIES OF FILAMENTARY STRUCTURES FUNDAMENTAL ASPECTS OF FIBRE REINFORCED PLASTIC COMPOSITES. NEW YORK: WILEYINTERSCIENCE; 1968.
- [8] TSAI SW, WU EM. A GENERAL THEORY OF STRENGTH FOR ANISOTROPIC MATERIALS. J COMPOS MATER 1971;5(1):58–80.
- [9] [23] LIU KS, TSAI SW. A PROGRESSIVE QUADRATIC FAILURE CRITERION FOR A LAMINATE. COMPOS SCI TECHNOL 1998;58(7):1023–32.
- [10] HASHIN Z, ROTEM A. A FATIGUE CRITERION FOR FIBER-REINFORCED MATERIALS. J COMPOS MATER 1973;7:448–64.
- [11] HASHIN Z. FAILURE CRITERIA FOR UNIDIRECTIONAL FIBER COMPOSITES. JOURNAL APPL MECH 1980;47:329–34.
- [12] GÜNTHER LUTZ VULKAN KUPPLUNGS- UND GETRIEBEBAU, THE PUCK THEORY OF FAILURE IN LAMINATES IN THE CONTEXT OF THE NEW GUIDELINE VDI 2014 PART 3
- [13] PUCK A, SCHUERMAN H. FAILURE ANALYSIS OF FRP LAMINATES BY MEANS OF PHYSICALLY BASED PHENOMENOLOGICAL MODELS. COMPOS SCI TECHNOL 1998;58(7):1045–67.
- [14] DÁVILA CG, CAMANHO PP. FAILURE CRITERIA FOR FRP LAMINATES IN PLANE STRESS. TECH. REP. NASA/TM-2003-212663; 2003.
- [15] T PINHO C G D´AVILA, P P CAMANHO L IANNUCCI, P ROBINSON FAILURE MODELS AND CRITERIA FOR FRP UNDER IN-PLANE OR THREE-DIMENSIONAL STRESS STATES INCLUDING SHEAR NON-LINEARITY. TECH. REP. NASA/TM-2005-213530; 2005.
- [16] Dvorak Gj, Laws N. Analysis Of Progressive Matrix Cracking In Composite Laminates. Ii. First Ply Failure. J Compos Mater 1987;21:309–29.
- [17] Pinho St, Iannucci L, Robinson P. Physically-Based Failure Models And Criteria For Laminated Fibre-Reinforced Composites With Emphasis On Fibre Kinking. Part I: Development. Composites Part A: Appl Sci Manuf 2006;37(1):63–73.
- [18] Pinho St, Iannucci L, Robinson P. Physically Based Failure Models And Criteria For Laminated Fibre-Reinforced Composites With Emphasis On Fibre

Kinking. Part Ii: Fe Implementation. Composites Part A: Appl Sci Manuf 2006;37(5):766–77.

- [19] St Pinho, R Darvizeh, P Robinson, C Schuecker And Pp Camanho - Material And Structural Response Of Polymer-Matrix Fiber-Reinforced Composites.
- [20] NX Nastran User's Guide
- [21] SIEMENS - Element Library Reference
- [22] FEMAP API Reference Manual.
- [23] Grasso Amedeo - Detailed explanation of failure criteria api for Femap
- [24] Manish Nagaraj - Report:Evaluation of Failure Indices using LaRC05
- [25] [https://en.wikipedia.org/wiki/Visual\\_Basic](https://en.wikipedia.org/wiki/Visual_Basic)
- [26] [https://en.wikipedia.org/wiki/Application\\_programming\\_interface](https://en.wikipedia.org/wiki/Application_programming_interface)
- [27] <https://techterms.com/definition/api>
- [28] <https://www.zerounoweb.it/software/erp-crm-scm/cosa-sono-le-api-e-quali-impatto-hanno-sul-business/>
- [29] <[HTTP://WWW.ADMC.ESRTECHNOLOGY.COM/BACKGROUND/FAILURE/](http://www.admc.esrtechnology.com/background/failure/)>.

## **Appendice A – Breve riassunto in italiano della tesi**

### **Introduzione**

Nell'industria aeronautica e aerospaziale l'uso dei materiali compositi è in continua crescita anno dopo anno, rendendo necessario la costante evoluzione delle metodologie di progettazione delle strutture in composito.

In questo contesto è emersa la necessità di comprendere meglio i meccanismi di rottura dei laminati in composito, studiando più dettagliatamente i fenomeni fisici alla base. Negli anni diversi studiosi hanno lavorato su questo aspetto riuscendo ad arrivare a diversi criteri che identificassero quando si possa verificare la rottura, e durante la prima edizione dei WWFEs (World Wide Failure Exercises) è stato dimostrato che il criterio di Puck fosse il più corretto.

Partendo dalle idee di Puck al NASA Langley Research Center sono stati ideati e studiati una serie di criteri, conosciuti come LaRC. Questi durante la seconda edizione dei WWFEs hanno riscontrato un'ottima correlazione con i casi esaminati. Ad oggi l'ultima versione è il LaRC05 che estende l'approccio ad uno stato di tensione 3D.

Poiché i criteri della famiglia LaRC sono recenti e quindi non ancora applicati nell'industria, i codici commerciali usati normalmente per la progettazione non li implementano per valutare gli indici di rottura ("*Failure Index*"). Perciò è stato sviluppato un tool, sotto forma di API, che si integri con il software commerciale Siemens Femap e permetta la valutazione dei FI del criterio LaRC05.

In questo documento è riportata una prima parte di descrizione dello stato dell'arte riguardo i criteri di rottura, da quelli classici a quelli più moderni e adeguati alle strutture in composito (Capitolo 2). Successivamente nel terzo capitolo viene descritto da prima il concetto di API e il "computational framework" che ha permesso lo sviluppo dell'API; e infine è presentata l'API stessa e le sue diverse funzionalità.

Durante tutta la programmazione del software è stata svolta costantemente e quasi per ogni più piccola parte un'attività di debug e validazione del codice. Infine la validazione finale di ogni singola macro funzione è stata svolta sfruttando i risultati già ricavabili con le analisi FEM, o scrivendo dei fogli Excel apposta o confrontando i risultati con quelli ricavabili da procedure aziendali standard. Tutto ciò è oggetto del quarto capitolo.

Il capitolo 5 riporta un confronto, tratto dalla letteratura e dall'applicazione del tool, tra i risultati ottenibili con i metodi classici e quelli più moderni. Infine, nell'ultimo capitolo è riportato un caso reale su cui sono state sfruttate le funzionalità dell'API.

### **Capitolo 2 – Stato dell'arte**

I primi ad attribuire la rottura dei laminati in composito a fenomeni fisici differenti sono stati Hashin e Rotem. Nel criterio di Hashin sono state proposte quattro condizioni di rottura dipendenti e non tra loro, per distinguere tra rottura della matrice e della fibra, causata da carichi a trazione o a compressione.

Successivamente questo concetto è stato ripreso e migliorato negli studi di Puck, che è stato il primo a supportare l'idea di rottura delle fibre e tra le fibre (FF e IFF).

Le ipotesi alla base della teoria di Puck sono:

- Analisi non lineare degli stress e deformazioni prima dell'IFF.
- I due criteri di rottura sono legati dal concetto di piano d'azione fisico
- Degradazione continua dopo l'inizio dell'IFF
- Considerazioni sulla rottura complessiva del laminato

Puck modifica le idee di Coulomb e Mohr per applicarle ai compositi unidirezionali.

### ***Criteri LaRC***

Successivamente per predire accuratamente la rottura di pannelli laminati in FRP, sottoposti a uno stato di tensione piano, senza dover ricorrere ad una ricerca dei parametri che meglio approssimano le curve, è stato definito un set di sei criteri denominato LaRC03.

Questo è ispirato dall'ipotesi fondamentale di Puck: la matrice si rompe con una rottura fragile. Di conseguenza entra in gioco il concetto di piano d'azione, già affrontato nella teoria Mohr-Coulomb.

La matrice può rompersi sotto carichi di trazione o compressione. Nel primo caso la rottura avviene lungo un piano normale al piano degli strati e parallelo alla direzione delle fibre.

Per ottenere un criterio che descriva la rottura della fibra per kinking, si deve calcolare il disallineamento delle fibre sotto un carico e applicare il criterio di rottura della matrice nel sistema disallineato di coordinate.

Successivamente i criteri LARC03 sono stati estesi al caso più generale di carichi tridimensionali e al caso di non linearità del taglio nel piano. Sono stati ottenuti così altre sei espressioni di failure index che costituiscono i criteri LaRC04.

Una prima differenza tra i due LaRC riguarda la rottura della matrice a trazione, perché viene esteso il concetto del rateo di rilascio di energia per valutare la geometria della rottura (introdotto da Dvorak e Laws) nel caso di materiali ortotropi lineari (già adottato nel LaRC03) anche nel caso di comportamento non lineare a taglio.

Invece è stato osservato che la matrice dei provini compressi si rompesse a taglio. In particolare dagli esperimenti si è osservato che l'angolo di rottura sotto compressione uniassiale è generalmente  $\alpha_0=53^\circ\pm 2^\circ$  per molti materiali compositi, invece di  $45^\circ$  come ci sarebbe aspettati. Questa rottura è stata modellizzata basandosi, come i precedenti criteri, sul criterio di Mohr-Coulomb per ottenere l'angolo di frattura.

Riguardo la rottura delle fibre, nel caso che siano caricate a trazione viene adottato il criterio di massimo stress ammissibile; mentre nel caso di carico a compressione a seconda del materiale sono possibili diversi modi di rottura. In particolare viene studiato il fenomeno del kinking.

Il kinking delle fibre è attivato da un angolo di disallineamento iniziale delle fibre e dalla rotazione di queste durante un carico a compressione. Si è osservato che il fenomeno del kinking è il risultato di una rottura prevalentemente a taglio della matrice in un sistema

di riferimento disallineato, sotto una compressione longitudinale. Tuttavia, se la compressione non è elevata, può succedere che la rottura della matrice provochi solamente lo splitting delle fibre ma non il kinking.

I valori che si trovano usando il LaRC04 correlano molto bene con I dati sperimentali, più degli altri criteri esistenti. L'ottima correlazione è attribuibile alla profonda conoscenza del fenomeno fisico alla base del modello della rottura.

### Capitolo 3 – API

Le **API** sono degli strumenti di programmazione che le maggiori industrie del mondo informatico mettono a disposizione degli sviluppatori per facilitare il loro compito nella realizzazione di applicazioni di vario genere.

Le API possono assumere diverse “forme”: possono essere delle librerie di funzioni che permettono al programmatore di interagire con un programma o una piattaforma software o semplicemente una serie di “chiamate” a parti di un programma che uno sviluppatore può utilizzare per abbreviare il suo lavoro.

Utilizzando un'API, un programmatore può far interagire due programmi (o due piattaforme, o un programma e una piattaforma) altrimenti tra loro incompatibili. Utilizzando, quindi, degli “artifici” di programmazione, si possono estendere le funzionalità di un programma ben oltre le reali intenzioni dello sviluppatore o della software house che l'ha realizzato.

In questo lavoro è stata creata un'API che si interfacciasse con il software CAE “Simens Femap”, ed È stato necessario utilizzare anche l'ambiente di lavoro di “Visual Studio Express”. Infatti il codice sorgente del tool è scritto in linguaggio Visual Basic, con l'integrazione delle librerie di Femap e Excel.

Per permettere un utilizzo più semplice e intuitivo possibile da qualunque utente, che non conosca fin da subito le capacità dell'API, è stata creata un'interfaccia grafica “user friendly”. In questo modo l'utente è guidato in tutte le operazioni da fare, e l'utilizzo si riduce alla semplice compilazione dei parametri di input di volta in volta necessari.

Le funzioni svolte dall'API sono:

- Calcolo dei «failure index» usando due possibili teorie:
  1. Hoffman
  2. LaRC05 – per laminati unidirezionali in composito
- Valutazione dei margini di sicurezza per il buckling di pannelli sandwich:
  1. Con pelli in metallo: dimpling, wrinkling, tensile yielding, compression yielding e tensile ultimate.
  2. Con pelli di laminati in composito

Nella valutazione dei margini di sicurezza per l'honeycomb è possibile valutarli sia che sia meshato con elementi di tipo “pcomp” (laminato) che con elementi solidi.

Valutati tutti i vari margini di sicurezza per ciascun elemento della mesh della struttura, il software valuta anche per quale condizione di carico, in quale elemento e in quale strato si è ottenuto il minimo valore.

Infine è prevista l'esportazione automatica in un file Excel dei risultati.

L'utente può scegliere quale stato tensionale usare nei calcoli:

- direttamente quello di Femap (ottenuto dall'analisi FEM basata su Nastran),
- da un file esterno.

## **Capitolo 4 – Validazione API**

Per validare la procedura di calcolo dei “failure index” secondo la teoria di Hoffman si è creato un file Excel “*Hoffman Failure Index*” e proceduto come segue:

1. Confronto numerico dei failure index prodotti da Nastran e dal file Excel,
2. Confronto dei contour plots prodotti direttamente dall'analisi con Nastran e l'API,
3. Confronto dei MoS calcolati dall'API e quelli del file Excel,

Inoltre è stata anche validata la funzione di «import» dello stato di tensione.

Per validare invece la routine che implementa il set di criteri LaRC05, non essendoci altre fonti, si è utilizzato il file Excel “*FAILURE INDEX CALCULATION-LARC05.xlsx*” creato apposta.

Infine per la validazione del calcolo dei MoS per diversi tipologie di pannelli sandwich sono stati confrontati i risultati ottenuti utilizzando l'API con quelli ricavati da diversi foglio di calcolo Excel usati in ambito aziendale. Nella tesi si riportano 3 esempi, evidenziando la perfetta correlazione ottenuta.

## **Capitolo 5 – Confronto criteri classici e criteri LaRC**

Nella prima parte del capitolo è mostrata la differenza nei valori tra i metodi classici e LaRC03 o LaRC04. Si osserva come i criteri LaRC e, anche quello di Puck, catturino dei fenomeni che prima venivano esclusi. Così da essere molto vicino ai dati sperimentali.

Nella seconda parte del capitolo invece si riportano due esempi di confronto dei risultati ottenuti utilizzando il criterio di Hoffman e LaRC05. Si osserva che a livello di distribuzione dei FI sono analoghi, tuttavia a livello numerico presentano un notevole differenza dovuta, probabilmente, al fatto che LaRC05 considerando una più dettagliata descrizione del fenomeno permettono di essere meno conservativi e più accurati nella scelta delle grandezze che contribuiscono alla rottura.

## **Capitolo 6 – Caso reale**

In questo capitolo sono riportati i risultati ottenuti applicando l'API ad un sun tracker, la cui struttura è costituita da pannelli con pelli in CFRP e honeycomb in alluminio.